University of Southampton

Faculty of Enginnering and Physical Sciences
School of Electronics and Computer Science
Smart Electronic Materials and Systems

E-Textile Based Electrostimulation for Wound Healing

by

Tom Greig

ORCID iD: 0000-0003-2745-235X

A thesis for the degree of
Doctor of Philosophy

September 2023

University of Southampton

Abstract

Faculty of Enginnering and Physical Sciences
School of Electronics and Computer Science

Doctor of Philosophy

E-Textile Based Electrostimulation for Wound Healing

by Tom Greig

Electrical stimulation has been known to have a positive effect on wound healing since the 1960s, although it has not yet been universally adopted as a recommended treatment for various types of wounds. A review of the clinical trials investigating the effectiveness of electrical stimulation confirmed its positive impact, with some studies reporting that stimulation doubled the rate at which wounds healed. However, the low numbers of participants and lack of consistency in these studies has prevented widespread adoption.

This thesis has investigated the underlying principals of electrical stimulation in the wound healing process and developed an e-textile device which can be used easily in a clinical setting and provide a platform for future studies. Dispenser printing was used to fabricate the electrodes directly onto existing wound dressings. To improve the consistency of the electrodes, a system was developed using laser displacement measurement which allows the printer to track the height changes of an uneven surface, reducing printing errors by 80%.

To understand how the current generated by these electrodes passes through the skin, two electrical models of the skin were developed. One, an equivalent circuit model derived from physical measurements, and the other, a simulation model using material properties from the literature, were compared to assess their accuracy. The two models agreed regarding the overall shape of the skin's impedance, but there were significant differences in their predictions of the DC resistance indicating an error in the modelling of the *stratum corneum*. These model was used to assess the ability of the various electrical stimulation waveforms to induce cell migration *in vitro*, but restrictions imposed by the coronavirus pandemic, mean there was not enough time to achieve meaningful results.

Finally, a miniature, flexible stimulation device was fabricated. This device consists of a battery powered circuit capable of generating a 30 V pulsed stimulation waveform, a novel magnetic connector to attach to a wound dressing and basic wound monitoring capabilities. The final device measured $50 \times 30 \times 10$ mm so can be worn under clothing and while performing other activities.

Contents

List of Figures

List of Additional Material

Dataset for chapter 4: http://doi.org/10.5258/SOTON/D2487.

Dataset for chapter 5: https://doi.org/10.5258/SOTON/D2487.

Dataset for section 6.3: https://doi.org/10.5258/SOTON/D2389.

Declaration of Authorship

I declare that this thesis and the work presented in it is my own and has been generated by me as the result of my own original research.

I confirm that:

1. This work was done wholly or mainly while in candidature for a research degree at this University;
2. Where any part of this thesis has previously been submitted for a degree or any other qualification at this University or any other institution, this has been clearly stated;
3. Where I have consulted the published work of others, this is always clearly attributed;
4. Where I have quoted from the work of others, the source is always given. With the exception of such quotations, this thesis is entirely my own work;
5. I have acknowledged all main sources of help;
6. Where the thesis is based on work done by myself jointly with others, I have made clear exactly what was done by others and what I have contributed myself;
7. Parts of this work have been published as: T. Greig, R. Torah, and K. Yang, "Electrical stimulation for wound healing: Opportunities for e-textiles," *IEEE Reviews in Biomedical Engineering*, pp. 1–14, 2022, doi: *10.1109/RBME.2022.3210598*; T. Greig, R. Torah, and K. Yang, "Investigation of Nozzle Height Control to Improve Dispenser Printing of E-Textiles," *Proceedings*, vol. 68, p. 6, Jan. 2021, doi: *10.3390/proceedings2021068006*; T. Greig, R. Torah, and K. Yang, "Investigation of the effects of ink pigmentation on substrate profiling for e-textile dispenser printing," in *2021 IEEE International Conference on Flexible and Printable Sensors and Systems (FLEPS)*, pp. 1–4, 2021, doi: *10.1109/FLEPS51544.2021.9469756*; T. Greig, K. Yang, and R. Torah, "Evaluation of a spring-finger based, magnetic connector concept for reliable e-textile interconnects," *IEEE Transactions on Components, Packaging and Manufacturing Technology*, vol. 12, no. 10, pp. 1723–1725, 2022, doi: *10.1109/TCPMT.2022.3209591*; T. Greig, K. Yang, and R. Torah, "Miniature flexible reprogrammable microcontroller circuits for e-textiles," *Engineering Proceedings*, vol. 30, no. 1, 2023, doi: *10.3390/engproc2023030015*; T. Greig, K. Yang, and R. Torah, "A comparative evaluation of equivalent circuit and finite element electrical skin modelling techniques," *Biomedical Engineering Express*, 2023, doi: *10.1088/2057-1976/acfb04*

Signed:..... Date:.....

Chapter 1

Introduction

1.1 Research Motivations

Wounds of all types are a significant problem for health systems, carrying a high chance of long term hospitalisation, occupying staff time, decreasing bed availability and increasing care costs. Wounds fall into several categories, the most notorious of which are traumatic wounds, those caused by a physical event. Traumatic wounds however are often the simplest to heal; as long as the wound has not significantly damaged any of the body's core functions, the natural process of wound healing should be able to proceed unimpeded.

Other categories of wounds include pressure ulcers and vascular ulcers, which can be much more difficult to heal. Pressure ulcers are caused when a prolonged pressure acting on soft tissue (usually between a bony prominence and a bed or chair) causes the tissue's blood supply to be reduced. This means that the tissue cannot receive oxygen and nutrients as it normally would and metabolic waste products cannot be taken away [7]. Similarly, vascular ulcers, often described as venous or arterial, are caused when a problem in the circulatory system impedes blood flow to a particular area, commonly exacerbated by diabetes [8]. These wounds can be more difficult to heal because the cause of the wound is hard to completely remove and will often hamper the healing process.

Ulceration is also a very common problem and therefore a significant target for assisted wound healing. Between 2015 and 2018, the NHS treated 33,155 cases of diabetic foot ulceration, though it is thought that at any one time, more than 64,000 people with diabetes in the UK have an ulcer [9]. Only 60% of these heal within 12 weeks [10]. Diabetic foot ulceration is also a common cause of amputations, leading to 7,000 each year in England. Having an ulcer also comes with a high chance of mortality for diabetic patients: only 60% survive for five years. The cost of diabetic foot care to the NHS was estimated at £1 billion in the year 2014-15 [9].

Typically, the treatment applied to a wound aims to create the best conditions in which the body can heal itself. Dressings may be applied to prevent further physical damage or blood loss, medications can be prescribed to rid the wound of infection, pressure redistribution equipment may be used to alleviate the cause of a pressure ulcer [11]. In many cases this is sufficient and the body can rebuild the damaged tissue in a timely manner. In other cases, particularly when the cause of the wound cannot be completely removed, the body is unable to repair itself and the wound becomes chronic.

One component that has been identified as being important to the wound healing process is the current of injury. This is a small, ionic current that starts flowing into the wound from the surrounding tissue when the skin is broken. It helps signal to cells that a wound has occurred and where that wound is. The cessation of this current, before the wound has healed, is strongly correlated with a wound becoming chronic [12].

By applying an external electric field to the wound, the cellular response to an injury can be increased even if the natural flow of current has broken down. Electrostimulation has shown promising results in several studies, in some cases doubling the weekly decrease in wound size, from 7 to 15% [13, 14]. However, there are still several problems that prevent the widespread adoption of electrostimulation therapy. The first is that there are numerous parameters that can be varied when defining an electrostimulation protocol: different studies have chosen various stimulating waveform shapes [13, 15], polarities [11, 15], durations of treatment [16, 15] and electrode locations [17, 15] meaning that it is hard to collate them into a cohesive body of evidence. Additionally, electrostimulation apparatus can be bulky and inconvenient to the patient.

The emerging field of e-textile technology provides an opportunity to develop electrodes that are much more ergonomic and potentially customised for a particular patient's wound. E-textiles are textiles that include some integrated electronic functionality. It is now possible to add several types of electronic device to textiles without compromising the fundamental textile properties of comfort and flexibility [18, 19, 20, 21, 22]. There are a variety of ways in which electrical connections can be fabricated on textiles, including weaving conductive threads into the fabric and printing them on the surface [23]. It is possible to add electrodes to a fabric using printing as well [24]. Dispenser printing in particular, wherein conductive pastes are deposited from a robotically actuated nozzle [22], is promising as it offers the ability to print on the varied surfaces that wound dressings present. The ability to print electronic circuits and electrodes onto textiles also means that it is possible to incorporate electrodes into existing wound dressings making electrostimulation more convenient.

E-textile technology also makes it possible to incorporate sensors into textile devices [18]. This is potentially useful in wound treatment, where maintaining the appropriate temperature, pressure and moisture levels are important [25], as it would allow these properties to be monitored without removing the dressing.

1.2 Objectives of this Research

This project first aims to develop a platform that can be used to fabricate electrodes on existing wound dressings using dispenser printing techniques. This will require work to ensure that the printer can produce electrodes on the varied surfaces that wound dressing present. These electrodes should be sufficiently reliable to function for as long as the dressing they are mounted on and should have a skin contact resistance low enough that they can effectively apply electrical stimulation to a wound.

To assess the ability of the printed electrodes to deliver current to the relevant parts of the skin, the project also aims to develop a model of the electrical behaviour of the skin. By creating models based on multiple techniques, for example equivalent circuit modelling and finite element simulation, the accuracy of the models can be evaluated.

The project also aims to evaluate the effect of using different stimulation waveforms, for example D.C, sinusoidal or pulsed current, on the cellular response.

Lastly, this project aims to produce a prototype e-textile device that could be attached to a wound dressing and provide an easy-to-use, unobtrusive means of delivering the stimulation voltage.

1.3 Statement of Novelty

The following novelties were the targeted outcomes from this project:

- The first use of laser displacement measurement for height control in dispenser printing. Along with optimisations of printing parameters (such as nozzle speed, clearance and pressure), this is used to facilitate the fabrication of electrodes directly onto wound dressing in a manner that can be adapted to an individual patient's wound.
- The comparison of two different techniques for electrical skin modelling gives new insights into what inaccuracies exist in the available data for the electrical properties of the skin.
- Miniaturisation of the circuitry required to provide wound healing electrical stimulation. E-textile techniques are used to construct a high voltage power source and controlling circuitry as a much smaller size and with more flexibility than previously achieved. This makes electrical stimulation treatment more comfortable and convenient for a patient.
- The development of new, e-textile compatible connectors, the first to use spring-finger contacts rather than the larger pogo-pins, allows the stimulation circuit to

be separated from the electrodes. This reduces waste when the dressing is changed while still allowing the stimulation circuity to be worn along with the dressing.

1.4 Thesis Structure

This thesis is divided into 7 chapters.

Following this introduction, chapter 2 provides a review of the literature, covering the basics of wound healing, the biological basis for electrostimulation as a wound healing treatment and a comprehensive review of relevant clinical trials. It also covers the developments within e-textiles that may be applied in this area.

Chapter 3 describes a system for dispenser printing flexible electrodes on to existing wound dressings, using a laser displacement meter to measure and account for the dressings' surface profile.

Chapter 4 describes the derivation of a simulation model representing the electrical properties of the skin and electrodes which was used in the design and testing of the stimulation circuitry.

Chapter 5 details the implementation of the model from chapter 4 to develop experiments and apparatus to investigate an electrotaxis cell migration assay to evaluate different stimulation waveforms.

Chapter 6 contains details of the device that was fabricated as an example of how e-textile technology could be used to produce an electrical stimulation system. It includes the miniature, high voltage stimulation circuit, a magnetic connector concept suitable for connecting the circuit to a dressing, and concludes with an investigation of the optimal way to integrate temperature sensing into the final proposed e-textile wound healing system.

Chapter 7 gives the conclusions from the thesis and a discussion of potential future work that remains in this area.

Additionally, appendix A describes a clip connector usable for programming small microcontroller circuits in e-textiles which was developed to aid in the integration of this e-textile system, but is applicable broadly in the research group for the development of e-textile demonstrators.

1.5 Publications Arising From This Thesis

- T. Greig, R. Torah, and K. Yang, "Electrical stimulation for wound healing: Opportunities for e-textiles," *IEEE Reviews in Biomedical Engineering*, pp. 1–14, 2022, doi: *10.1109/RBME.2022.3210598*
- T. Greig, R. Torah, and K. Yang, "Investigation of Nozzle Height Control to Improve Dispenser Printing of E-Textiles," *Proceedings*, vol. 68, p. 6, Jan. 2021, doi: *10.3390/proceedings2021068006*
- T. Greig, R. Torah, and K. Yang, "Investigation of the effects of ink pigmentation on substrate profiling for e-textile dispenser printing," in *2021 IEEE International Conference on Flexible and Printable Sensors and Systems (FLEPS)*, pp. 1–4, 2021, doi: *10.1109/FLEPS51544.2021.9469756*
- T. Greig, K. Yang, and R. Torah, "Evaluation of a spring-finger based, magnetic connector concept for reliable e-textile interconnects," *IEEE Transactions on Components, Packaging and Manufacturing Technology*, vol. 12, no. 10, pp. 1723–1725, 2022, doi: *10.1109/TCPMT.2022.3209591*
- T. Greig, K. Yang, and R. Torah, "Miniature flexible reprogrammable microcontroller circuits for e-textiles," *Engineering Proceedings*, vol. 30, no. 1, 2023, doi: *10.3390/engproc2023030015*
- T. Greig, K. Yang, and R. Torah, "A comparative evaluation of equivalent circuit and finite element electrical skin modelling techniques," *Biomedical Engineering Express*, 2023, doi: *10.1088/2057-1976/acfb04*

1.6 Impact of Coronavirus

The coronavirus pandemic prevented access to the biology laboratories for the majority of the project. This limited the time available for biological testing to the final six months. Because of these limitations, the focus of the bulk of the project shifted to concentrate on printing, connector design and integration. The time was also used to expand the literature review in chapter 2 into an independent paper.

1.7 Ethics Approval

The work in chapter 4 involved testing on human participants. This work was risk assessed and written consent was gathered. Data was processed in line with university and legal requirements. The study was approved by the University of Southampton's ethics process (study ID 64238).

Chapter 2

Literature Review

2.1 Introduction

The body naturally possesses the ability to heal most wounds. The purpose of medical treatment is to support this process: to ensure that the optimum temperature and moisture for healing are maintained and to prevent additional harm from occurring, either from physical damage or infection [25].

Once a wound has opened, the body first attempts to stop the loss of blood before rebuilding the lost or damaged tissue. While this is happening, a small ionic current develops, flowing into the wound. This current is one signal that indicates to cells that a wound has occurred and directs them towards the wound site. Blocking this current can cause a wound to become chronic. By amplifying and ensuring the continued presence of this current, electrical stimulation can make the process of wound healing more reliable.

This chapter gives an overview of the biological mechanisms involved in wound healing and how these are affected by the current of injury. It then discusses the various approaches that have been taken to model the electrical impedance of the skin and the experiments that have developed wound healing analogues *in vitro*. A comprehensive review of clinical trials is then given to identify the potential effectiveness of the treatment. Finally, they types of wound dressing currently available are listed and the e-textile technologies that may be used to integrate electrodes into them are discussed.

2.2 The Biology of Wound Healing

The natural process of wound healing is a complex system involving many types of cells and chemicals which all react to one another to produce a coordinated response. It is commonly divided into four chronological stages, though these stages will overlap and occur at different times in different parts of the wound.

2.2.1 Stage 1: Haemostasis

The purpose of this first stage is to prevent blood loss. It typically happens within a few minutes of a wound opening and is a job that primarily falls to platelets, a type of blood cell. When a blood vessel is broken, platelets detect and bind to collagen in the extra-cellular matrix (ECM), the structure that exists between cells and adds strength to a tissue. This binding causes platelets to change their morphology, allowing them to bind to other platelets and build up a clot [26].

Bound platelets also start releasing soluble mediators which initiate the coagulations cascade. Soluble mediators are chemicals, usually released by cells, that act as messengers to other cells or that form part of a chain of chemical reactions (a cascade). The coagulation cascade is a set of reactions that results in the protein fibrinogen being converted into another protein called fibrin. Fibrinogen is found on blood plasma and is also released by platelets, having been stored in their specific α granules, see figure 2.1. The fibrin generated by the cascade forms the bulk of the scab and is used as a temporary scaffold around which tissue can regrow. It is replaced later in the healing process by a permanent, stronger matrix made of the protein collagen [26].

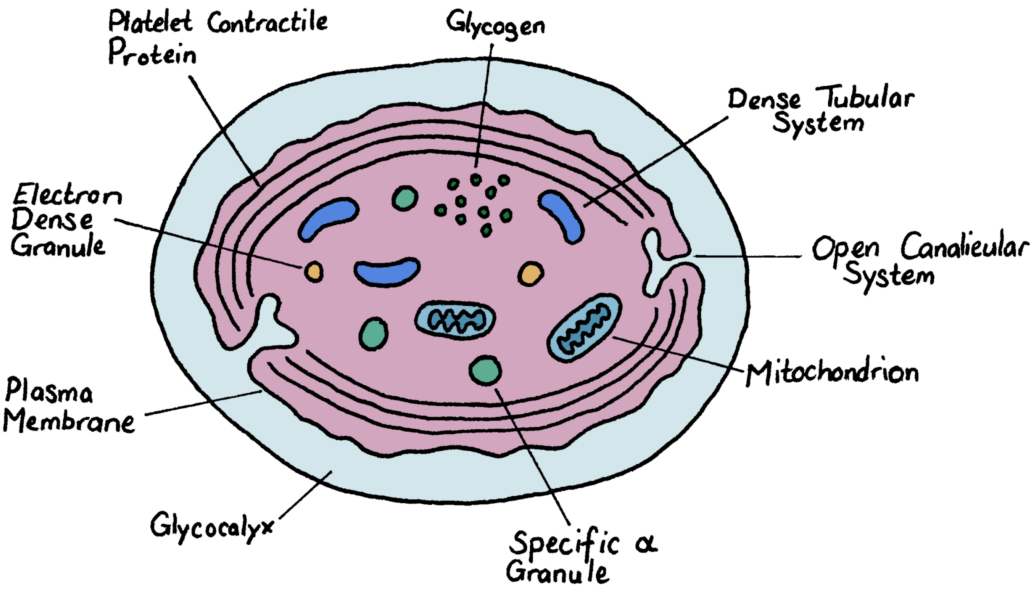

FIGURE 2.1: Structure of a platelet cell before it is activated. Once activated, it spreads out and extends pseudopodia to better aggregate with other platelets [26].

2.2.2 Stage 2: Inflammation

The purpose of the inflammation stage is to prevent or deal with infections. A break in the skin provides an ideal entry point for pathogens and the inflammation reaction

allows the body to swiftly kill any that do enter.

Inflammation is triggered by the release of inflammatory mediators, these include histamine, released by keratinocytes which make up the skin when it is broken, and some of the chemicals involved in the coagulation cascade [26, 27]. Several types of cells involved in the inflammation response also release inflammatory mediators when activated, creating a positive feedback loop [25].

The first effect of the inflammatory response is that blood vessels dilate and the endothelial cells that line them become less tightly packed and start expressing adhesion molecules. This allows cells to attach to the side of the blood vessel, stop themselves from flowing onward and move through the vessel wall into the wounded tissue [27]. The first cells to reach the wound site are neutrophils. Their job is to destroy pathogens and devitalised tissue via phagocytosis, engulfing a pathogen into a pocket called a phagosome where it is broken down by a variety of chemical mechanisms. Neutrophils are very short lived: even if activated, they die by apoptosis (preprogrammed cell death) within a few days [27, 28].

Once the neutrophils have been depleted, they are replaced by macrophages which carry on destroying pathogens and dead tissue. They also have the important task of cleaning up dead neutrophils; if the chemicals used by neutrophils to break down phagocytosed material are released into the extra-cellular environment, they can damage healthy cells and hinder wound healing [25]. Macrophages can also trigger the transition from the inflammatory stage to the proliferation stage through the release of more soluble mediators [25].

2.2.3 Stage 3: Proliferation

It is during the proliferation stage that the damaged tissue is actually replaced. It involves replacing damaged dermis with granulation tissue; angiogenesis, the process of regrowing blood vessels, and reepithelialisation [25].

Granulation tissue is mostly produced by fibroblasts. These cells migrate into the wound from the surrounding tissue when they detect the presence of mediators released by macrophages and platelets. They migrate by attaching themselves to the extra-cellular matrix and pulling themselves forward [25].

Once at the wound site, fibroblasts differentiate into myofibroblasts and start producing collagen to form the new ECM. As myofibroblasts, they also proliferate, though they can only do this a certain number of times before becoming senescent at which point their presence may become detrimental to healing [29].

Once the new ECM is in place, angiogenesis can begin. Angiogenesis is triggered by soluble mediators as well as environmental factors like oxygen and pH [25]. New branches

are formed when dividing epithelial cells in the wall of an existing blood vessel break through their basement membrane. When two of these branches meet, a new capillary is formed [25].

The last part of the proliferation stage is reepithelialisation; this is when damaged skin is replaced. Skin is made up of cells called keratinocytes which are divided into four layers, differentiated by their morphology, as shown in figure 2.2. Cells in the bottom layer, the *stratum basale*, are the only ones capable of proliferation. Normally, they divide to produce a new cell which steadily moves upwards, changing morphology as it goes, until it reaches the surface and is worn off. When reepithelialising however, basal keratinocytes change from their usual cuboidal shape, becoming flat and elongated and start moving out across the wound. They are propelled by their lamellipodia, these are processes extended out by the cell that grip onto the ECM and pull it forward. Once the basal keratinocytes completely cover the wound, they return to their original shape and start proliferating to build up the other layers [30].

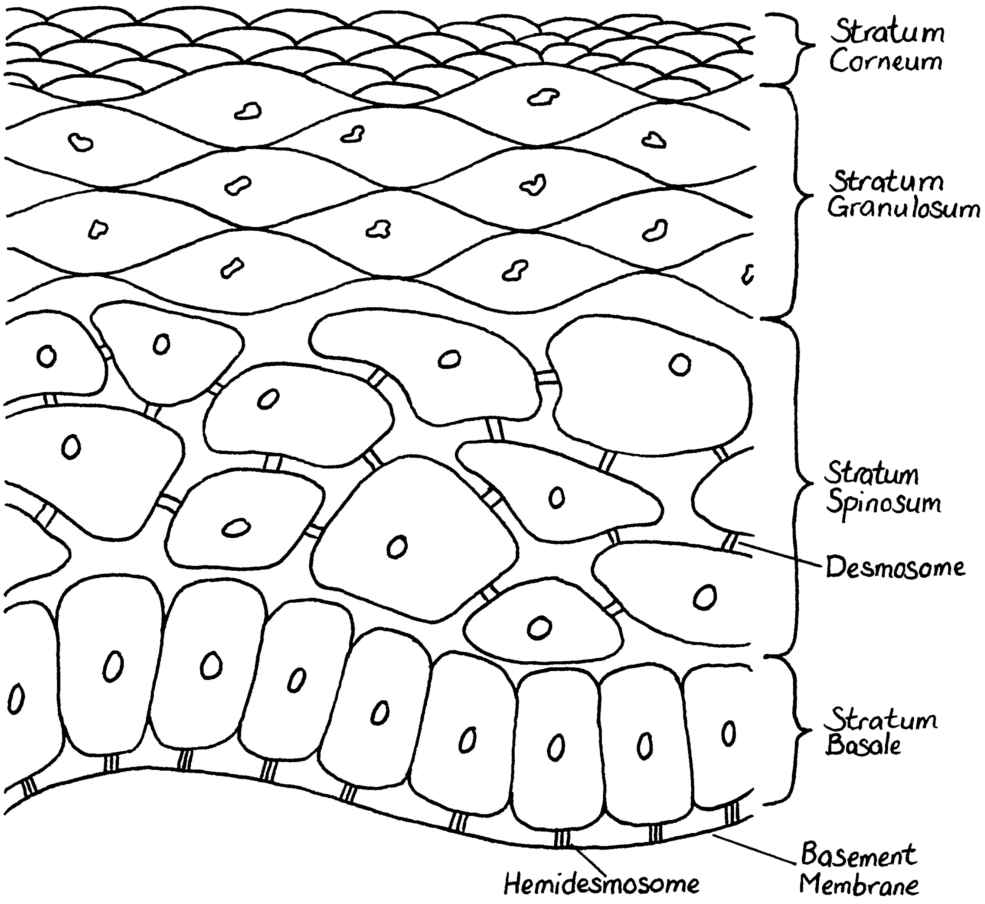

FIGURE 2.2: The layers of the epidermis. Cells in the *stratum basale* divide and then move upwards, changing morphology as they go from one layer to the next [30].

2.2.4 Stage 4: Remodelling

Because the earlier stages need to be completed as quickly as possible to restore the functionality of the tissue and the physical barrier of the skin, some stages are performed to a minimal functional standard. In particular, the extra-cellular matrix produced by the proliferative stage is laid down almost at random and has much less strength than that of healthy tissue. Over the course of a few months, the original type II collagen matrix is replaced with a more organised one made from type I collagen. This brings the tensile strength of the wound from about 25% of normal tissue up to around 80%. Repaired tissue never quite reaches 100% [29, 25]

2.2.5 Chronic Wounds

A wound will become chronic if anything prevents it from moving through these four stages. Most commonly, this occurs when a wound gets stuck in the inflammatory phase, for example, because of a prolonged infection. Neutrophils and macrophages contain proteases which they use to break down phagocytosed material. Upon their death, these enzymes are released and can begin to break down healthy cells. Additionally, macrophages destroy devitalised tissue using elastase and collagenase enzymes which can also break down newly grown granulation tissue. As such, allowing too many of these cells to accumulate will hinder the healing of the wound [29, 25].

Another potential cause of delayed wound healing is physical damage to delicate, newly grown tissue. Should new capillaries be broken for example, the whole process of wound healing can start again from the haemostasis stage [29, 25].

2.3 Electrical Currents in Wound Healing

2.3.1 Natural Current of Injury

During wound healing, a current naturally occurs, flowing into the wound from the surrounding tissue. This arises because of the potential differences that exist across the skin being short circuited by conducting fluids such as blood and wound exudate [12].

A potential difference across the skin is generated by moving sodium, potassium and chlorine ions through the cells of the epidermis. Most cells predominantly move negative ions (Cl^-) towards the surface and positive ions (Na^+ and K^+) away from the surface [31]. On average the surface of the skin is 23 mV lower than the dermis, though this varies between different parts of the body: the hands and feet can be 35 mV lower while the difference on the head and upper arms is only 15mV [32].

When the epidermis is broken, a conducting path can form between the dermis and the surface of the skin, as shown in figure 2.3. Here the current does not consist of free electrons, as in a metallic conductor, but the same charged ions that were moved to form the potential difference in the first place.

How the properties of this current are affected by the depth of the wound has not been thoroughly studied, though it is known that the dermis is more conductive than the fat or muscle that lies below it [33], meaning that the returning current will likely be concentrated in the dermis, regardless of the wound's depth.

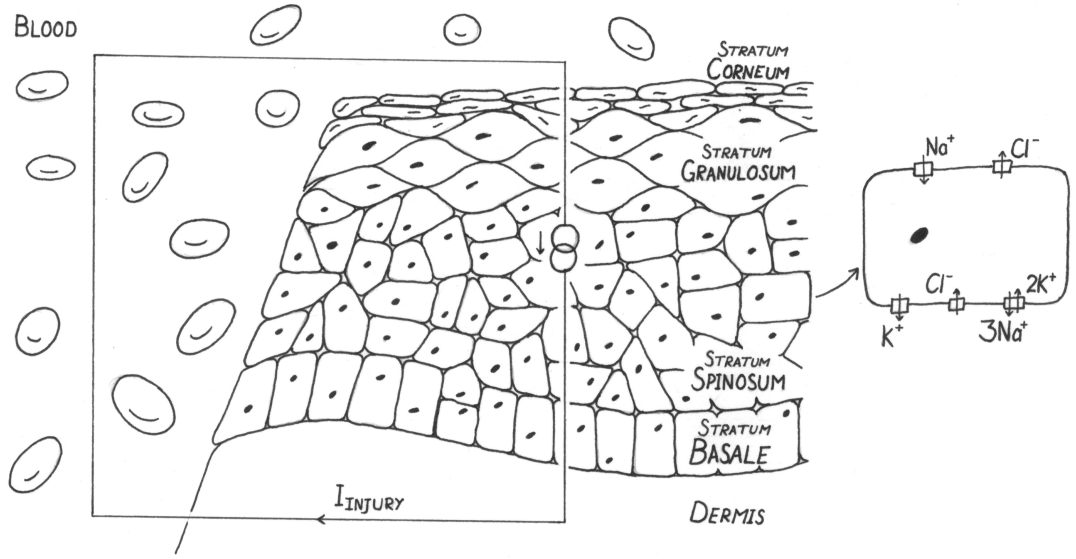

FIGURE 2.3: The structure of the skin and source of wound current. Cells in the *stratum basale* proliferate and move outwards, changing morphology as they go from one layer to the next [30]. These cells move charged ions through themselves, providing a current source. The circuit is completed when a conducting fluid, e.g. blood or wound exudate, connects the surface of the skin with the dermis [30, 31].

2.3.2 Responses to Current

Many different types of cell have been shown to migrate directionally in an electric field, through a process called electrotaxis [31]. Of the cells involved in the inflammatory phase, lymphocytes [34], monocytes and neutrophils [35] have been shown to migrate cathodically meaning they are directed towards the centre of the wound. Macrophages have been recorded migrating perpendicularly to an oscillating electric field [36] and granulocytes have been shown to migrate towards the anode in a constant field [37]. Several studies have examined how fibroblasts behave in an electric field and most record them travelling cathodically [38, 39, 40, 41, 42], but they have also been recorded moving towards the anode [43]. Keratinocytes also migrate towards the cathode [44].

There are a variety of mechanisms through which this migration may occur. The first is that charged proteins on the cells' surface will accumulate on one side or the other when

exposed to an electric field. Integrins, the proteins used by cells to bind to the ECM, are negatively charged in the region outside the cell and so accumulate cathodically when an electric field is applied [31]. Keratinocytes have been shown to cease their electric field induced migration when missing proteins involved in the functioning of integrins [45]. The same mechanism applies to the receptor proteins used to detect soluble mediators. Epidermal growth factor is a mediator the encourages keratinocytes to proliferate and to move across the wound [25]. The proteins that detect epidermal growth factor are negatively charged and accumulate on the cathodic side of their cells within 10 minutes of an electric field being applied [31].

It is also thought that electric current can inhibit the growth of bacteria [12]. Several clinical trials reported that electrical stimulation treatment helped to heal infections and that rates of infection were higher in control group patients than those receiving stimulation [15, 46]. However, it is hard to determine exactly how this inhibition takes place given the complex systems involved and the number of mechanisms the stimulation could be utilising.

One potential reason for the lower incidence of infection is that electrical stimulation is simply aiding the body's own immune system. As stated above, monocytes and neutrophils are attracted to the cathode in an electric field [35]. Thus, cathodic stimulation will cause a greater number of them to reach the wound site and make it more likely that an infection is quickly eradicated.

While this is certainly one way in which electric fields can affect bacteria, it cannot be the only one. This is because several *in vitro* studies have also demonstrated the antibacterial effect of electric current. The first of these was done by Rowley in 1952. He placed E. coli from a colony in its logarithmic growth phase into a liquid growth medium and applied DC or AC of varying frequencies in the range of 0.2 - 140 mA. AC had very little effect, but DC had a significant impact on the growth rate of the bacteria. Also having a large effect was how close the bacteria were able to get to the electrodes themselves. This was because the area around the electrodes had a significant change in pH due to electrolysis effects. With filters keeping the bacteria away from the electrodes and at a constant pH, 140 mA of DC increased intergeneration time - the time between a cell dividing and its daughter cells dividing - by 14.5%. Without filters, the intergeneration time was increased by 38.8%. The electrodes used in this study were made of platinum - iridium which is particularly resistant to leaching into the growth medium and so will not have had a direct effect on the bacteria [47].

Later Spadaro et al. performed a similar test using four different types of bacteria: staphylococcus aureus, escherichia coli, pseudomonas ærugionsa and proteus vulgaris; and five types of electrode: platinum, stainless-steel, gold, copper and silver. It was found that silver had a large bacteriostatic effect (it prevented the growth of bacteria, but did not kill them) even at very low currents (0.4 µA) where no change in pH was

caused. With larger currents (40 & 400 µA), the other electrodes started to have an effect, though when applying currents this strong, large changes in pH were caused [48]. This implies that the antibacterial effect of electrical stimulation is not a direct result of the current or electric field, but more a result of silver's antibacterial properties or the environmental changes the currents caused.

These two studies show that electrical stimulation is able to inhibit bacterial growth, but imply that this is achieved by inducing a pH change in the environment. This makes the results hard to apply to practical wound healing, where pHs must be controlled to prevent damage to surrounding tissue.

2.4 Electrical Modelling of the Skin

When studying electrical stimulation as a wound healing treatment, it is essential to understand the electrical properties of the different skin layers. Without this, it is impossible to know where an induced current will be flowing or what magnitude of electric field will be present in the different regions of the skin.

Relying on physical measurements alone, it is difficult to gain this understanding: doing so would require the insertion of needle electrodes into a test subject which can be painful and only gives data about a few specific points. For systems that are this hard to observe, mathematical models and simulations are a crucial way of developing a more complete understanding. Unlike physical measurements, they can provide detailed information about any point within their scope and can be used to rapidly evaluate stimulation systems without the need for physical fabrication or testing.

The weakness of modelling is that results can be less accurate than those from a physical experiment. A model will never perfectly match the real equivalent, particularly in a system as complex and variable as biological tissue.

There are two main approaches available for modelling electrical behaviour: the first is using an equivalent circuit model, wherein the different parts of a system are represented with combinations of resistors, capacitors and inductors which provide an equivalent impedance [49]. The second is to use a tool such as finite element analysis to simulate a full, three dimensional model of the system, built using the dimensions and material properties of its components.

2.4.1 Equivalent Circuit Modelling

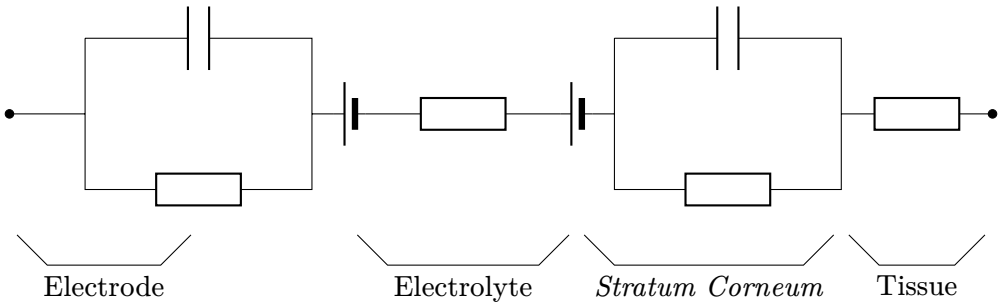

FIGURE 2.4: Neuman's equivalent circuit model of a skin – electrode system including the external electrode, electrolyte, epidermis and underlying tissue [50].

An equivalent circuit model that has been widely used in the field of biopotential monitoring [49, 51, 52] was derived in 1989 by Kaczmarek and Webster [53] before being further developed and matched to the physiology of the skin by Neuman [50]. This model is shown in figure 2.4. Kaczmarek and Webster's equivalent circuit consisted of a second order filter of two, parallel resistor – capacitor networks, plus an additional series resistance.

The first of these RC pairs was attributed by Neuman to the interface between the electrode and the electrolyte (either sweat or an applied gel interface). This is a result of the double layer capacitance effect that occurs at the boundary between ionic and electronic conductors. (This capacitance forms because the electronic conductor generally holds and excess charge near its surface. This is balanced out by a complementary change of the ion distribution in the electrolyte. These two layers of opposite charge, separated by an atomic scale distance, produce a large capacitance [54].) The parallel resistor represents the leakage current across the electrode – electrolyte boundary [50].

The second RC pair is attributed to the *stratum corneum*, the thin, poorly conducting, upper layer of the skin. The electrolyte itself and the deeper layer of tissue are considered to be purely resistive.

Neuman also adds two potentials to the circuit, represented by the cells in figure 2.4, one caused by the half-cell between the electrode and the electrolyte, and the other caused by the difference in ion concentrations across the *stratum corneum* [50].

This model was developed for biopotential monitoring (for example ECG or EMG measurement) where the voltage source exists within the body itself and has to be conducted to an electrode where it can be measured. It could however be adapted to the electrical stimulation case by duplicating the electrode, electrolyte and epidermis sections to represent the returning current path.

A limitation of this model is the presumption that the *stratum corneum* and electrode – electrolyte interface present pure, frequency independent capacitances. Factors including the inhomogeneity of tissues and the polar nature of water molecules mean that is not the case. There are several ways of accounting for this which are discussed in section 2.4.3, below.

This type of model has been used to investigate the effects of electrode material [52] and to show that the interface impedance decreases as more pressure is applied [51]. Its simplicity means that all the parameters can be derived from physical measurements.

2.4.2 Finite-Element Simulation Modelling

A drawback of equivalent circuit models, it that they are specific to a particular geometry. If the size of the electrodes, or the thickness of a skin layer changes, the entire model must be reconstructed. Finite-element models solve this issue by specifying the geometry of a system separately from the other properties. They work by dividing a model into many small elements, then solving the relevant equations within each one using numerical methods.

When constructing a finite-element simulation model of the skin, the model will generally be divided into a number of sections, corresponding to the different skin layers, each parametrised by their geometry and electrical properties. The accuracy of the model is largely dependent on how accurately these properties are known.

The geometric properties of the skin are well documented as they can be measured easily using microscopy techniques [55, 56]. When developing a model, it is important to use skin thickness data appropriate for the part of the body being considered as skin in certain regions, particularly the hands and feet, is much thicker than elsewhere on the body, but the data necessary to do this is also widely available [55].

A much greater challenge is identifying the electrical properties of the various skin layers. Because of how thin the upper layers of the skin are ($>100\,\mu m$), it is difficult to isolate a sample that can be used for impedance measurement [57]. For deeper tissue layers that are somewhat thicker, or in studies where the skin layers are lumped together, this is less of an issue [58].

One early study measuring the impedance of *stratum corneum*, Yamamoto and Yamamoto, 1976, circumvented this issue by measuring the impedance between two electrodes before and after stripping away the *stratum corneum* using tape and then calculating the difference. This was only possible because the *stratum corneum* is the outermost layer of the skin and it can be removed without significant harm to the patient [59].

A different method of measuring tissue impedance that doesn't require isolating the individual layers is using an open-ended coaxial probe butted against the skin [60, 61].

The coaxial line is pressed against the skin and the S_{11} reflection coefficient is measured using a network analyser [62]. From this, the permittivity and conductivity of the reflecting material can be derived. The depth into the sample that the electric field penetrates can be controlled by varying the inner and outer diameters of the coaxial probe [63]. This technique is effective for measuring the skin impedance at radio frequencies, it's development driven by the need to understand how wireless communication signals interact with the body [64, 61, 65, 66]. Because of this, there are no published results from this method below 1 kHz which would not be relevant to wireless networks. This limits its applicability to wound healing stimulation which primarily uses frequencies from D.C. to 1 kHz [67].

2.4.3 Modelling Dispersion Characteristics

One of the complexities that must be considered when modelling biological tissues is the propensity for materials' properties to change with frequency. Because tissue is non-homogeneous and because it contains polarised dissolved molecules, its permittivity, and thus capacitance, will change at different frequencies.

These are referred to as dispersion effects. There are three main dispersion mechanisms that are present in biological tissue, labelled α, β and γ which occur at around 10^2, 10^6 and 10^{11} Hz respectively [68]. The γ dispersion effect is caused by the polar properties of water [68]. The β dispersion effect it thought to be a result of the structure of cells: at low frequencies, cell membranes present a significant impedance to conducting ions, whereas at high frequencies, the cell membrane can be capacitively bypassed, decreasing the relative permittivity of the tissue [68]. The cause of the α dispersion is not yet known. It has been shown to disappear within a few hours of death [69] and it has been suggested that it is also a result of cellular structure but though a different mechanism than the β dispersion [70].

There are a number of ways of representing dispersion effects mathematically, allowing them to be incorporated into both equivalent circuit and finite element models. The most accurate method is shown in equation 2.1.

$$\epsilon^*(\omega) = \epsilon_\infty + \sum_n \frac{\Delta\epsilon_n}{1 + (\mathrm{j}\omega\tau_n)^{(1-\alpha_n)}} + \frac{\sigma_i}{\mathrm{j}\omega\epsilon_0} \tag{2.1}$$

This equation calculates complex permittivity, a value that contains both permittivity and conductivity according to equation 2.2.

$$\epsilon^*(\omega) = \epsilon_r - \frac{\mathrm{j}\sigma}{\omega\epsilon_0} \tag{2.2}$$

Here, ϵ_∞ is the permittivity at infinite frequency and σ_i represents the intrinsic conductivity of the material. The summed term in between them, referred to as the Cole-Cole term, is used to represent each dispersion effect, parametrised by $\Delta\epsilon_n$, the change in permittivity caused by that effect, τ_n, the inverse of the frequency at which it occurs, and α_n, a parameter which encodes the frequency range over which the dispersion effect takes place [71].

A simpler representation, which approximates the effects of a single dispersion mechanism on the effective value of a capacitor, is to change the capacitor's impedance from $(j\omega C)^{-1}$ to $(j\omega C)^{\alpha-1}$ where α has a value between 0 and 1 [72]. This representation is particularly useful in equivalent circuit models.

(The α terms in these equations have no relation to the α dispersion effect specifically.)

2.4.4 Conclusions

Models are a vital tool for understanding the electrical properties of complex systems such as biological tissue.

Equivalent circuit models have the advantage of greater simplicity; having fewer parameters means that their values can be derived from physical measurements [52, 49]. However, equivalent circuit models are less detailed; they provide no information about the flow of current within a tissue layer, only what the electrical potential is on either side. They are also harder to generalise: the circuit model for an electrode on a 1 cm diameter wound cannot easily be converted into a model for an electrode on a 2 cm diameter wound, for example.

3D finite element simulation models solve this problem by specifying the geometry separately from the material properties. These added degrees of freedom come with the drawback of making the model more challenging to derive.

Accurate models of the skin are very useful for the development of electrical stimulation protocols. They allow stimulation devices to be tested without the need for patients, or long term trials. Modelling is also necessary when conducting *in vitro* experiments to ensure that the currents and electric fields being used match what cells would be exposed to *in vivo*.

2.5 Electrotaxis

Electrotaxis, sometimes referred to as galvanotaxis, is a phenomenon observed in some cells that causes them to move when in the presence of an electric field. Directed

cellular migration is one of the most important effects of the natural current of injury, and therefore of any external electrical stimulation treatment [12].

2.5.1 Experimental Methodologies for Investigating Electrotaxis

The majority of experiments on electrotaxis are conducted on a glass substrate, whether in a Petri-dish [73, 74]; a custom-made chamber [38, 75] or, in some cases, a simple trough built from a stack of cover slips [40, 43]. A typical experimental setup is shown in figure 2.5.

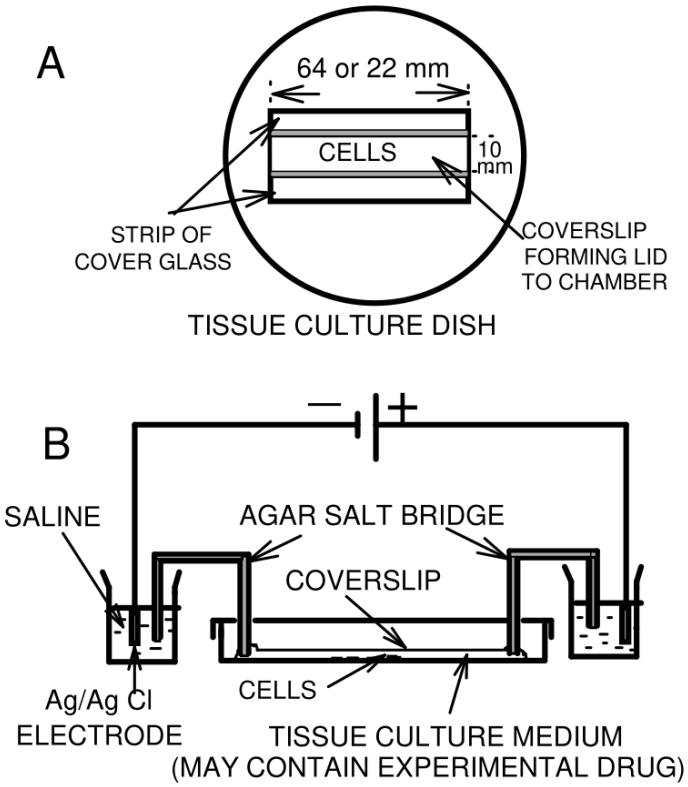

FIGURE 2.5: Experimental setup used by Zhao et al. 1996. Similar apparatus is used in most other electrotaxis studies. Image taken from [73].

Most studies chose to supply the electric field through metallic electrodes placed in a reservoir of saline solution that is connected to the electrotaxis chamber by bridges of saline solution with 2% agar [73, 38, 41, 43, 74, 75, 76, 77, 78, 79, 80]. These bridges are at least 10 cm long and connected to the medium the cells are in. This means that any chemicals released from the electrodes or produced by electrolysis cannot reach the cells [43].

In most cases, the cell culture being studied is placed on a glass cover-slip which was then placed in, or formed part of the electrotaxis chamber. Some studies [44, 77, 75] coated their glass slips with collagen, a major component of the extra-cellular matrix;

this makes the experiment more closely resemble *in vivo* conditions. Doing so did not otherwise affect the experimental setup or method, however Sheridan et al [44] showed that human keratinocytes will migrate approximately three times further on a substrate of type I collagen than on plastic. The substrate had no effect on the directionality of the migration however.

A variation on this standard setup was used by Moarefian et al. [81] who built a microfluidic enclosure, a few millimetres across, with a central chamber for the cells connected to four additional chambers on the sides. These could be used to insert additional chemicals creating a chemical gradient, or to connect steel electrodes to apply an electric field. From a cell's perspective though, this produces the same environment, just on a smaller scale.

Since around 2000, the most common medium for electrotaxis experiments has been Dulbecco's modified Eagle's medium (DMEM), usually with 10% foetal bovine serum (FBS) added. This creates an environment where the cells have all the nutrients they need to survive and proliferate. No work in the literature has so far investigated whether the differing electrical characteristics of this media mean that the effects of an electric field applied in one of these assays would be different from that in the body.

One study that did not follow the standard setup was Bullock et al. 2007 [82]. They constructed a full model of a skin wound by growing human epithelial cells in a ring shape on top of deepithelialised dermis. They then applied stimulation in various ways and compared the rate at which the hole in the centre closed. The stimulation method in this study was wireless, using an alternating current (AC) excited coil placed under the culture dish. Therefore, this study offers no indication as to whether such a model is suitable for testing printed electrodes.

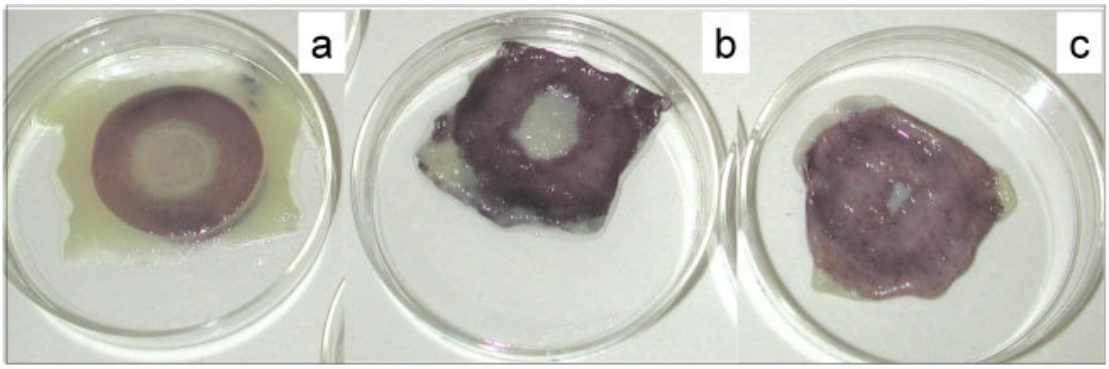

FIGURE 2.6: Wound model from Bullock et al. 2007 after 0, 7, and 13 days (a, b and c respectively) of being cultured at an air liquid interface. Image taken from [82].

2.5.2 Discussion of Electrotaxis Results

All studies reviewed managed to record electrotaxis occurring in their cell samples, thought the voltage at which this occurred varied significantly between cell types and between studies. The study that found an effect with the weakest electric field was by Nuccitelli and Smart in 1989 and was testing on embryonic neural crest cells from quails [76]. They managed to record cathodic migration at only 10 mV/mm. The majority of studies observed electrotaxis beginning at a few hundred mV/mm. This lines up well with the field strength observed in wounds which is between 100 and 200 mV/mm [31].

The majority of cells were recorded migrating towards the cathode; this equates to moving towards the centre of the wound. Notably, one study recorded fibroblasts from rabbits moving towards the anode [43], however several more recent studies recorded them moving cathodically [39, 40, 41].

2.5.3 Electrotaxis Conclusions

The conventional apparatus and configuration of electrotaxis experiments provides a reliable method of finding how cells will respond to a known electric field. The ability to change the substrate on which the cells are placed allows the environment, from a single cell's perspective, to be very similar to *in vivo* conditions.

However, to be able to observe and track cells during an experiment, electrotaxis chambers need to be made from transparent materials. This means that it is difficult to observe the effects of electric fields on cells in an environment that physically resembles human tissue and that the electric field produced by an electrostimulation device could not be directly tested this way. Instead, the electric field produced in the tissue by such a device would need to be measured or calculated beforehand, then artificially reproduced in an electrotaxis chamber.

One other way in which electrotaxis experiments could be useful in the development of electrostimulation devices is testing the cellular response to different waveforms. There have been studies conducted with biphasic waveforms [82] and pulsed electric fields [74], the latter successfully inducing directional migration. One study, Tsai et al. 2012 [41], tested various waveforms including high voltage pulsed current, finding it ineffective. However, no attention was given to the electrical differences between their electrotaxis chamber and human tissue. This means that there is no guarantee that the electric field the cells in the experiment were exposed to was the same as they would experience *in vivo*.

2.6 The Effectiveness of Electrical Stimulation for Wound Healing

The first true research into the effects of electricity on wound healing came in the 1960s after it was found that applying conductive gold leaf to ischaemic skin ulcers significantly improved their ability to heal [83, 84], though this was first noted in 1668 by Sir Kenelm Digby in his *Choice and experimented receipts in physick and chirurgery* where it was described as a 'most certain remedy for all Scars of the Small-pox' [85].

Reviewed below are the studies the tested an active electrostimulation treatment, observing its effects on wound healing in human patients. They were identified by searching the PubMed database and EBSCO MEDLINE with the query 'wound AND heal* AND electr* AND stimulation'. Each paper also had its references and, where available, papers that cited it, checked for other studies that fit the criteria.

2.6.1 Low Intensity Direct Current

The first type of active stimulation investigated is known as low intensity direct current (LIDC). It typically involves currents of under 1 mA delivered either continuously or as a low frequency square wave with an on-period of at least one second [67].

The first study to investigate LIDC was by Wolcott et al. in 1969 [15]. Patients with ischaemic skin ulcers were treated with a constant DC current between 400 and 800 µA. Current was applied in sessions lasting two hours, three times a day. For the first three days, the electrode on the wound itself was negative with the positive electrode 15 cm proximal to the wound. The polarities were then reversed the next two times that healing 'plateaued' (usually two to three weeks later, then another week after that). From then on, the polarities were reversed daily. Of the 75 ulcers treated during the 18 month study, most of which had not responded to their previous treatment, 31 healed completely. Eight patients had two or more ulcers and so were able to serve as their own controls. Among these patients, the average weekly wound size decrease was over five times higher in the treated wounds than the controls.

The reason for the polarity switching, explained in a later paper by the same authors [86], was that negative stimulation appeared to have an antibacterial effect but hindered wound healing, while positive stimulation aided both healing and bacterial growth. Despite providing no evidence for this nor giving a precise definition of a healing plateau, several further studies used polarity reversing schemes inspired by this one.

The first of these was conducted in 1976 using an identical methodology but only reversing the polarity after the first plateau. Here 48 out of 100 total ulcers healed completely

and in the six patients with control ulcers, the mean weekly healing rate was twice as high in wound treated with electrostimulation [16].

In 1985 the same stimulation was tested again, this time using three days of negative stimulation following each plateau and positive the rest of the time. This study used 15 pairs of subjects, matched by age, wound type, wound size and wound location, one of whom received simulation, the other only standard wound care [87]. The treatment lasted for five weeks. The average wound volumes in the two groups were similar at the start of the study, but by the third week, the treatment group's wounds were, on average, less than a quarter of the volume of the control group's.

Despite the poorly defined methodology, these three studies' overwhelmingly positive results imply that the potential benefits of electrostimulation treatment are very large, but the lack of rigour and consistency make it hard to identify the principal driver of these results.

In 1987, Katelaris et al. [88] tested LIDC stimulation combined with dressings soaked in saline solution or povidone-iodine. They used a stimulator that provided 20 µA of current with the cathode over the wound. They were unable to find any evidence that electrical stimulation sped up the healing of venous ulcers. In fact, it was found that electrical stimulation combined with povidone-iodine significantly slowed healing. A possible cause of this is that the negative electrode over the wound would repel the negatively charged iodine molecules, causing them to penetrate deeper into the tissue instead of killing bacteria on the surface as they were meant to [89]. These results show that, while electrostimulation may be generally helpful, care must be taken when considering the materials used alongside it to ensure that there are no detrimental side-effects.

In the same year, Fakhri and Amin investigated the effects of LIDC on chronic burn wounds. Their treatment consisted of 25 mA of current applied on either side of the wound for 10 minutes, twice a week. In all of their 20 patients except one with anaemia, reepithelialisation began within three days and the wounds completely healed within three months. In addition to this, several patients, on whom skin grafts had previously been attempted, had them succeed when retried after electrical stimulation [17].

These studies show that the potential benefits of electrostimulation are substantial, but offer little information about what the best polarity is. The earlier studies get positive results by alternating the orientation of their electrodes, though offer nothing to compare that against and no evidence for why that method was chosen. Meanwhile Fakhri and Amin shows that having current flow across the wound, rather than into or out of it, can also result in a substantial benefit to patients. A complicating factor is that prolonged exposure to DC currents, even below 1 mA, can cause the tissue under the cathode to become alkaline and under the anode, acidic. This can cause irritation and create a

sub-optimal environment for the cellular processes necessary to facilitate wound healing [67, 90]. As a result, LIDC is rarely used in modern settings.

2.6.2 Pulsed Current

An alternative to continuous DC that alleviates some of its problems is pulsed current. Pulsed current usually takes the form a square wave that is on for less than 1 ms and has a small duty cycle, typically less than 5%. This stops it from causing the pH changes and irritation that occurs with continuous current while still being a polar signal [67].

The first studies investigating pulsed current for stimulation were done to test wound healing stimulators made by Staodynamics Inc.: the Dermapule [13] and Vara/Pulse [91]. Both stimulators could be configured to provide a square wave with an amplitude of 35 mA and a frequency of 64 or 128 Hz. Regardless of frequency, the output had an on period of around 140 µs. In both cases the stimulation was applied in 30 minute sessions, twice a day for four weeks. Initially, the electrode over the wound was negative and the frequency set to 128 Hz. This was maintained until the wound cleared itself of necrotic tissue (debrided itself). After that, the polarity was switched every three days. Once a wound reached stage III (descending into subcutaneous tissue, but not muscle), the frequency was reduced to 64 Hz and the polarity was reversed daily. In both studies, the healing rate was twice as high in the stimulation group than in the control group.

The Dermapulse device was tested again over a period between 1997 and 2006 by Jünger et al. using a similar protocol to the original studies, except the stimulation was repeatedly cycled between 7 days of negative and 3 days of positive. At the end of the four month study, it was again found that stimulated wounds shrank at over twice the rate of the controls, backing up the previous tests. Significant improvements were also found in reported pain, transcutaneous oxygen partial pressure (a measure of oxygen levels in a tissue) and capillary density [92].

In 1993, Wood et al. tested a device that applied 300 - 600 µA of current at frequencies below 1 Hz [93]. In their study, the electrodes were placed on either side of the wound, on healthy skin. After eight weeks of treatment, with one session (of unspecified length) every other day, the treatment group's ulcers had healed by about 80% on average and those from the control group had mostly deteriorated.

In 2001, Adegoke and Badmos tested an electrostimulation device that provided pulsed current with a duty cycle of one third and a frequency of 30Hz. They gave spinal cord injury patients with stage IV ulcers 45 minutes of stimulation each session just below the minimum perceptible intensity. While their treated patients showed much better results than the controls, there were only three patients in each group and within groups, there was a lot of variation, reducing the result's significance [94].

One other study, published in 1996 by Baker et al, used stimulation protocols that could be considered pulsed current. Here, three different stimulating waveforms were tested. The first consisted of a positive pulse of a high intensity followed by a longer negative pulse of a lower magnitude, such that the total charge transferred in each direction was equal, as shown in figure 2.7a. The second waveform, figure 2.7b, was the same except that the negative pulse was of the same duration as the positive one (but still had a lower amplitude). The final waveform was similar to the second but scaled to have a lower amplitude overall: 4mA for the positive pulse, the first two waveforms having their amplitudes set just below the motor threshold, figure 2.7c.

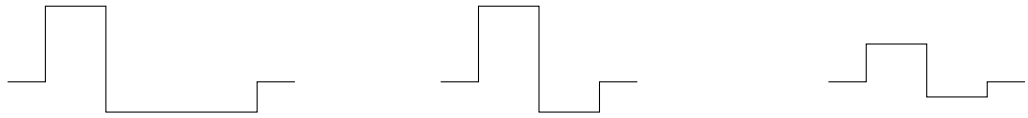

(A) (B) (C)

FIGURE 2.7: Stimulation waveforms used in Baker et al. 1996 [95].

No statistically significant difference was found between the healing rates of the three different groups, or the control group when all patients in the groups were analysed together. When just the patients that completely healed during their treatment were analysed, the balanced waveform appeared slightly better than the unbalanced and significantly ($p < 0.05$) better than the lower amplitude or controls [95]. The applicability of this result is limited however, not just by the complicated method required to obtain a significant result, but also by the fact that both the electrodes were placed on intact skin on either side of the wound, when compared to the more common configuration of one on intact skin and the other directly on the wound. As such, this study does not provide any clarity on what the effects of charge flowing into or out of the wound are.

2.6.3 High Voltage Pulsed Current

A sub-type of pulsed current that has become one of the most widely studied waveforms is high voltage pulsed current (HVPC). This furthers the principal of using more current for less time, applying voltages of up to 200V but only for a few microseconds and with a duty cycle under 1% [67].

An early study using HVPC was done by Kloth and Feedar in 1988. They applied HVPC to nine patients with stage IV ulcers and compared the results to seven controls. Their stimulation waveform had two peaks, 50 µs apart repeated at 105 Hz as shown in figure 2.8. The intensity of the peaks was set just below the motor threshold (the current intensity that induces involuntary muscle movement). This was at an amplitude between 100 and 175 V. After 16 weeks of treatment (45 minutes, 5 days a week) all the treated patients had healed completely, while most of the control group's wounds had deteriorated [96].

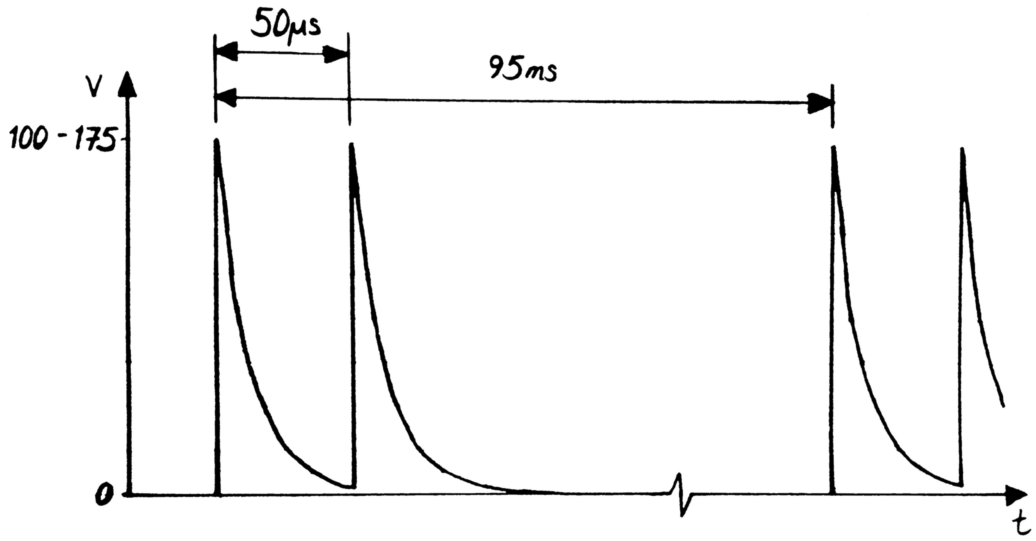

FIGURE 2.8: HVPC stimulating waveform used by Kloth and Feedar. The waveform consists of two peaks, 50 µs apart, repeated 105 times a second [96]. This format is used by all studies investigating HVPC, though the exact timings and amplitudes vary.

Kloth and Feedar did not give the rationale for using specifically a double peaked, exponential waveform. Nonetheless, the shape has become a standard for HVPC studies; while the exact voltages and timings vary, most studies keep to a waveform of two exponential peaks.

In 1991, Griffin et al. studied the effects of HVPC on pelvic ulcers in patients with spinal cord injuries. Using twin peaked pulses of 200 V, 100 Hz and 75 µs per pulse, they found that patients receiving the treatment had their wounds' size decrease by significantly more than the control's on days 5, 10 and 20 of the 20 day trial [97].

Further, similar studies tested HVPC on leg ulcers [98], diabetic vascular ulcers [14] and pressure ulcers [99, 100], all of which recorded positive results, showing that HVPC's effectiveness is not contingent on the etiology of the wound. These studies used between 50 minutes and 2 hours of stimulation per day and in the case of leg ulcers, achieved better results with electrostimulation than with topical medicine or compression therapy [98].

In 2001, Peters et al. tested HVPC's effect on diabetic foot ulcers by having patients wear a Dacron-mesh silver stocking which delivered 50 V stimulation for 20 minutes each hour. It was found that patients that had the real stocking were much more likely to heal that those using a placebo. Though in both groups, those who used the stocking for more than 20 hours a week were more likely to heal than those who used it for less than 20 hours [101]. This indicates that some flexibility is available in how the stimulation is delivered. However, because no further details about how the current was transferred to the wound were provided, no specific lessons can be drawn.

In 2016, Zhou et al. tested HVPC in conjunction with a silver collagen dressing on 10 patients. They recorded a significant decrease in wound size, though there were no controls to compare against. Additionally, several adverse events occurred during the study including one wound becoming infected (which silver dressings are designed to prevent) and one patient noticing an increased foul odour after using the dressing [102].

In 2017, the effects of changing polarity were tested by Polak et al. Their study ran for six weeks with one group of patients receiving a typical cathodic HVPC treatment the whole time while the other group received cathodic stimulation for only the first week before switching to anodic stimulation. The results showed that the cathodic treatment was slightly superior, though the difference was not statistically significant. Both polarities resulted in at least twice the healing rate of the control however [11].

2.6.4 Other Stimulation Waveforms

There have also been studies that used alternative waveforms to the above categories. One such waveform is TENS - transcutaneous electrical nerve stimulation - which consists of an up to 100 Hz wave with an intensity of up to about 50 mA [103, 104]. TENS is mostly used as a treatment for chronic pain as it can disrupt the signals of the nervous system [104]. There have been four studies investigating TENS' use in wound healing. The first, by Kaada and Emru in 1988 [103], tested it on 19 patients who had had leprous ulcers lasting at least 2 months. All the patient healed completely within 12 weeks of the treatment starting, though there were no controls to compare against.

TENS stimulation has been shown to reduce the size of diabetic [105] and pressure ulcers [106] in controlled trials. In their investigation of pressure ulcers, García-Pérez et al. found that while TENS did reduce wound size, it had no effect on other wound properties such as wound depth or the state of the wound bed. This implies that the stimulation effects were limited to the edge of the wound [106].

In 1988, Lundeberg et al. applied TENS at an intensity three times the sensory threshold to ischaemic skin flaps resulting from reconstructive surgery. It was found that the stimulation increased blood flow more than a sham control, drastically reducing incidents of necrosis [107].

In 1994, one of the few studies investigating biphasic stimulation was published by Jerčinović et al. They used an FES - functional electrical stimulation - waveform consisting of trains of pulses which, as they return to zero, overshoot slightly and slowly, exponentially decay back up, keeping the overall charge transfer balanced at zero. This waveform, shown in figure 2.9, was used to treat 61 pressure ulcers in spinal cord injury patients, while 48 patients received only traditional treatment and were used as controls. They recorded 1.5 to 2 times faster healing in wounds treated with electrostimulation [108]. This indicates that biphasic stimulation can be as effective as monophasic, though

again, this result offers little as to whether monophasic or biphasic stimulation is better as there was no monophasic treatment to directly compare against.

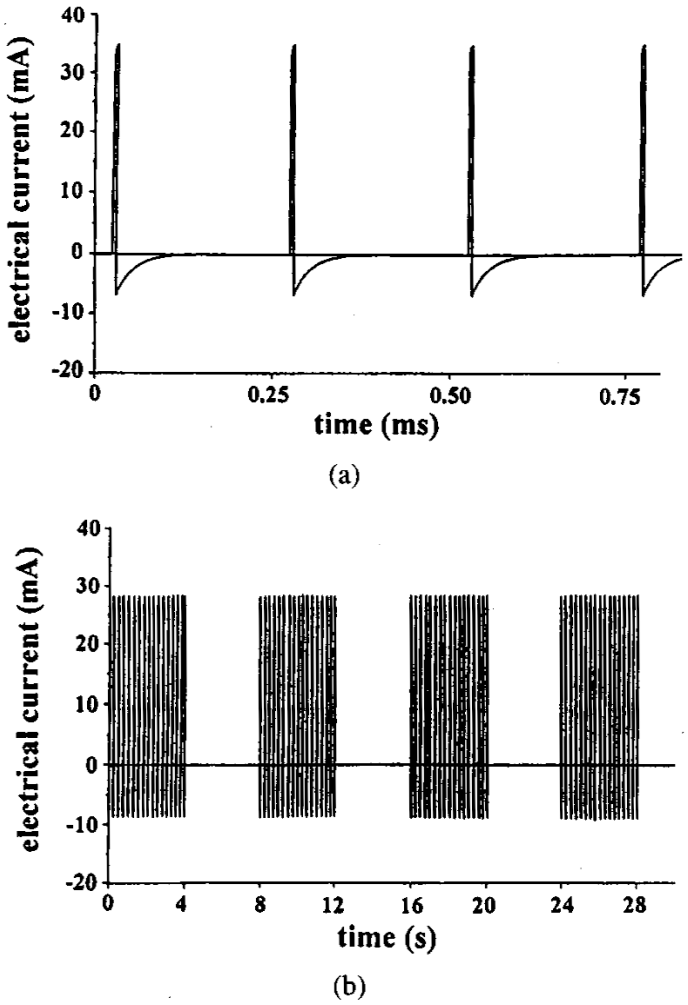

FIGURE 2.9: Waveform used by Jerčinović et al, 1994, showing the trains of pulses used. The initial spike and the exponential decay were balanced so that the net charge transfer was zero (a). These 4 kHz pulses were grouped into trains 4 seconds long, with one train being applied every 8 seconds (b). Image from [108].

Another study to investigate biphasic stimulation was conducted in 2019 by Ibrahim et al. on patients with severe partial thickness burns. They compared the effects of electrical stimulation to negative pressure wound therapy, a treatment that involves applying a suction force to the wound to drain excess fluids as well as stimulate blood flow and tissue regrowth. The electrical stimulation used a 1 Hz, 300 µA amplitude square wave. Both the electrical stimulation and the negative pressure performed significantly better than the standard wound care control, both in terms of wound size decrease (1.6 and 1.3 times respectively) and bacterial colony count (both caused a slight decrease compared to the almost two time increase seen in controls). Patients treated with electrical stimulation showed slightly better wound size reduction while those treated with negative pressure showed fewer bacterial colonies [46]. It is possible that combining

both electrical stimulation and negative pressure could give superior results on both metrics, but this was not tested.

In 2007, Lawson and Petrofsky published another study investigating biphasic stimulation. They were interested in whether applying electrostimulation to chronic wounds while in a warm environment would increase blood flow and improve healing. Their study involved 10 patients with diabetes and 10 without, all of whom had stage III or IV ulcers that had not healed for 2 months. All patients received stimulation in the form of a biphasic square wave of width 200 µs, frequency 30 Hz and amplitude 20 mA for 30 minutes, 3 times a week for 4 weeks. It was found that electrical stimulation, given in a room with an ambient temperature of 32°C, did increase blood flow and that this correlated with increased healing among diabetic patients [109]. This increase could only be measured against the base line of no healing for the previous two months however, as there were no dedicated control patients. Additionally, there is no way to know to what extent the temperature of the room affected the results as there were no controls in that regard either.

FREMS - frequency rhythmic electrical modulation system - is a waveform similar to HVPC which has been used in a few studies. A FREMS signal consists of several short pulses occurring at rapidly changing frequencies. It was first used 2004 to treat musculoskeletal pain [110]. Since then, much of the research into FREMS has been focused on its potential to lessen diabetic neuropathy (nerve damages as a result of diabetes), at task at which it shows some promise [111, 112, 113]. The reasoning behind the use of varying frequency pulses is that these variations 'probably permit a modulation on the peripheral and central [nervous] systems' [110].

Between 2008 and 2013, there were four studies published evaluating the efficacy of FREMS stimulation on chronic leg ulcers. The first of these was done by Janković and Binić and comparing standard topical treatment (15 patients) to topical treatment plus FREMS stimulation (20 patients), and showed that FREMS reduced the size of ulcers and the perceived level of pain significantly more than the control treatment ($p < 0.01$) [114].

In the same year, Magara et al. found that wounds treated with FREMS shrunk significantly more than the control group's wounds 15 and 30 days into the treatment period, though this significance did not persist to day 60 [115].

The third study also found positive when testing FRENS solely on venous ulcers, isolated from he effects of diabetes. This study, by Santamato et al, had a treatment group of 10 patients that saw decreases in wound surface area approximately six times greater than those of the 10 patients in the control group after 15 days of treatment and 30 days of follow up. The levels of pain reported by patients in the treatment group were also significantly lower than those reported by the control group [116].

The final study, by Magnoni et al, containing 16 treated patients and 14 controls with chronic ulcers of all types, also recorded significantly better results, both in terms of wound size and reported pain, in their treatment group, though exact values were not given [117].

While they do present universally positive results, none of the studies investigating FREMS used a sham treatment meaning that patients knew whether they were in the treatment or control group. Because of this, it is difficult to know whether the benefits to wound healing were a result of the treatment or of the placebo effect.

Most recently, in 2021, electrical stimulation treatment was shown to be effective on surgical wounds inside the mouth. Miguel et al. tested a stimulation treatment consisting of 100 µA AC currents at 9 kHz on wounds from palatal surgery. This was applied for only 120 s each day for five days. Despite this short treatment period, wounds in the treatment group shrunk at a rate approximately 2.5 times quicker than in the control group [118].

2.6.5 Conclusions

Figure 2.10 provides a summary of the different electrostimulation studies from the literature which reported the rate of wound size reduction. Studies are grouped according to the simulation waveform that was used and the number of patients enrolled in the study. Most studies, particularly those conducted more recently and with a large sample size, report an improvement in the rate of wound size decrease of roughly two times, but there is still al large amount of variation between studies.

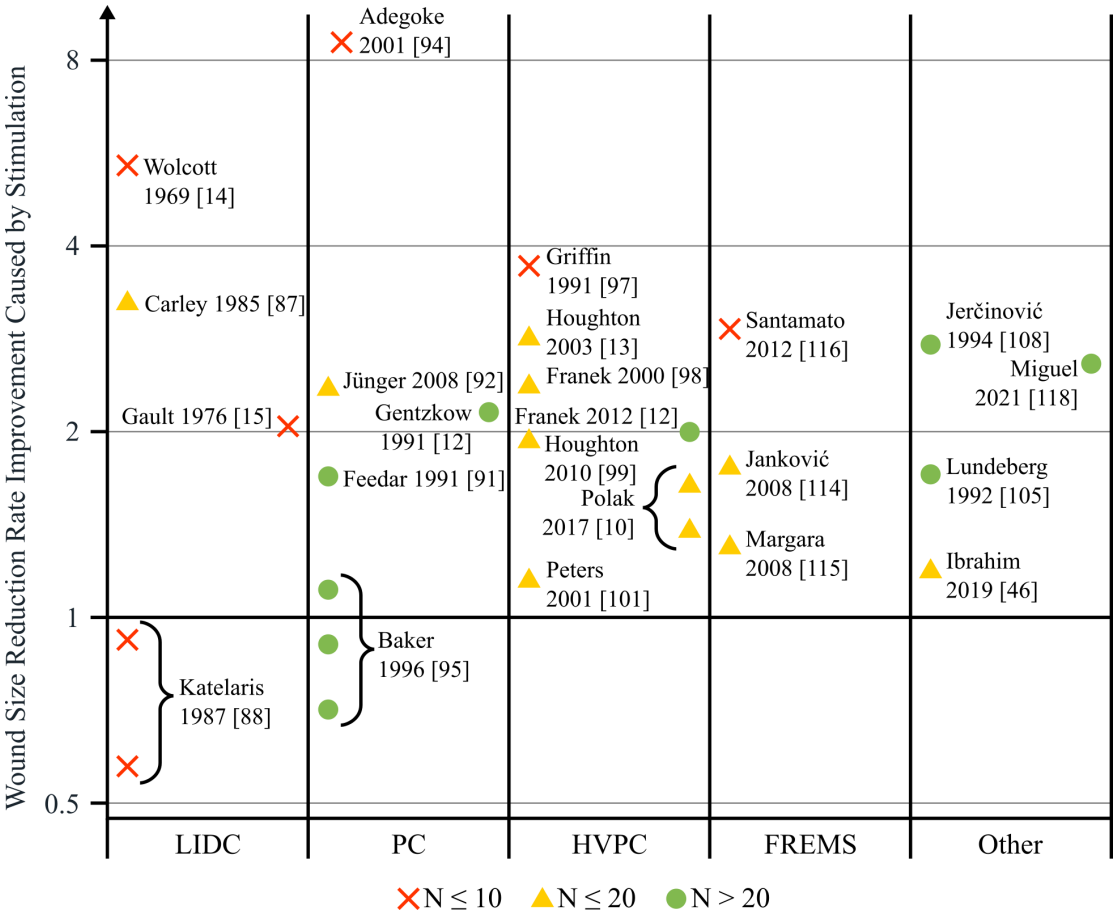

FIGURE 2.10: Comparison of results from controlled studies that report wound area decrease. The y-axis shows the improvement in percentage decrease in wound area per week that the treatment group had over the control group. Data points are colour / marker coded by the number of participants in the study as shown at the bottom of the figure, where N is the number of patients in the treatment group or the control group, whichever is fewer. Where a study tested multiple treatments, the results of each treatment group are shown separately.

Taken together, these studies clearly show that electrical stimulation can have a positive effect on the healing of several types of wounds. The fact the many studies claim that the healing rate in their treatment group was twice that of their control group, suggests that the potential benefit of electrical stimulation treatment, if adopted, could be very large.

However, no single study has had enough participants to be considered conclusive evidence on its own. The only one to have over 100 participants was carried out by Gault and Gatens in 1976 [16] and the median of all the studies reviewed is less than 40. In addition to this, the fact that each study uses a different treatment protocol and inclusion criteria means that it is hard to combine them into a single piece of evidence supporting a particular treatment. Because of this, electrical stimulation is not yet recommended by the National Institute for Health and Care Excellence (NICE) for treatment of diabetic foot ulcers [119, 120].

There have also been few direct comparisons between stimulation treatments, none of which recorded statistically significant results. As such, it is not even possible to say which protocol should be the focus of further research. This means that a device that allows many centres to perform compatible experiments and encourages the accrual of sufficient evidence for electrical stimulation to gain NICE approval would be worthwhile.

2.7 Conventional Wound Dressings

Wound dressings are materials which are applied to the area of a wound to protect it during the healing process and directly or indirectly aid healing. Dressings can either be classified by whether they are passive inert or interactive or whether they are absorbing, non-absorbing or moisture donating.

2.7.1 Passive Inert Dressings

The most basic passive inert dressing are made of loose fibrous textiles like gauze or lint. These are rarely used in modern wound healing as they adhere to the wound as it heals and are painful to remove [29].

Passive absorbent dressings are used on highly exuding wounds, wounds that produce a lot of fluid. They can be made to be very low-adhesive - though not completely non-adhesive - and hold onto fluid even under pressure. If used on wounds that are low exuding, they can dry the wound excessively. This impedes healing by preventing the movement of cells and chemicals (as well stopping the current of injury) [29].

Passive, non-absorbent dressings are typically used when all this is required is a physical barrier to prevent contact with a second dressing. They are permeable to moisture and bacteria. If made impermeable, the increase the risk of maceration, where tissue loses its integrity due to excessive moisture [121].

2.7.2 Interactive Dressings

Interactive dressings are ones that actively regulate the moisture in a wound. Non-absorbent interactive dressings include film dressings that stick to the healthy skin around a wound. They are impermeable to bacteria and liquids, but allow moisture vapour to pass through. They are often used over hydrogels or alginate dressings (discussed below) to hold them in place [121].

Another type of non-absorbent interactive dressing is wound contact layers. These are made from a soft silicon polymer and sit between the wound and another dressing,

preventing the dressing from sticking and reducing pain. They are not absorbent themselves, but allow moisture to pass through to the dressing above [29].

Alginate dressings are absorbent dressing made from a chemical derived from seaweed. Sodium from the wound exchanges with calcium in the dressing to form a hydrophilic gel which absorbs excess water while keeping the wound damp. They fit into the category of interactive absorbent dressings [29].

2.7.3 Hydrocolloid Dressings

Hydrocolloid dressings consist of a matrix of fibres that form a gel when moistened. They can adhere to wound while keeping it moist, absorbing some exudate (they are unsuitable for highly exuding wounds though) and providing pain relief. They are impermeable to bacteria, but also to gas and water vapour. Hydrocolloids come in many forms including gelling fibres which are particularly absorbent and hydrogels which are complex polymers capable of up to 90% water content [29].

2.7.4 Protease Modulating Dressings

Protease modulating dressings specifically bind protease enzymes to themselves as they absorb wound exudate, rendering it inactive. Excess protease in the wound breaks down proteins and slows healing. Protease is necessary in fighting infections so these are only used in uninfected chronic wounds [29]

2.7.5 Antibacterial Dressings

There are several dressings available that have antibacterial properties. These include cadexomer iodine dressings which release iodine into the wound as they absorb exudate. The iodine is in a sufficiently low quantity to not harm the body's cells but still has an antibacterial effect. Povidone-iodine dressings are also available and have a similar function. Both can be incorporated into hydrogels.

Honey dressings have a range of antimicrobial properties including the provision of small amounts of hydrogen peroxide, the creation of an acidic environment, and the binding of water molecules to their sugars, robbing bacteria of their food. They can also help with wound malodour [29, 121].

Dressings are also available that have silver added to them, though their antibacterial properties have been contested [29]. Lastly, dressings containing polyhexamethyline biguanide, which is effective against many types of bacteria as well as biofilms, are available [29].

2.8 E-Textile Opportunities within Wound Healing

E-textiles are textiles that have electronic devices fabricated on or incorporated into them. E-textiles have been developed which include sensors [18], energy harvesters [19], integrated circuits [20], antennas [21] and displays [22]. E-textile devices benefit from the inherent properties of textiles, while adding electrical functionality with which the user can interact. The ability to mount electronic devices directly onto fabric is promising for the world of wearable technology. Where previously adding electronic functionality to clothing meant including rigid, bulky and thus uncomfortable and obtrusive PCBs, connectors and other components, more recent e-textile techniques, such as printing [23], weaving [122] and embroidery [123], allow these to be included in a much less disruptive manner.

More ergonomic wearable technology also means improvements in the field of wearable medical devices. Wearable formats are particularly useful for medical devices as they benefit from the ability to be on the body for long periods of time. For example, new continuous glucose monitoring patches provide an alternative to finger prick monitoring for diabetic patients [124]. Wearable EEG sensors such as the one presented in [125] can be used for long term emotion monitoring as well as tasks like epileptic seizure detection [126]. In the context of wound healing, wearable electronics has the potential to make electrostimulation much more user friendly and ergonomic so that patients can receive stimulation in a manner that does not interfere with other activities or limit their movement.

Most modern commercial electrodes are based on hydrogel [20]. Hydrogels are made from a mesh of hydrophilic polymers that can hold a very large amount of water [127]. Because of its gel like consistency, hydrogel can form a good electrical connection to the skin. However, if the moisture in the gel evaporates, this advantage is lost. Hydrogel electrodes are also quite bulky: on top of the gel, there is usually a metallic cup connecting to a signal wire which is then connected to external electronics to measure or provide the signals. This means that hydrogel electrodes are unsuitable for long sessions and often prevent the patient from doing anything else while wearing them.

An alternative to gel based electrodes are dry textile electrodes. Here, the electrode and the wire that carry its signal are mounted on or incorporated into a textile. There are a variety of materials and fabrication techniques that have been used to make textile electrodes, each with their own advantages and disadvantages, however textile electrodes have been shown to behave comparably or even better than standard hydrogel ones [128, 129, 130].

2.8.1 E-Textile Material Options

One intuitive material option for making e-textiles is metals and these are often used for the connections to the electrodes. Silver is common choice because of its high conductivity; stretchable, silver based inks have been developed with conductivities as high as 3200 Scm^{-1} [131]. Silver is also chemically stable and biocompatible, but being a precious metal, its cost can be prohibitively high [132]. Copper also has a high conductivity and is significantly cheaper than silver, making it another common choice for e-textile applications, though is is more prone to corrosion [132]. Steel has been used to create conductive yarns for e-textiles because of its balance of good physical and electrical properties [133].

An alternative to metals are conductive polymers, of which there are several suitable options, for example polyaniline [134, 135], polypyrol [136, 137] or poly(3,4ethylenedioxythiophene) polystyrene sulphonate - PEDOT:PSS [138, 139]. These materials can be made into yarns by a variety of spinning techniques, e.g. electrospinning, where an electric field is used to extract a thin strand of polymer from a solution [140], or wet spinning, where the polymer precipitates from a solution in a liquid bath [134]. It is also possible to coat existing fibres or textiles with conductive polymers or metals.

However, these polymer fibres have a conductivity at least ten times lower than metallic conductors so are less suited for long conductive paths. As shown by Merhi et al. [141], it is possible to combine metals and polymers to create a material with the physical properties of the polymer but with much lower resistance. Merhi et al.'s work mixed PEDOT:PSS with silver nanowires (short silver fibres) creating a stretchable screen printable ink with a sheet resistance of 6 Ω/sq.

A common material choice for the electrodes themselves is carbon loaded rubber which can be used to make a soft pad suitable for attaching to the skin. Printed electrodes made of this material have been shown to have a lower impedance than conventional gel electrodes [142].

When designing e-textile devices, the choice of materials must be carefully considered. To function on a textile substrate, they must be flexible, and in some cases stretchable, without breaking or losing their conductivity. In wearable contexts, particularly medical ones, biocompatibility is also essential. Some e-textile fabrication techniques also place requirements on the substrate. It is desirable for the substrate to absorb some of the ink when printing, in order to provide a more mechanically robust bond after curing [143]. Most printed electronic inks have curing temperatures between 100 and 150 °C, sustained for 5 - 30 minutes [129]. Some inks alternatively require exposure to high intensity ultraviolet light in bursts of 5 - 60 seconds [24]. Therefore, the substrate must be sufficiently robust to sustain this post-processing, typically repeated for several layers of printing [144].

2.8.2 E-Textile Fabrication Methods

There are two broad groups of methods used in the manufacture of textile electrode systems: the first is incorporating the conductive material into the textile itself, either through weaving, knitting or embroidery. The second is printing the conductive materials onto the surface of an existing textile.

The first methods require a conductive yarn. This could be a conductive fibre manufactured using one of the techniques described above or simply a metallic wire with the right physical properties to be incorporated into the textile [122]. There are a variety of different weaving techniques that can be used to create the topography of yarns necessary for complex circuits [145], however, the conductive paths will always be constrained by the orthogonal paths of the weave. Embroidery offers more geometric flexibility, though is more difficult to realise on an industrial scale as most conductive threads lack the necessary strength and elasticity for machine sewing [23], though recent advancements are making it more practical [146].

Knitting is rarely used to make e-textile circuits as it offers limited options for controlling the topology of a yarn or for integrating conductive yarns with non-conductive ones. However, it is good as a method for producing topographically simple elements such as electrodes [147]. Here, it haves the advantage of good flexibility and stretchability while being securely integrated into the host textile. This comes at a cost however, in applications where precise electrode size and positioning are important, a knitted electrode may stretch and move in undesirable ways.

There are numerous different methods by which it is possible to print conductive material, the simplest of which is stencil printing. Here, a frame with openings cut to the desired pattern is filled with conductive paste. The paste is then polymerised via heat or UV cured and the frame removed [20, 142]. This method is most suited to simple patterns as the frame can become too fragile if particularly small details (< 1 mm) are required, resulting in deformation of the stencil and inaccuracies in the print. Additionally, all parts of the stencil must be connected, meaning that free-standing, concentric designs are not possible. Stencil printing is good for thicker deposits of material ($>$ 1 mm) because large amounts of paste can be applied at once while other techniques, originally developed for graphic printing, would require several layers to reach the same thickness [23].

A method that works similarly to stencil printing is screen printing. The screen used in the printer is a dense wire mesh, partly covered by a mask of the design. The material being printed is forced through the uncovered parts of the mesh by a squeegee and onto the substrate below [24].

Dispenser printing is a third method by which conductive material can be applied to fabrics. Here, a nozzle is positioned by a robotic actuator, with conductive paste being

dispensed, either pneumatically or mechanically, onto a substrate. Because they can only print in a series of individually deposited lines, typically under a millimetre in width, dispenser printers can be slow to print large areas. They are, however, much more versatile than screen or stencil printers. Using one of those methods, changing the design requires the manufacture of a new mask or stencil for each layer. Being a digital printing technique, dispenser printing required only that the printer be reprogrammed with a new design. Dispenser printers also offer the ability change the vertical position of the nozzle during printing, making it possible to print on uneven surfaces. It is also a non-contact process; nothing touches the substrate apart from the paste, making it possible to print on adhesive and other non-standard materials [148].

Inkjet printing uses a similar process to dispenser printing; a cartridge is positioned close to the substrate and inks are ejected from it. While dispenser printers typically print with a continuous stream of paste, the ink used in an inkjet printer is deposited as individual drops, typically only picolitres in volume. To form such small drops, inks used in inkjet printing have a much lower viscosity that those used in screen, stencil or dispenser printing [149]. Drops may be produced continually or only when needed depending on the desired pattern [150]. Inkjet printing has benefited from large amounts or research interest, being on of the most common methods used in graphic printing.

There are several other printing methods that are occasionally used in the fabrication of e-textiles. Aerosol printing, a technique similar in principle to dispenser and inkjet printing, sprays ink droplets from the nozzle to the substrate using a stream of gas, kept accurate by another sheath of gas around it [151]. Aerosol printing provides some of the same advantages of dispenser printing, though requires a significantly more complex system.

There are also methods that involve setting up ink in the required pattern on one surface, then transferring it to the substrate. These include gravure and flexographic printing, where the design is engraved on a roller, the engraving filled with ink and then rolled onto the substrate. The cost of producing the rollers and the stringent requirements on the ink rheology mean that these methods are rarely used in small volume e-textiles production [152].

Printing techniques such as these generally require a very smooth surface that the ink can adhere to. If this requirement is not met, the ink may delaminate or increased quantities may need to be deposited to create a complete, conducting path. Because most textiles do not meed these requirements, interface layers can be placed between the conductive ink and the fabric. Polyurethane is a common choice for this as it is flexible and adheres well to textiles. It can be printed as a paste [129] or applied as a laminated sheet [153].

Often, several different fabrication techniques will be used in the production of one e-textile device. For example, the electrical interconnections may be woven into a fabric

before the electrode contact material is printed on top, as in [122], see figure 2.11. It is also possible to combine prefabricated flexible PCBs with textiles using a range of sewing techniques. This allows for the utilisation of standard electronics microfabrication techniques while, so long as any rigid components are sufficiently small, maintaining the benefits of a textile form-factor. This is particularly helpful when prototyping e-textile devices as it can be much quicker and more reliable to place several electronic components on to a single circuit board than to integrate them each into the textile separately [154].

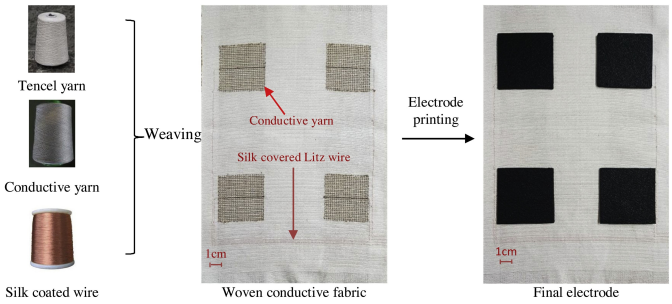

FIGURE 2.11: Pain relief electrodes built by Yang et al. showing electrical connections woven into the fabric (centre) and the carbon rubber electrodes printing on top (right). Image from [122].

Recent advancements have also been made improving the physical characteristics of e-textile devices. In 2015, Komolafe et al. showed that optimising the thicknesses of the encapsulation above and below the conductive layer of a printed circuit, so that the conductive path was on the neutral axis and was not compressed or tensioned when flexed, reduces the change in a path's resistance caused by bending and washing [155]. Several other techniques, including thermally bonding polyurethane interface layers [153] and introducing a catalyst to facilitate electroless deposition [156], have also been proven successful in this regard.

A greater understanding has also been gained of the failure modes of textile electronics. In 2019, Komolafe et al. showed that breaks in an etched flexible copper circuit tended to develop because of cracks in the copper or buckling as the traces came away from their substrate. It was found that these mostly occurred in the thin traces ($< 200\,\mu m$), close to the large connection pads [18]. This implied that the high stresses at the transition between more rigid and more flexible parts of the system are the primary cause of failures for flexible circuits.

2.8.3 Electrodes for Wound Healing

In general, little attention has been paid to the electrodes used to deliver electrical stimulation for wound healing. Most early studies used steel [87, 91, 102] or other metallic mesh [17, 14, 15, 88, 97] placed on top of a saline soaked gauze. Later studies

mostly used carbon rubber electrodes [11, 13, 92, 98, 100, 95], though several simply do not specify. No clinical trials have compared the effectiveness of different electrodes, though one, Houghton et al. 2010 [99], did note that switching to a carbon rubber electrode alleviated redness caused by the original adhesive electrodes used by one of their participants.

One study has been published in which the authors tested a stimulator that combined the electrodes and stimulation circuitry onto one device. The circuit was configured to provide 30 - 40 V pulses, lasting 100 µs at 100Hz. It was integrated into a chitosan-Vaseline gauze dressing and tested on rats where the combination of chitosan-Vaseline and electrostimulation showed better results than either individually. The circuit itself, shown in figure 2.12 was fabricated on polyamide film and consisted of a boost converter with its output being switched by a microcontroller driven MOSFET [157]. While this work serves as a good proof of concept, showing that flexible stimulators integrated into dressings are possible and effective, the large component sizes, particularly the dual in-line package ICs significantly increase the circuit's size and reduce its effective flexibility. Given also that the circuitry is underneath the adhesive layer of the dressing, with the components pointed inwards it is also likely to be very uncomfortable to wear over a prolonged period. Using surface mount components and positioning the circuit so that only the electrodes themselves are under the pressure of the dressing wound make the overall device much more ergonomic. Additionally, having the electrodes and the circuitry permanently attached to one another makes it harder to reuse the device with new dressings than if they were separable, but is a good proof of concept and highlights the growing interest in developing this new technology and thus the timeliness of this thesis.

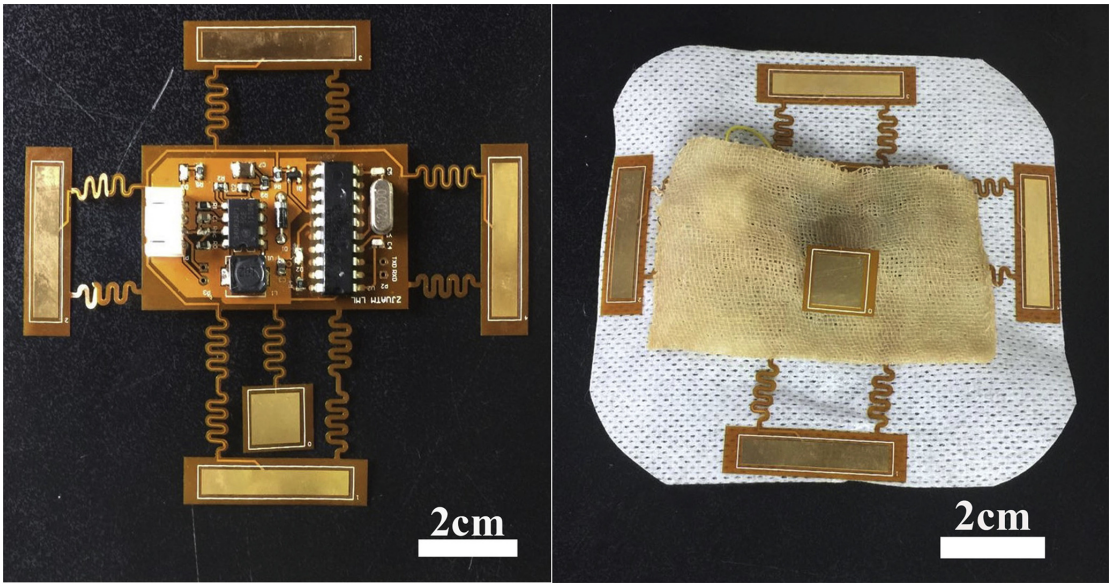

FIGURE 2.12: Stimulator used in Wang et al, 2021, showing the flexible circuit (left) and its integration into a dressing (right). Image from [157].

2.8.4 E-Textile Electrodes

One thing that new electrode printing technologies, particularly dispenser printing, allow is the ability to completely customise the layout of a set of electrodes. Traditionally, electrodes were only available in certain shapes, usually circles or rectangles, and in a defined range of sizes. However, with printed electrodes, any layout that conforms to the printer's size limit and resolution is possible.

There have been a small number of studies investigating the effects of electrode size and layout. The first of these was by Petrofsky et al. who studied the current output of modern self-adhesive electrodes. They found that the size of self-adhesive hydrogel electrodes has very little effect on how the current was passed into the skin. This was because the electrodes themselves have a fairly large resistance meaning that the current only flowed through the centre, close to where the lead wire was attached. Thus, adding extra electrode space far from the lead wire had little effect on the current distribution. This was not the case with carbon electrodes which often have a much lower resistance and create a more homogeneous current distribution over their whole area [158].

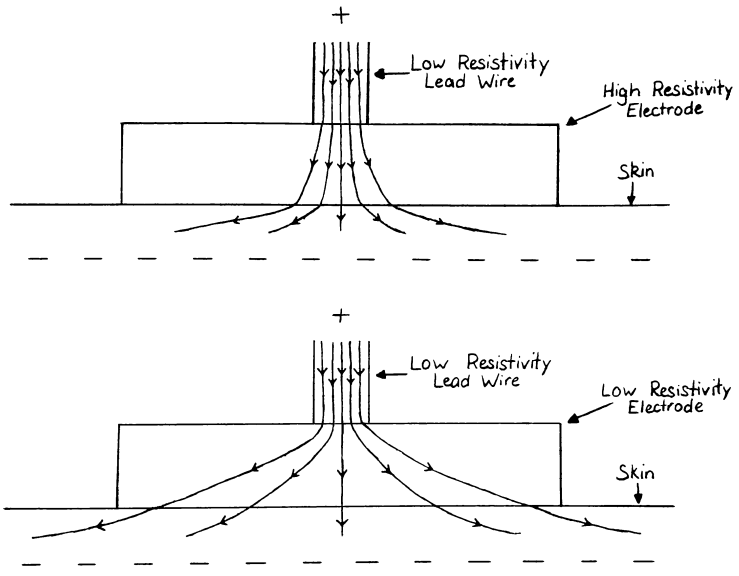

FIGURE 2.13: Flow of current though high and low resistivity electrodes. When the electrode resistivity is high, the current can only travel a short distance and so remains concentrated under the lead wire. When the electrode resistivity is low, the current can spread out and enter the skin in a more distributed fashion [158].

In 2007, Petrofsky and Schwab modelled the flow of exogenous (externally generated) current through the body. They concluded that because blood has such a low resistivity (1.6 Ωm^{-1}), current is likely to concentrate wherever it is present; if there is a lot of blood near the surface of the skin, that is where current will flow, if not, the current will penetrate deeper [159].

In 2009, Suh et al. studied the effects of using a three electrode system for treating diabetic wounds. They placed three electrodes in a triangle centred on the wound. One electrode was active and the other two were connected to ground. These roles were switched once per second. On healthy skin, measurements with needle electrodes showed that the three electrode structure caused a greater distribution of current and caused the current to penetrate deeper into the muscle [160].

The finite element modelling software COMSOL, has been used to simulate the electric field that would result from applying electrical stimulation with various shapes of electrodes with the aim of identifying the electrode configuration which would produce the largest electric field at the edge of the wound. The results suggest that the best configuration had the negative electrode over the wound itself, with the skin around the wound covered by the positive electrode. With an applied voltage of 30 mV, this generated an electric field of 40 mV/mm at the edge of a 5 mm wound. This study was limited however in that it dealt only with constant DC stimulation, used a simplified model of the skin and only considered a circular wound of a single size [161].

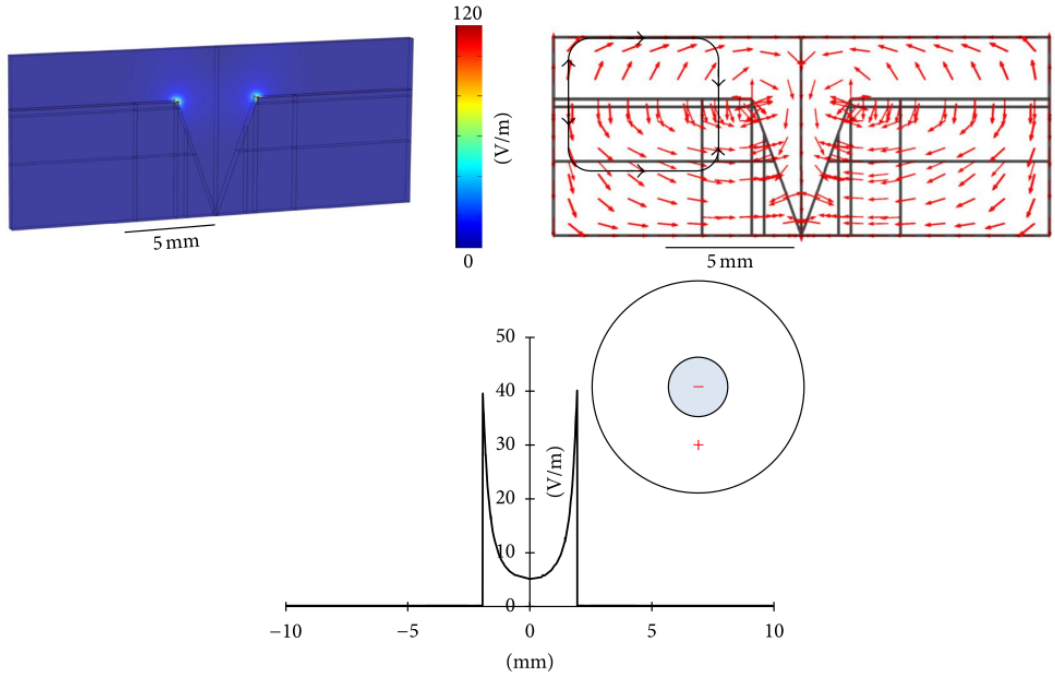

FIGURE 2.14: Results of Sun's simulation of a concentric electrode over a circular wound. A 3D heat map of the generated electric field is shown in the top right, the direction if current flow in the top left and the magnitude and electrode design at the bottom. Image from [161].

E-textile electrodes have already been successfully used in other electrostimulation treatments. Functional electrical stimulation (FES) is a treatment used to increase the functional movement available to patients with damage to their nervous systems, for example stroke survivors [128]. In 2014, Yang et al. published details of an FES system which

used 24, small, printed electrodes, shown in figure 2.15. The smaller electrodes, approximately 1 cm^2 in size, allowed stimulation signals to be delivered to specific areas of muscle and the system was able to induce multiple different hand positions in patients. The electrodes in this case were screen printed with interface and encapsulation layers of polyurethane sandwiching the conductive silver traces in between. The electrodes themselves were printed carbon-rubber [129].

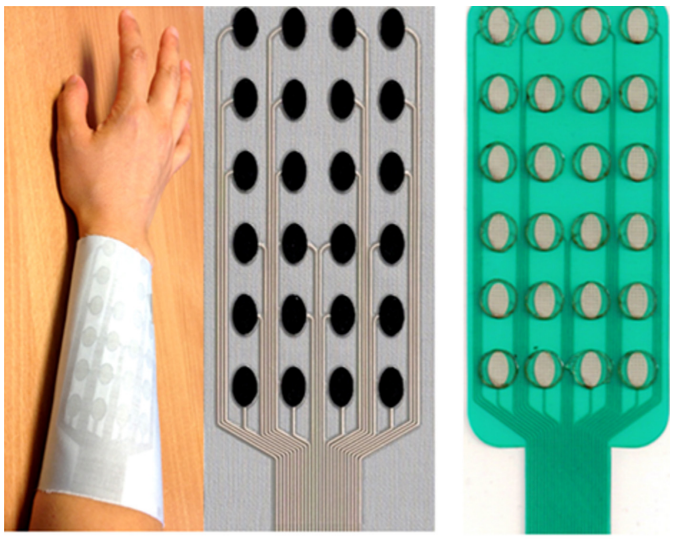

FIGURE 2.15: Electrode array used by Yang et al. 2014, showing 24 small carbon electrodes connected by scree printed traces. Image from [129].

E-textiles electrodes have also been incorporated into clothing, as in one study by Moineau et al. [130]. They designed and tested a pair of garments, a shirt and a pair of leggings, containing electrodes knitted from conductive yarn. An FES stimulator was connected to them and the system was used to identify the minimum amount of current that could be perceived, induce any movement, induce a full range of joint movement and the maximum amount of current that the test subject could withstand. These were found to be comparable to the equivalent values found with hydrogel electrodes.

Another treatment that e-textiles have been successfully applied to is pain relief. It is possible to use electrical stimulation to interrupt the signal the body uses to communicate chronic pain. In 2020, Yang et al. tested a device that used interferential current, a signal consisting of two frequencies between 1 and 10 kHz delivered at < 100 mA between two pairs of electrodes across the subject's knee. The electrodes used in this study were made of carbon loaded rubber, printed on top of a textile containing woven copper wires. The soft rubber material was able to form a good electrical contact. Tests shown that the current was delivered uniformly and subjects reported that the device was comfortable and easy to use [122].

The successes imply that, if e-textile technologies were applied to wound healing, similar results to those seen in the studies presented in section 2.6 could be achieved while creating a device that has all the ergonomic benefits e-textile technology can provide.

2.8.5 E-Textile Testing

Beyond the standard tests applied to any electronic device, testing of e-textile primarily focusses the performance of the sample during bending and during washing.

One way of testing the durability of a device while bending is by passing the test piece over an axle, for example using the bending rig used in [18] (figure 2.16).

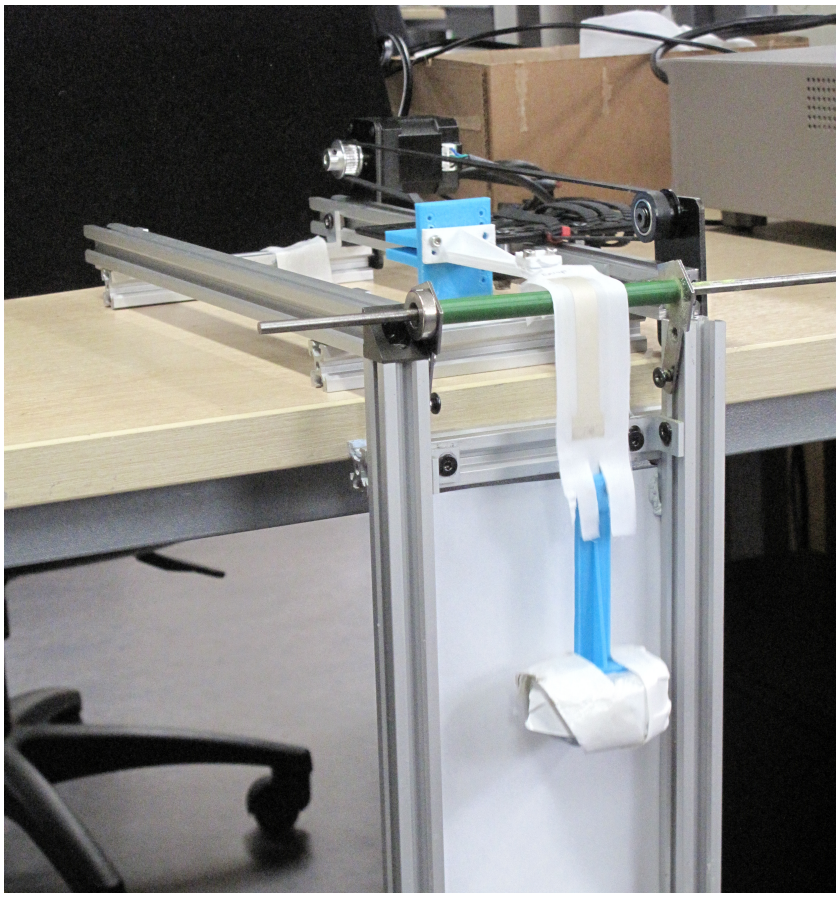

FIGURE 2.16: The bend testing rig used in [18]. A stepper motor moves the sample back and forth over an axle with an adjustable radius while a weight holds it under tension. It can be configured to repeat for a pre-defined number of cycles.

Another method of assessing bending stress is by using a limb model, as proposed in IEC draft standard 63204-204-2 [162] and shown in figure 2.17. This method provides a more realistic model of the bending a garment might experience and, by rotating the sample around the joint, can test bending a device in the plain to the textile. It can also account for the stretching garments undergo when limbs move. However, it is limited to

only testing devices that take the form of a sleeve and is hard to use for testing bends at smaller radii.

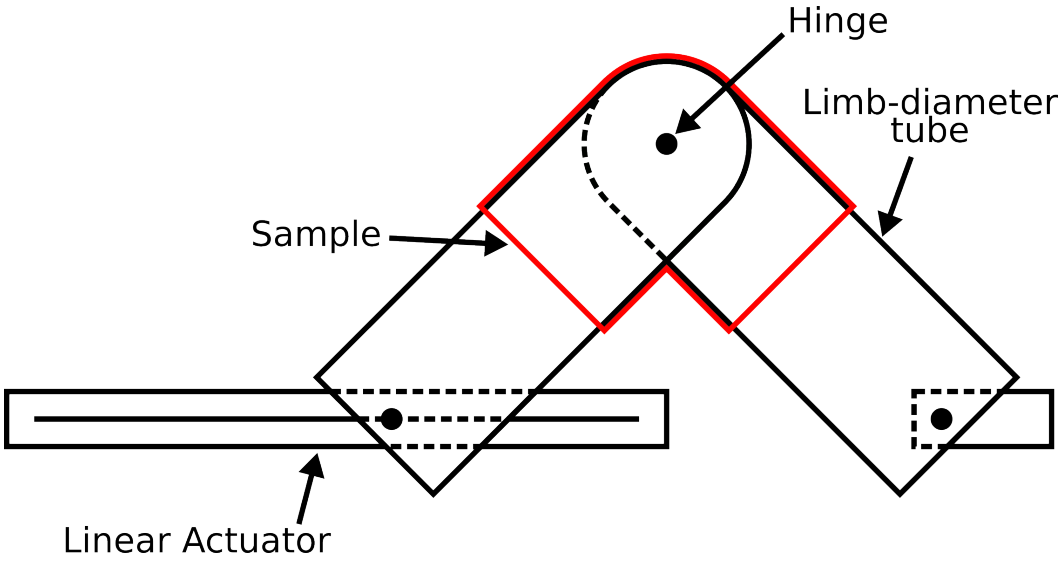

FIGURE 2.17: Bend testing system proposed by IEC draft standard 63204-204-2 [162]. Two tubes are attached together at a hinge to create the equivalent of an elbow or knee. The joint is rotated using a linear actuator attached to the other end of one tube while the sleeve shaped sample is held over the joint.

The other common test e-textile device are subject to is wash testing. Machine washing involves a number of environmental factors which can be harmful to e-textile devices: mechanical stress, moisture and high temperatures [163]. Mechanical stress and high temperatures can weaken the adhesives used to encapsulate electrical components and bond them to textiles while the ingress of moisture can damage the components themselves.

Several standards exist, giving the parameters for wash testing; the most commonly used in e-textiles is ISO 6330. However, not all investigations follow these standards and there is disagreement about how many washing cycles a test should include [163].

Through these tests, a greater understanding has also been gained of the failure modes of textile electronics. In 2019, Komolafe et al. showed that breaks in an etched flexible copper circuit tended to develop because of cracks in the copper or buckling as the traces came away from their substrate. It was found that these mostly occurred in the thin traces ($< 200\,\mu m$), close to the large connection pads [18]. This implied that the high stresses at the transition between more rigid and more flexible parts of the system are the primary cause of failures for flexible circuits.

On top of this, e-textile electrodes need specific testing to ensure that they are effectively delivering or receiving voltages to or from the skin. This can involve testing the

impedance between the electrode and the skin, compared to an existing electrode technology [142], or a functional test, for example ensuring that FES electrodes can induce muscle movement [129].

2.8.6 Remaining Challenges for E-Textile Based Stimulation

Several challenges still exist, which have hindered the development of e-textile based electrical stimulation. Primarily among them is the supply of power. The state of the art for powering small electronic devices is currently lithium based batteries due to their high energy density. While these are available in small sizes, down to a few centimetres square, they are not currently flexible and are thus difficult to use while retaining the comfort and flexibility otherwise afforded by e-textiles [164]. For high voltage stimulation, the power requirements are more strenuous; while the power transferred to the skin is still low, boost converters require significant amounts of power to maintain their output at a high voltage, and even lithium based batteries are incapable of sustaining their operation. Research is ongoing, developing battery solutions that better fit e-textile devices, however these are still far from providing the power necessary for wound stimulation applications [164]. Alternatives such as energy harvesting have been considered [165, 166, 167], but these are currently very lower power, in the nano- and micro-watt range, and therefore also insufficient for wound stimulation.

A second challenge relates to sustainability. Wound dressings are inherently single use products and as such, any electronics integrated into them must either be removable or be safe and sustainable to discard. This is an area in which current e-textile solutions perform poorly and little consideration has so far been given [168]. Increasing the modularity of devices can alleviate this problem, but doing so requires impermanent connectors between modules, which remain difficult to realise without compromising the properties of the textile [169].

Another limitation of e-textile electrodes is the need for wetting. To maintain a low impedance connection to the skin, textile electrodes need to be kept moist. During use, electrodes will naturally dry out and so can need rewetting as often as every 10 minutes [130]. This is less of an issue in the context of wound healing because wounds must be kept moist anyway to allow effective healing. Interventions such as hydrocolloid dressings already exist to accomplish this if necessary [25].

2.9 Conclusions

While the processes that are involved in wound healing are complicated, electrostimulation can clearly provide a significant benefit. The vast majority of studies that investigate the treatment record positive effects arising from its use. Most studies that

detail the rate of wound size decrease, saw the weekly rate increase by one to four times. In addition, electrical stimulation was reported to decrease the incidence of infections [46] and the reported pain [92, 114, 116, 117]. However, none of the individual studies reviewed has enough subjects with conclusive enough results to be considered sufficient evidence for this effect on its own. The fact that a wide variety of treatment protocols have been investigated in the literature means that it is hard even to combine them into a cohesive body of evidence. Meanwhile, the lack of direct comparisons between treatments means that it is hard to know where further research attention should be directed.

One of the main ways in which wounds are treated is by selecting an appropriate dressing. As a result, electrostimulation apparatus should be usable in conjunction with a variety of dressings. E-textile technology, particularly dispenser printing, allows the fabrication of circuits and electrodes on arbitrary fabrics meaning that an electrode could be placed on a physician's dressing of choice and the patient could receive the benefits of both the dressing and the electrostimulation treatment.

Finally, the versatility of dispenser printing allows for investigations into the effects of different electrode properties. Variations in electrode layout and material are known to influence their behaviour in the context of wound healing, but little work has been done to optimise these parameters.

Chapter 3

Dispenser Printing Conductive Traces on Wound Dressings

3.1 Introduction

As detailed in section 2.7, existing wound treatments rely heavily on the wide variety of wound dressings that are available. For electrical stimulation to be practical, the treatment should be compatible with as many of those dressings as possible. The adhesive nature of many of these dressings makes it hard to use printing techniques such as screen or stencil printing as they require a mask to make contact with the substrate. Dispenser printing, because it is a non-contact process and because it is compatible with a wide variety of inks, is more promising.

Investigations into printing electrodes on wound dressings were conducted with a Fisnar F7300NV, shown in figure 3.1, along with a Nordson EFD Ultimus V pressure controller. Syringes and nozzles were purchased from Fisnar. The dispenser has a moving stage to control the y-axis position and moving print head gantry to control the x- and z-axes. Pastes can be loaded into a syringe attached to the print head and dispensed pneumatically using the pressure controller.

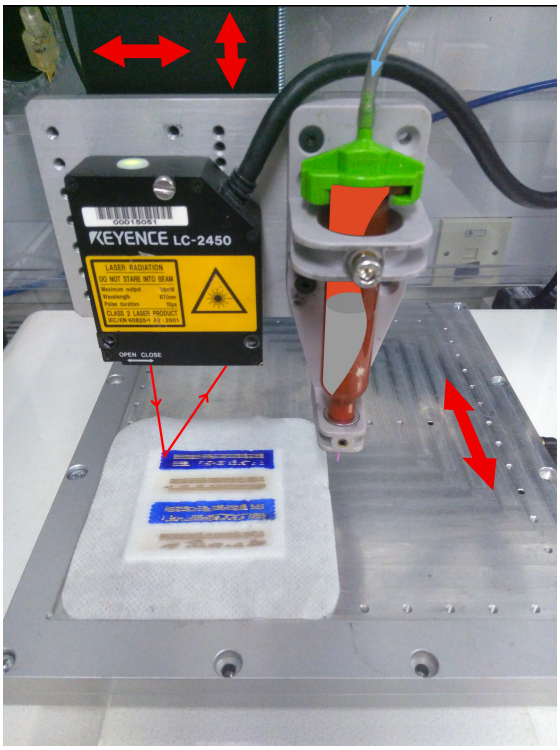

FIGURE 3.1: The Fisnar F7300NV dispenser printer. The gantry holding the syringe and laser is able to move in the x- and z-axes while the stage moves in the y-axis. Pneumatic pressure generated by an external pressure controller is used to push pastes out of the syringe's nozzle.

Previous work, using screen printing techniques, established a three layer system for fabricating electrodes on textiles, shown in figure 3.2: first an interface layer is printed onto the fabric. This provides a smooth surface for subsequent layers and also adds strength and waterproofing to the device. Having a smooth surface means that less of the conductive silver paste, which forms the next layer, needs to be printed to ensure electrical continuity. This also makes the process more economical, as the silver paste is relatively expensive. Finally, the carbon-rubber pad is printed on top. It is also necessary to add another layer of the interface material on top of silver areas that are not covered by carbon-rubber to provide physical protection and electrical insulation [23, 129].

In these tests, the interface and encapsulation layers were printed with Smart Fabric Inks' Fabinks UF-IF-1004, the conductive layers were Fabinks TC-C4001 and the carbon rubber electrode material was Fabinks TC-E0001.

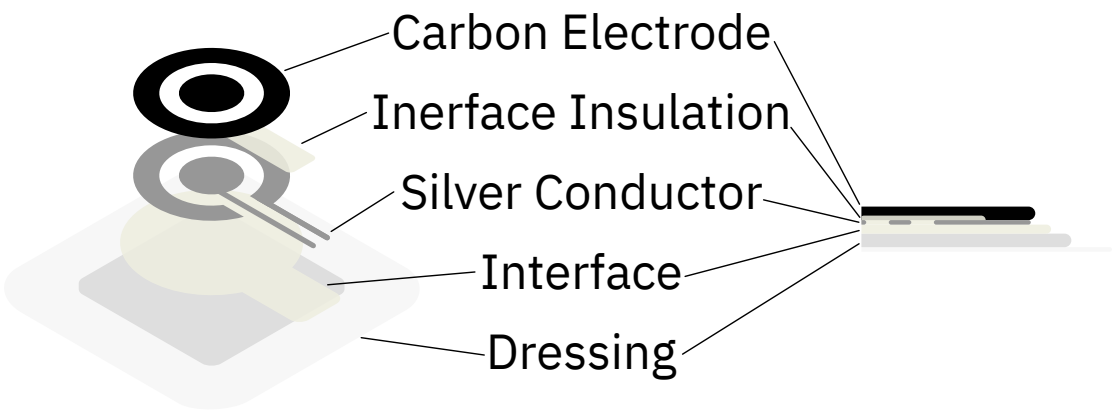

FIGURE 3.2: The structure of the printed electrode system. The printed silver connections are surrounded by layers polyurethane interface, providing protection and insulation. Areas of silver are left exposed for electrical connections and the carbon rubber electrode that is printed on top.

When configuring this dispenser printer, there are several parameters that need to be set: the nozzle speed, diameter, clearance and the pressure can all be varied and the ideal values are different for each paste. Very viscous pastes such as the carbon-rubber need a large nozzle and high pressure (approximately 500 kPa with a 1 mm nozzle diameter). This creates a wide, slow moving stream of paste so the distance between the nozzle and the substrate can be large but the nozzle speed should be slow. More fluid pastes such as the interface, require a lower pressure (less than 10 kPa for a nozzle with half the diameter). Though, because the interface is usually printed over a large area, a large nozzle and high speed can be used to print a large volume quickly.

The silver paste is the most challenging to print reliably. Because finely detailed designs are often needed and because of its higher cost, it is advantageous to print using very thin lines of paste. This makes it necessary to use a smaller nozzle which puts stringent requirements on the spacing between the surface and the nozzle tip.

In order to print successfully with any paste, it is necessary to keep the distance between the nozzle tip and substrate within a certain range: the correct clearance will produce a consistent line, but if the distance gets too small, the nozzle effectively becomes blocked; if the distance is too large however, individual drops will form and be deposited one at a time, once they get large enough to bridge the gap. The three possible cases are illustrated in figure 3.3. These effects typically occur on a scale comparable to the diameter of the nozzle so for detailed conductive patterns when the nozzle tip is only 100 - 200 µm wide, the clearance needs to be controlled to within a similar range.

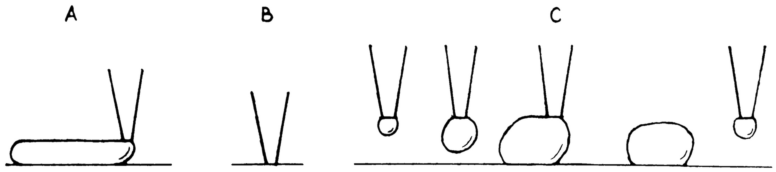

FIGURE 3.3: Behaviour with various different nozzle clearances. A: Correct clearance produces a consistent line. B: Low clearance risks making contact with the substrate, blocking the nozzle. C: High clearance allows space for large droplets to form on the nozzle tip which only get deposited once they are large enough to reach down to the substrate.

Because many textile substrates, particularly those used in wound dressings, vary in height by more than this, it becomes necessary to have the dispensing nozzle's path compensate for the height changes. It is possible to perform height compensation manually. This and most other dispenser printers allow the print head to be moved manually when it isn't actively printing and will report the current nozzle coordinate though their user interface. By positioning the nozzle above a points in the design, moving it slowly down until it makes contact with the substrate surface and recording the displayed position, the height of the substrate at that point can be effectively measured. If this process is repeated at enough points along the print path, a sufficiently detailed and accurate height map can be derived and the printer can then be programmed to interpolate between the recorded coordinates. While this method works, it is very slow and susceptible to human error.

Alternatives to this that have been developed for CNC manufacturing include probes that use contact force to find an object's position [170]. This have been used for dispenser printing electronics [171], but cannot be used on substrate which can compress, as this would reduce the accuracy of the readings. It is also common to use electrical conductivity to identify when a probe has made contact with a work piece, but as e-textile substrates are necessarily non-conductive, this is not applicable either.

A more practical alternative is to use a laser displacement meter attached to the print head, to measure the distance down to the surface [172]. This allows the height to be measured quickly and automatically at a large number of points on the design, creating a detailed surface topography map which can be used to derive the tool path.

Laser displacement meters work by projecting a laser dot onto an object and calculating its distance from the path along which the light returns. To work effectively, the laser light needs to reflect off the surface and disperse such that enough light reaches the detector for it to make a measurement [172]. This can be an issue when using translucent layers, such as the Fabinks UV-IF1004 interface targeted for this study, which allow the laser's light to penetrate some distance beyond the surface before bouncing back.

3.2 Characterising the Effect of Nozzle Clearance

In order to identify the range of nozzle clearances that result in successful prints, a series of lines of Fabinks TC-C4007 silver were printed on on polyamide (DuPont Kapton) film. The film provides a flat surface, completely parallel to the print bed, that the silver could adhere to without the need for an interface layer. This setup removed as much uncertainty as possible from the nozzle height settings. The test lines were printed with a 30 gauge nozzle (0.16 mm inner diameter), 35 kPa pressure and a print speed of 2 mm/s. Straight, 40 mm long lines were printed with nozzle heights ranging from 0 to 400 µm. These were then cured in a box oven at 120°C for 3 minutes before the trace resistances were measured with a multimeter.

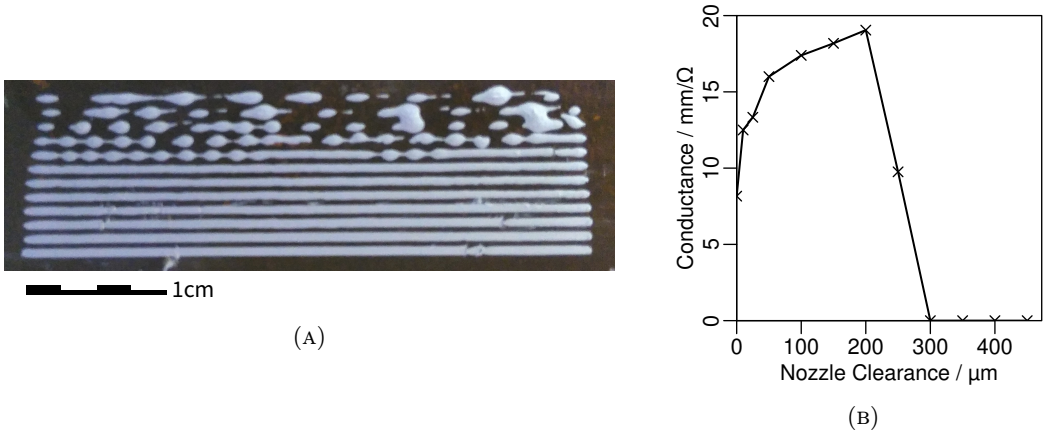

(A) (B)

FIGURE 3.4: (a) 40 mm long test lines printed on Kapton film with nozzle clearances of 0 µm (bottom line), 10, 25, 50, 100, 150, 200, 250, 300, 250 and 400 µm (top line). (b) The change in trace conductance with nozzle clearance.

The results of this test are shown in figure 3.4. Figure 3.4a clearly shows the droplet effect that occurs when the clearance is too high. Figure 3.4b shows that the best conductance is achieved by printing with a clearance similar to the diameter of the nozzle. It also shows that there is a margin of approximately 50 µm above and below outside of which the conductance of the printed track starts to fall rapidly.

3.3 Increasing Interface Layer Opacity

It was hypothesised that adding coloured pigment to the interface would increase its opacity and thus the displacement meter's accuracy. Initial tests using an available blue pigment showed that colouring the interface did indeed improve the laser's accuracy. However, it was clear that the blue colour was not ideal for use with the red light of the Keyence LC-2540 laser as it often failed to take a measurement at all, reporting that it was receiving too little light.

To more thoroughly test the effect of colouring, three different pigment colours were purchased: 1391C yellow, 2629C-A red and 5249P blue from DCC Colourants' Dynaco range. These provided a range of hues of varying distance from the laser's red. The exact pigments were chosen for their good opacity and ability to be mixed into the interface paste.

The three pigments were added to the interface at concentrations of 2.5% and 5% by mass. With the addition of uncoloured translucent interface, this made a total of seven colours. The tests were conducted on two layers of interface where one layer was printed and cured, then another layer printed on top, as this was found to produce the best surface for the subsequent layers [173].

The primary method of determining the accuracy of the laser's measurements was by comparing them to measurements taken by manually lowering the printer nozzle to the substrate's surface, shown in figure 3.5. Therefore, identifying the amount of error typical in these manual measurements was a necessity. This was achieved by printing small areas of each colour onto a Mölnlycke Mepore wound dressing then taking five measurements at each of five points on each surface. The standard deviation of each point's measurements was calculated and then averaged with the other points on that surface to get a value for the typical error.

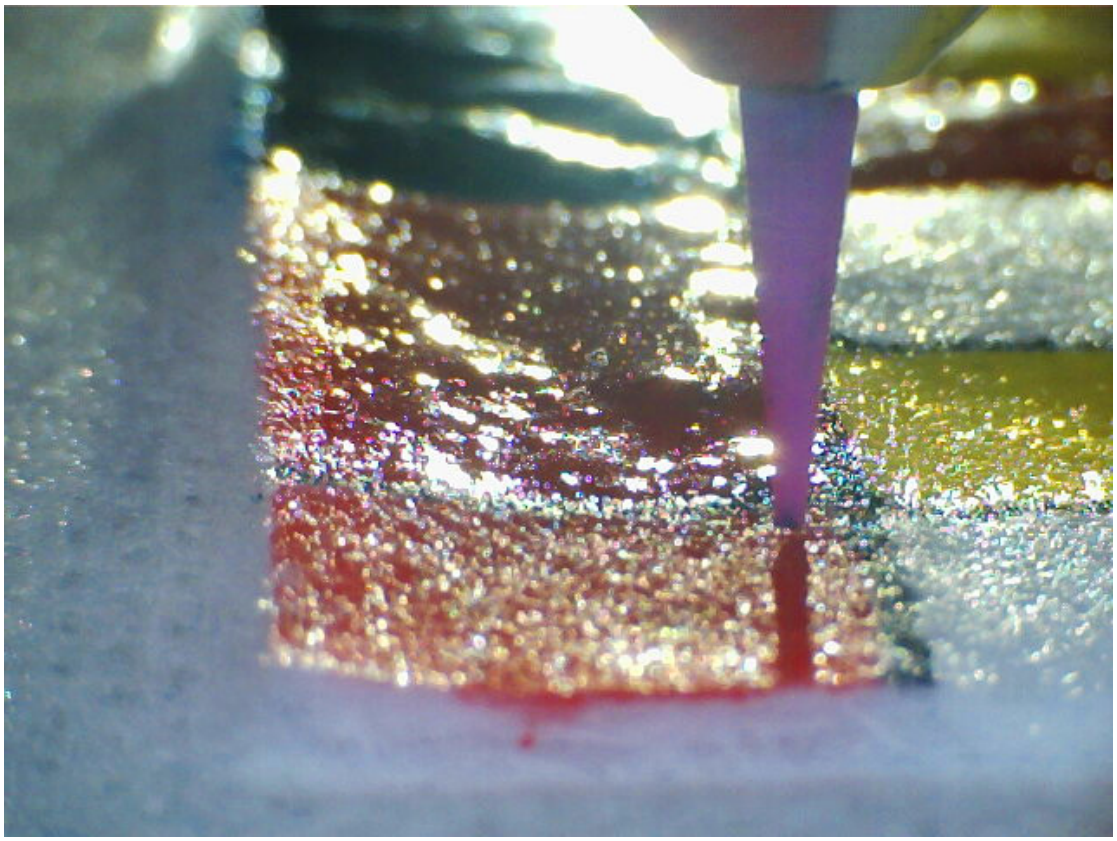

FIGURE 3.5: Conducting a manual height measurement on a single layer of red interface. This image comes from the same camera that is used to view the nozzle close up so shows the level of clarity available when determining whether the nozzle has made contact with the surface.

The laser's measurement error was then calculated by measuring the height of another five points on each surface, first with the manual nozzle moving technique, then again with the laser. Because the laser can only give relative measurements, thus needs to be calibrated against at least one manual measurement during normal use, the important result from this test was not the difference in measured values themselves, but how much those differences vary between points on a given surface.

3.3.1 Discussion of Profiling Results

Adding pigment to the Fabinks interface paste had no noticeable effect on the ability of the dispenser to print the interface layers: both the 2.5% and 5% concentrations produced a substantial change in opacity without affecting the interface's viscosity.

There was however a significant effect on the curing process. Fabinks-UV-IF1004 is cured by exposing it to a 365 nm UV light. The effect of adding red or yellow pigment was minor, compensated for by curing the print for 25 to 50% longer. However, the blue pigment severely hampered curing, preventing the UV light from curing more than a

thin layer at the top, producing a skinning effect. The uncured paste left underneath would then bleed into the surrounding fabric causing the cured skin to wrinkle as shown in figure 3.6 (left).

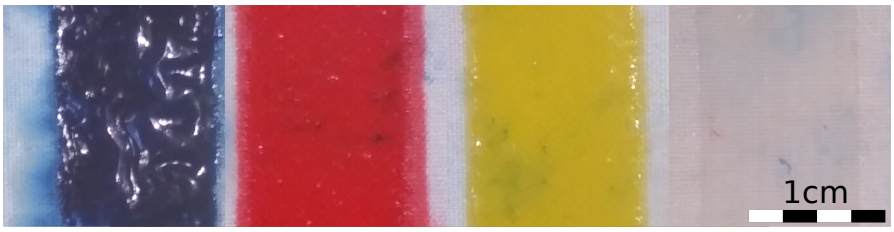

FIGURE 3.6: Four areas of interface from left to right: blue, red, yellow and clear. The blue area is much less even than the others. Uncured blue interface has bled out into the surrounding fabric.

In an attempt to quantify this effect, the laser was used to measure a detailed profile of 2.5 cm of each surface, printed on the much flatter A1656 polyester-cotton from Whaleys Ltd. of Bradford. The results of this are shown in figure 3.7.

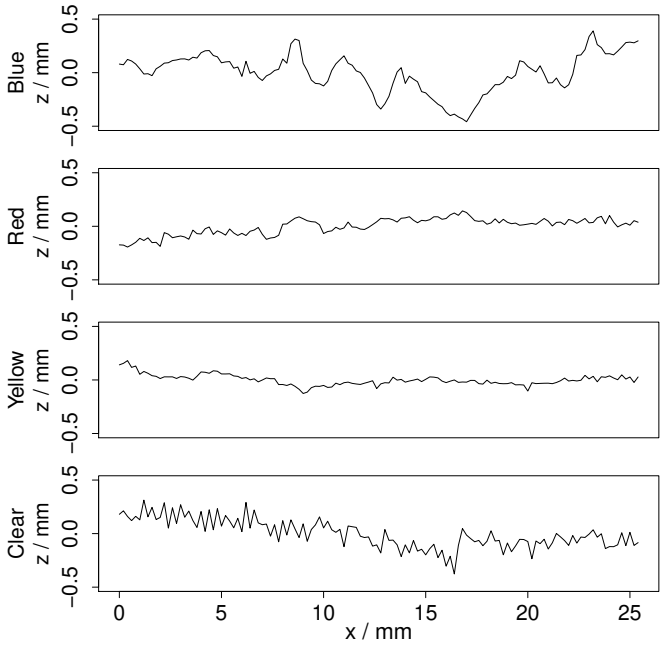

FIGURE 3.7: Laser output showing height change across 2.5 cm of each colour. The height of the blue interface is much more variable than the red or yellow. The clear interface's height is fairly consistent over a horizontal distance of a few centimetres, but has a high frequency oscillation with a period of 0.6 mm superimposed on top of it.

Although the accuracy of the laser's measurement on these surfaces had not been fully established at this point, it was clear that blue interface presents a much less even surface than red or yellow. It is also worth noting that oscillations in the clear measurements match the spacing of the fibres in the polyester-cotton base fabric. This implies that the

laser's light was travelling all the way though the interface layer instead of measuring the distance to the surface, a fact that would be confirmed by the results below.

Figure 3.8 shows the variation in the manually conducted measurements. The graph plots the average standard deviation of the measurements conducted at five different points on each surface. The standard deviation for all surfaces was below 40 µm. This is not insignificant, but is considerably lower than the 150 µm found to be available for successful prints in section 3.2 as well as the errors that would later be seen in the laser measurements.

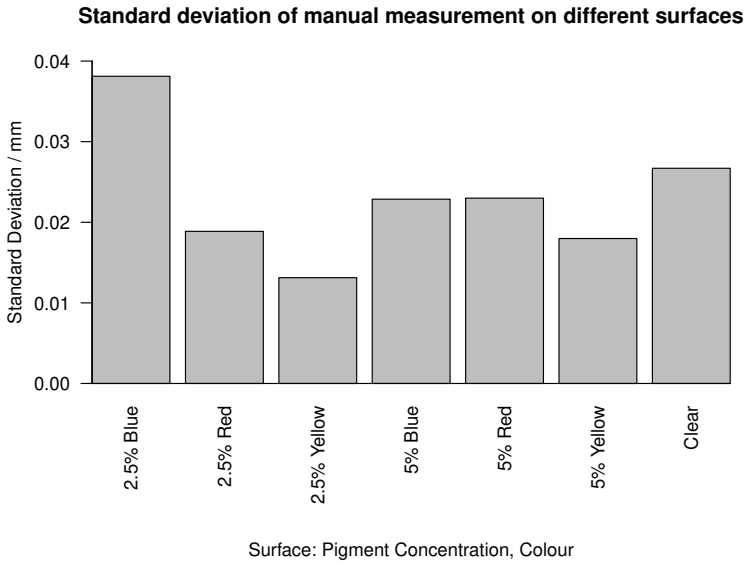

FIGURE 3.8: Results of calculating the standard deviation of manual height measurements on each surface. The y axis shows the amount of error that can be expected from a manual measurement on that surface.

Figure 3.9 shows the variation in the difference between manual and laser measurements. As expected, clear interface gives a very wide variation because of the laser penetrating into the material instead of reflecting off the surface. The blue surfaces also introduce a large error in the laser's measurements. This is likely a result of the blue pigment absorbing most of the red laser light. This was corroborated by the laser receiving unit's received intensity readout which showed a value approximately ten times lower than it did when profiling the other colours.

The smallest variations are shown by the red and yellow surfaces which manage to be sufficiently opaque and reflective enough to produce an accurate measurement.

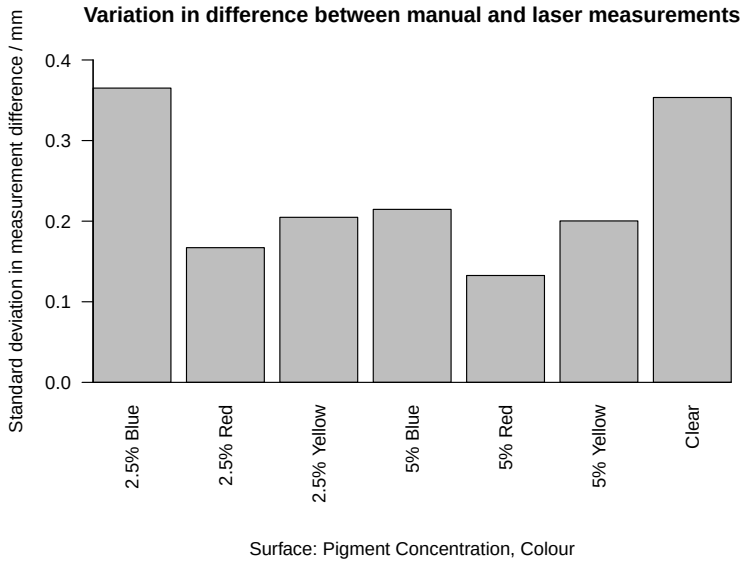

FIGURE 3.9: The standard deviation in the difference between manual and laser measurements. Similarly to figure 3.8, the y axis shows the amount of error that can be expected from a laser measurement relative to a manual one.

3.4 Semi-automatic Height Compensation for the Dispenser

To perform the laser height measurements without needing to manually position the print head over each point and apply those measurements to a design, a custom application was written. With existing software, it was not possible to move the print head to a specific location and record a height measurement once it had arrived. By using the printer's telnet interface and reading the laser's output over RS-232, the new application was able to do this for the first time. Once all the necessary height data had been collected, the program was able to combine this with the 2 dimensional design, creating a 3 dimensional toolpath that could be sent to the printer.

The main interface of the program is shown in figure 3.10. The design is stored in an XML file that contains the file settings and the list shapes that constitute the full design. Designs are composed lines, which can be made up of several segments, and rectangles which are printed in a meander pattern. The file can also set parameters controlling how the design is profiled, including the distance between each measurement point and how many measurements are averaged. It is also possible to set the printing speed and the spacing between the lines which make up rectangles.

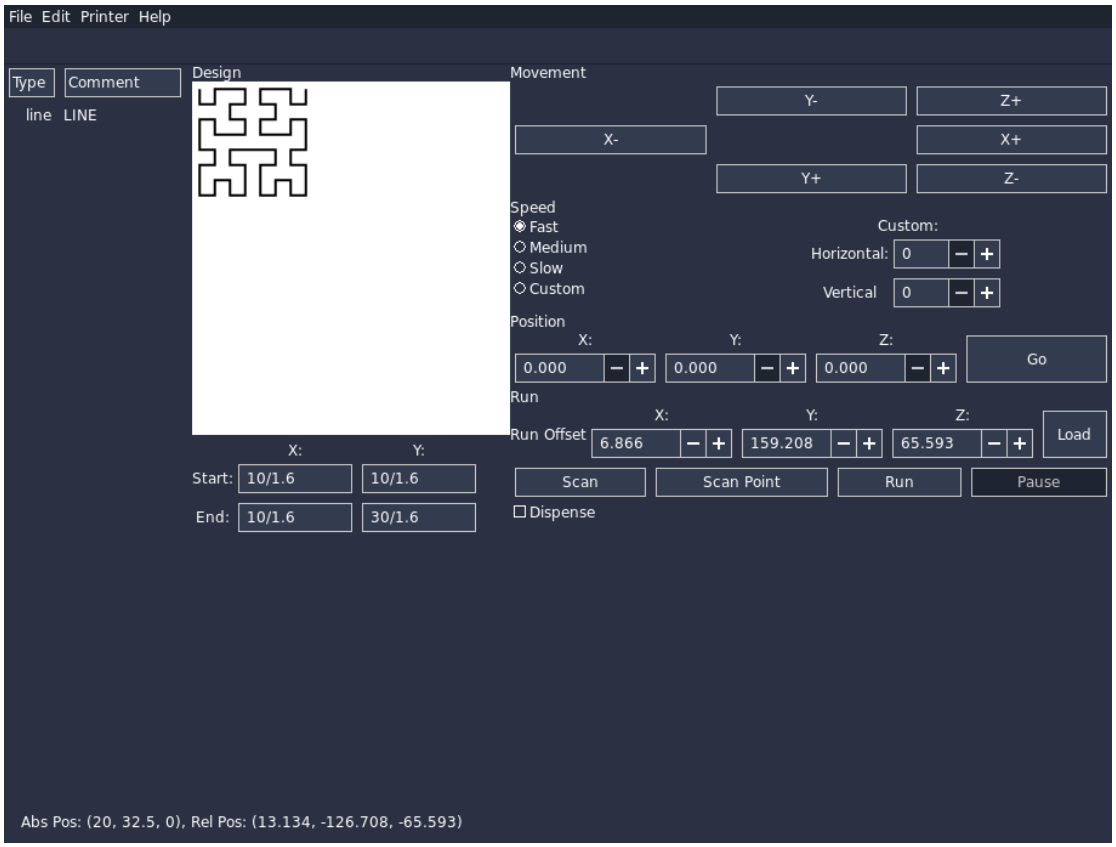

FIGURE 3.10: The main interface of the bespoke program which was written by the author to control the printer and the laser. On the left is the design being used, on the right are controls for manually positioning the print head and running scans or prints of the design.

To determine whether using laser profiling affected the success rate of dispenser prints, a design consisting of a third order Hilbert curve, occupying just under 1 cm^2 in area as shown in figure 3.11, was printed with and without height compensation and compared. The Hilbert curve design was chosen because it gives a relatively long line, 7.65 cm, that remains in a small area. Thus, any irregularities in the surface would only affect one print and could be identified as anomalies. The program was set up to measure the height at approximately one point per millimetre, with the spacing being rounded down to fit a whole number of points per straight line segment.

The design was printed using Smart Fabric Inks Ltd. TC-C4001 silver paste with a 30 gauge nozzle, 35 kPa of pressure and a print speed of 3.5 mm/s using one pass. Using these settings makes printing less reliable because only a small amount of paste is deposited, but doing so meant that any small change caused by enabling or disabling the height control wound have a noticeable effect on the resulting print.

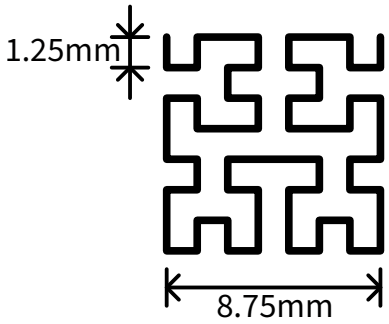

FIGURE 3.11: Design used to test the printing system. This shape, a third order Hilbert curve, creates a line 7.65 cm long in an area less than 1 cm².

Height compensated test prints conducted on polyester-cotton showed similar results to those done at a fixed height. This was because the surface of the red and yellow interface on the flat polyester-cotton generally did not vary enough over the one by one centimetre print area for the height control have a significant effect. It does show though, that the laser's measurements do not have any detrimental effect on the printer's performance.

The test was repeated, swapping the thin polyester-cotton for a much less even wound dressing (Mölnlycke Mepore). On the less even surface, the effect is more pronounced and using height compensation resulted in a significant improvement. As shown in figure 3.12, prints which utilised height compensation only failed to accurately print 5% of the complete path length, compared to 25% for those printed at a fixed height.

The correctly printed length was calculated by superimposing the design over an image of the result and measuring the percentage of the design's length where silver had been deposited.

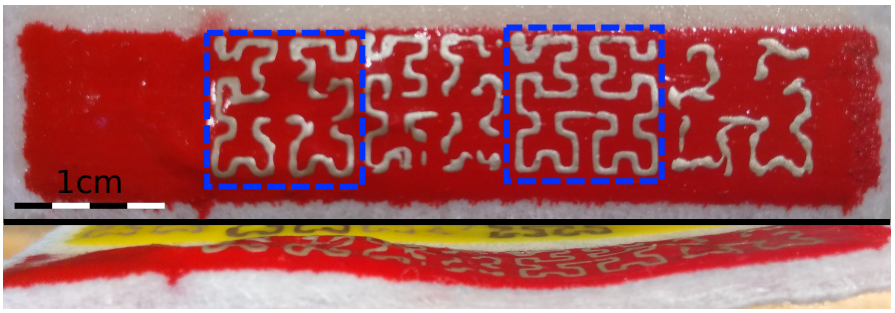

FIGURE 3.12: Four test prints on red interface on a Mölynlycke Mepore dressing. The two highlighted in blue dashed squares were printed with height compensation, the other two were printed at a fixed height. The height compensated prints show significantly fewer breaks than the others, despite the leftmost one being printed a particularly uneven section of interface.

While many of the height controlled prints made during testing do still have one break along their length, printing with multiple passes or with a larger nozzle makes the process

much more reliable. This would make it practical to use for producing prototype and bespoke e-textiles without needing to deposit large amounts of paste.

3.5 Conclusions

Dispenser printing is a very useful technique for developing new e-textile devices. Being a digital printing technique, it can be used to rapidly iterate a design. Because of the ability to control the nozzle position in three dimensions and the fact that contact with the substrate is not required, it is also good at printing on a wide variety of surfaces. However, the fact that the vertical clearance must be kept in a range that can be as small as 150 µm makes printing on uneven substrates difficult.

A laser displacement meter can be used to measure the surface topography to compensate for its fluctuations, but the laser used here struggled to measure the height of the translucent interface layer onto which the conductive silver layers were printed. Adding red pigment at a 5% concentration brought this error within the 150 µm range required for successful prints, allowing, for the first time, dispenser printing on the varied, uneven and compressible surfaces, existing wound dressings present. It is likely that red pigment performed the best because it matches the colour of the laser's light.

Care needs to be taken to ensure that the pigment doesn't adversely affect the fabrication process however. It was found that blue pigment prevented the interface from curing completely leaving uncured interface to bleed out into the surrounding fabric.

In order to collect height measurements and apply them to a design efficiently, it was necessary to write a custom application that could interface with both the printer and the laser. This program was capable of generating the list of points that needed to be measured for a particular design, coordinating the printer and the laser to measure them and then applying those heights to the toolpath it sent back to the printer. This allows a design to be printed on any laser measurable surface with minimal manual intervention.

Comparing prints with and without height compensation on a smooth fabric, one with less than 150 µm of roughness, showed little difference between the two, however on red and yellow interface printed on the uneven surface of a typical wound dressing, introducing height compensation reduced the percentage of the test design that failed to print by 80%.

Chapter 4

Modelling of Skin and Tissue Impedance

4.1 Introduction

Knowledge of the electrical properties of the skin is crucial to understanding the effects of electrical stimulation as a wound treatment, as well as for many other stimulation and diagnostic techniques like functional electrical stimulation and electrography. Modelling makes it possible to analyse how the electrical current is passing though the different physiological layers of the skin. This information can be used to evaluate stimulation waveforms without having to test them on patients. Being able to calculate the electric field in specific parts of the tissue also means that more accurate *in vitro* experiments can be set up, allowing detailed investigations into the effect of electrostimulation on specific cells or cellular mechanisms.

As discussed in section 2.4, there are two main approaches for modelling the skin's electrical behaviour: equivalent circuit models and finite-element models. Equivalent circuit models are simpler, having fewer parameters, and can be derived from physical measurements of the system as a whole, but are hard to generalise beyond a particular geometry and offer little detail about how current passes through individual tissue layers. Finite-element models offer much more detail in their predictions, but need more detailed information about the properties of the different skin layers when being put together. In the case of skin modelling, this presents a particular challenge as it can be difficult to measure the properties of the thin upper layer of the skin, to the extent that there is only one study which gives details of the properties of the stratum corneum.

A disadvantage of modelling in general is that all models contain inaccuracies, particularly for a system as complex as biological tissue. It can also be hard to quantify

exactly how large these errors are when the physical system being modelled cannot be accurately measured.

A large amount of research into the electrical properties of the skin has been conducted, as enumerated in section 2.4, but it all suffers from the limitation where the accuracy of the proposed model is hard to access. The aim of the work in this chapter was to produce both an equivalent circuit model and a finite-element model of the skin, and to compare their predictions as a way of evaluating their accuracy.

4.2 The Equivalent Circuit Model

4.2.1 Equivalent Circuit Model Derivation Method

The equivalent circuit model of the skin was created by fitting the circuit model described above to impedance spectra measured as parts of this study.

Bespoke carbon rubber electrodes, made from Fabinks E-0003 carbon paste, were used to collect these measurements. Silver connections (Fabinks TC-C4007) and a polyurethane interface (Fabinks UV-IF-1004) were dispenser printed onto a polyester–cotton backing using the dispenser printing method described in [174]. A 28 × 28 mm, carbon rubber pad was then stencil printed on top [142], giving it a total thickness of 2 mm. These were chosen because they were the materials used to manufacture the custom electrodes. Stencil printing was chosen over dispenser printing for the carbon pad because, when creating a simple square electrode, it allowed them to be created more quickly and uniformly.

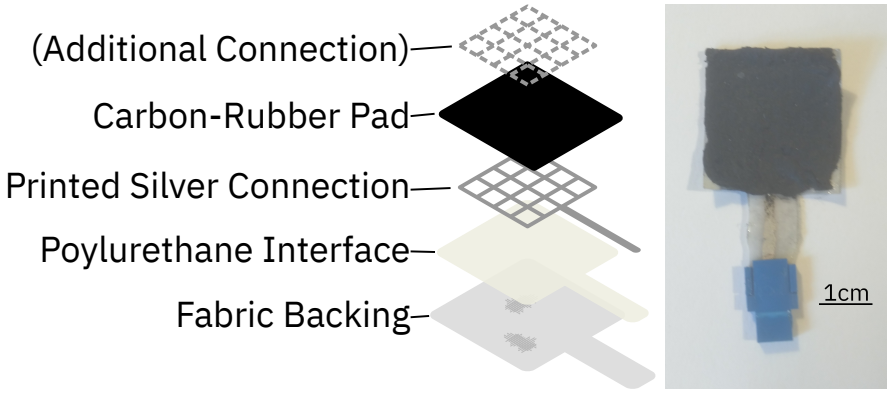

FIGURE 4.1: Electrodes used for physical measurements in this chapter. The printed electrodes consisted of a polyester–cotton base, a layer of polyurethane interface, a printed silver connection and a carbon rubber pad. A second set of electrodes were printed with an extra silver grid on top, to measure the impedance of the electrode pad alone.

Impedance measurements were taken using a Wayne Kerr 6550B impedance analyser. Amphenol Clincher connectors were attached to the ends of the printed silver, from there, copper wires could connect to the impedance analyser's probes. The impedance analyser was capable of recording both the magnitude and phase of the impedance connected to it within a range of 100 Hz and 50 MHz. When making measurements above 1 MHz, the analyser's output included an additional equipment error, equivalent to a parallel resistor, inductor and capacitor as well as a fixed time delay added to the phase, see figure 4.2. This persisted after running the manufacturer recommended calibration procedure but was consistent enough that it could be reliably removed from the data after exporting, using equation 4.1.

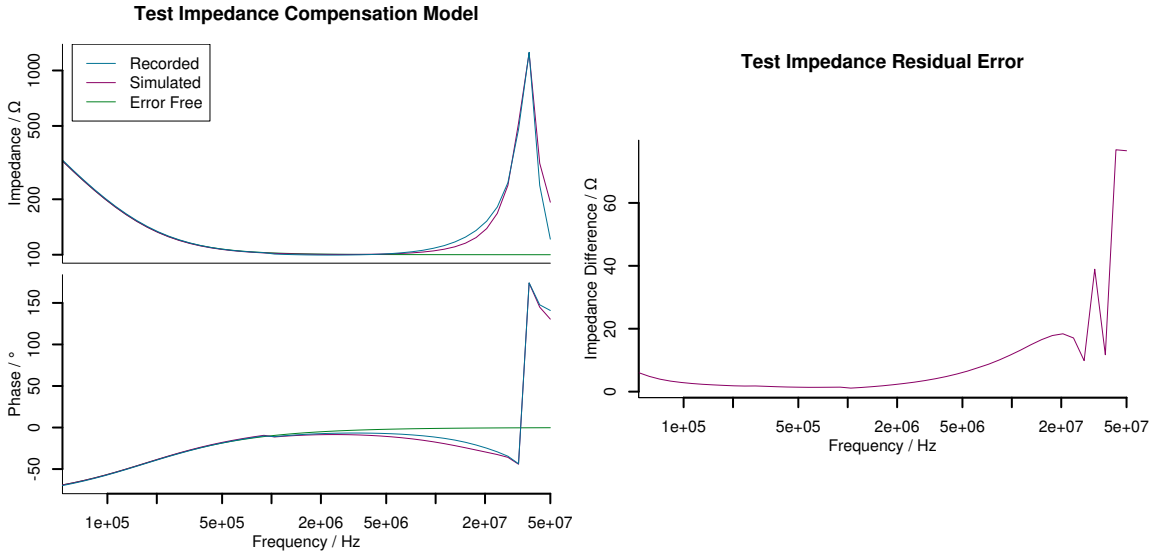

FIGURE 4.2: Recorded and expected impedances of a 100 Ω resistor in series with a parallel 100 kΩ resistor and a 10 nF capacitor. Left: The expected, error free impedance is shown in green, while the measurement from the impedance analyser is shown in blue. The purple line shows the expected impedance with compensation added to fit the blue measurement as closely as possible. The purple line in the right hand graph shows the residual error left over after the compensation is applied.

$$
\begin{aligned}
&Z_{true} = \left(Z_{measured} - \left(R^{-1} + \left(\frac{1}{\mathrm{j}\omega C} \right)^{-1} + (\mathrm{j}\omega L)^{-1} \right)^{-1} \right) \times e^{-\mathrm{j}\omega t \times (f > 1\mathrm{MHz})}, \\
&t = 4.61\mathrm{ns}\ (\sigma = 0.2\mathrm{ns}),\ R = 35\mathrm{k}\Omega\ (\sigma = 2\mathrm{k}\Omega), \\
&C = 25.4\mathrm{pF}\ (\sigma = 1.0\mathrm{pF}),\ L = 707\mathrm{nH}\ (\sigma = 49.1\mathrm{nH})
\end{aligned}
\tag{4.1}
$$

Before attempting to measure the properties of the skin, a series of tests were conducted, identifying the properties of the electrodes themselves. The first of these, designed to measure the impedance of just the electrode's carbon pad, used a duplicate electrode, fabricated as described above, but with an additional lead wire printed on top of the

pad as well as underneath it. This allowed the impedance of just the carbon rubber to be measured, with minimal effects from connection interfaces. Such measurements were taken with 0, 50, 100 and 150 g masses compressing the electrode.

This range of masses, applied by placing small metal weights on top of the electrode, was used in this test, and the later ones, to access how the compressive forces of a bandage would affect the electrode performance.

Following this, the impedance between a normal, single lead wire electrode and a copper sheet was measured. This gave an insight into the interface impedance between the electrode and the surface it is contacting. The impedance between the electrode and the copper was tested with 3 different masses applied: 50, 100 and 150 g, and with the interface both wet and dry. During wet tests, 0.05 ml of tap water was applied to the electrode surface using a syringe. This was enough that, under a 150 g mass, small amounts of water could be seen seeping out from the sides. This test was performed independently with two different electrodes: A and B, that would later be used together for measuring the tissue. These two electrodes were produced using the same method but due to variations in the materials and the texture of the electrode surface, could have had slightly different properties and so were tested separately.

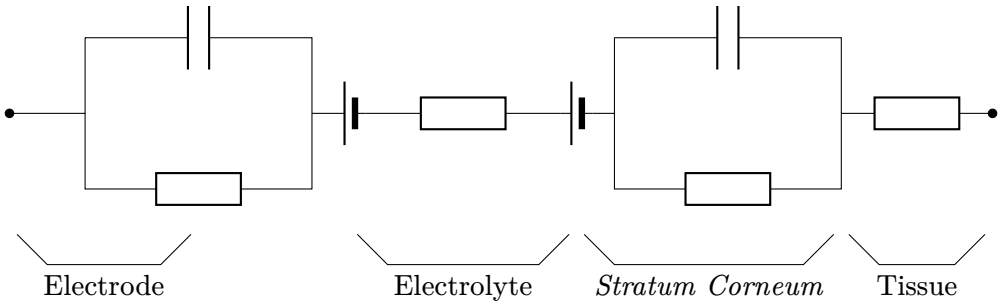

FIGURE 4.3: Neuman's equivalent circuit model of a skin – electrode system including the external electrode, electrolyte, epidermis and underlying tissue [50].

These measurements were fit to the electrode and electrolyte sections of the equivalent circuit shown in figure 2.4 (copied as figure 4.3). Because only the impedance was being considered, the electrode – electrolyte half–cell potential was ignored. The R language's [175] non–linear least squares routine [175] was used to find the parameters to equation 4.2 which best matched the recorded impedance curves, where R_S is the series resistance, R_P the parallel resistance, and C_P and α the properties of the capacitor.

$$Z = R_S + \frac{1}{\frac{1}{R_P} + (\mathrm{j}\omega C_P)^{1-a}} \tag{4.2}$$

The tests on skin were performed similarly, with 50, 100 or 150 g of mass and dry or with 0.05 ml of water, on each electrode. Electrodes were placed 30, 50, 70 or 90 mm apart, centre to centre, on the ventral forearm.

Because the recorded impedance was approximately three orders of magnitude higher in these measurements than in the ones conducted on copper, and because there was no sign on the impedance curve of a second break frequency, the impedance recorded on skin was fitted against just the epidermis and tissue sections of figure 4.3. Again, the half–cell potential was ignored.

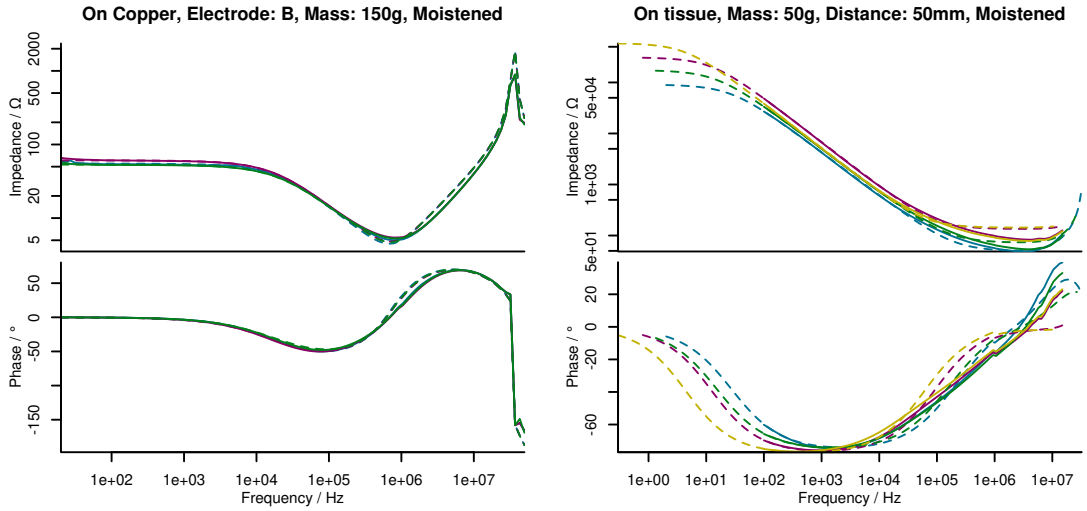

FIGURE 4.4: Recorded (solid) and fitted (dashed) impedance curves. The different colours are multiple repeats of the same measurement. The graph on the left is from measuring the impedance between a single electrode and copper sheet. The graph on the right is the impedance between two electrodes placed 50 mm apart on the ventral forearm.

4.2.2 Equivalent Circuit Model Results

Measurements of the properties of the two–lead–wire electrodes revealed that the bulk of the electrodes' pads presented a purely real impedance of no more than 5 Ω. This was consistent across the entire frequency range and did not change with the amount of mass applied.

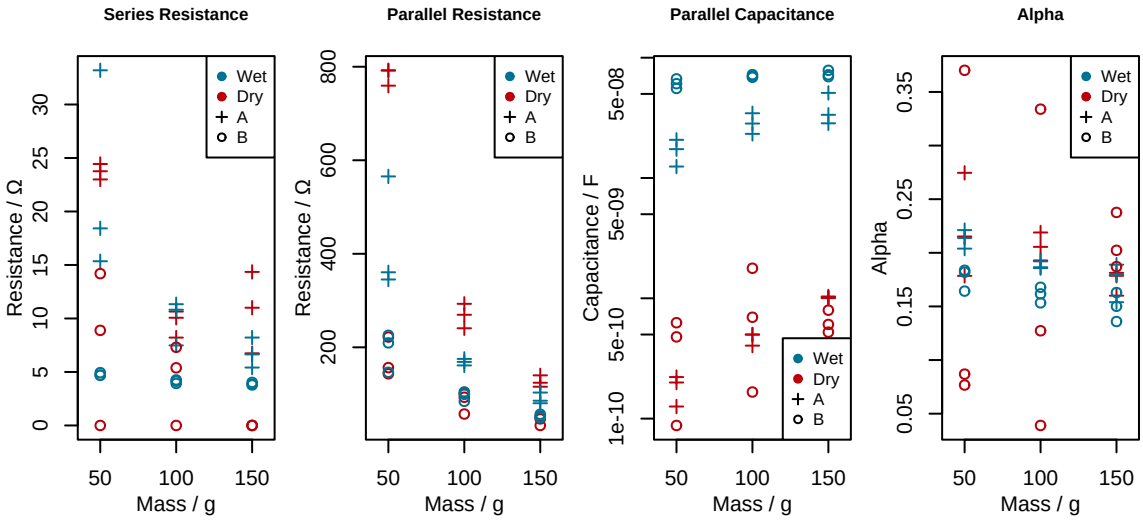

FIGURE 4.5: Fitted model parameters for electrodes placed on a copper sheet. The data points come from independently fitting to three repeats of each measurement. Note that the capacitance is given on a logarithmic scale as the result for that parameter occupies such a large range.

The fitted model parameters derived from electrodes on copper are shown in figure 4.5. Contrary to the predictions of the model in figure 4.3 the parallel resistance and capacitance behave as if they were not entirely being produced by the electrode interface, but, at least in part, by the electrolyte beneath them. The appearance of a capacitance in the dry tests, when no double–layer producing electrolyte is present, shows that a capacitance can arise directly between the electrode and the skin. The positive correlation with mass corroborates this; as more mass is applied, the electrodes and skin will move closer together, decreasing the dielectric width and increasing the capacitance. These results show that moistening the electrodes increases the capacitance by approximately two orders of magnitude. This is close to the difference between the permittivities of water and air: approximately 80 at room temperature [176], implying that a significant portion of the capacitance recoded in the moistened cases is across the whole electrolyte as well.

The parallel resistance shows a pronounced negative correlation with the applied mass. This was not observed in the electrode pads themselves when measured alone, but could be expected from an electrolyte space decreasing in thickness as more pressure is applied. Likewise, the capacitance shows a slight increase with increasing pressure, as the distance between the conductive regions of carbon rubber and copper is decreased.

The derived series resistance values show a wide variation in a way that does not correlate well with either dampness or applied mass. The reason for these variable results has to do with how series resistance is extracted from an impedance curve. The series resistance is found by looking at the value at which the impedance becomes constant at high

frequencies. In this case though, because of the meter's built in error, the impedance magnitude starts increasing again before this can happen. The result of this is that the series resistance never becomes the dominant impedance in the circuit and so it cannot be measured accurately.

The one configuration that produced a consistent result for series impedance was the measurement of electrode B with a wet interface (the blue circles in figure 4.5). The constant resistance of just under 5 Ω for all applied masses matches the measurements of the electrode pad alone, implying that the series resistance originates mostly from within the electrode. However, the variability of the results from other configurations means that this cannot be stated with confidence.

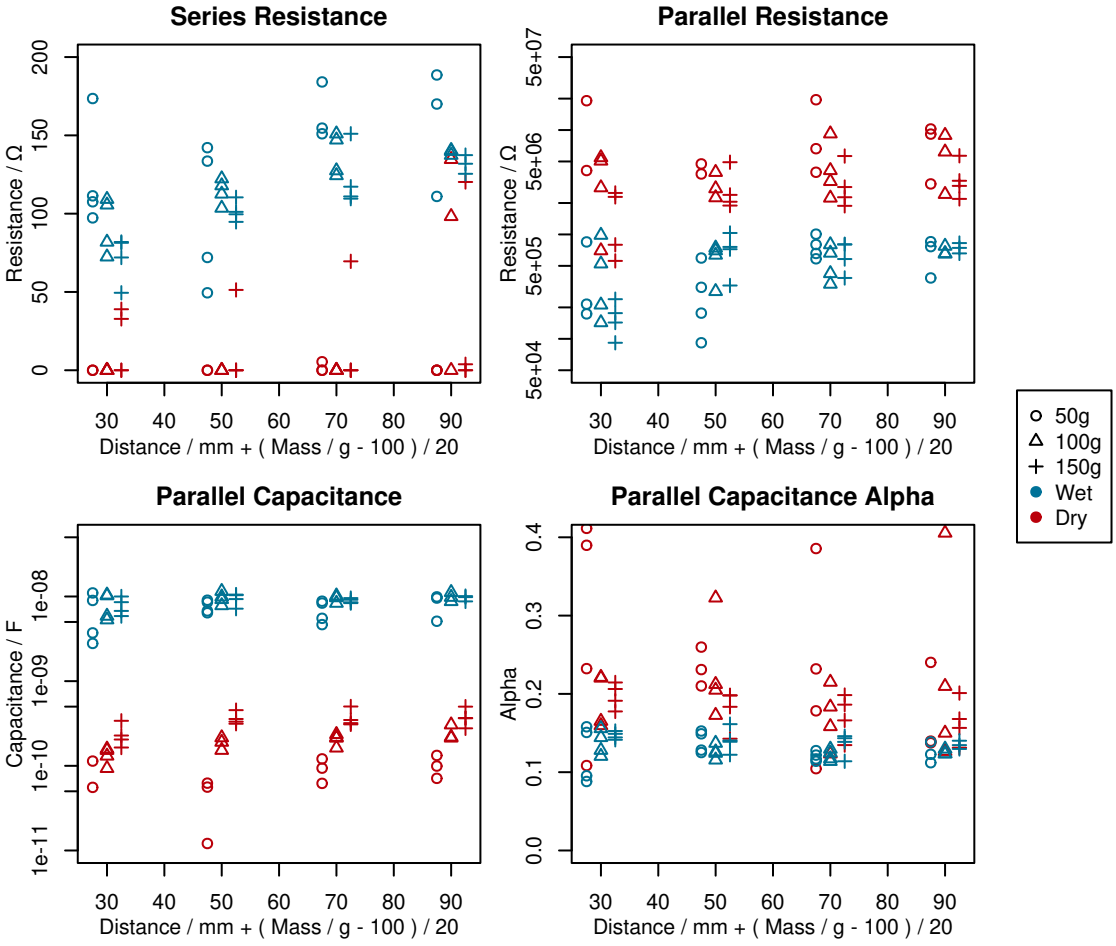

FIGURE 4.6: Fitted model parameters for a pair of electrodes on tissue. The x axes primarily plot the distance between the electrodes, however, to also show the effect of changing mass, measurements taken under 50 g are shown the equivalent of 2.5 mm left of their true position, and those with 150 g, 2.5 mm to the right, despite all having been measured at the same set of distances.

The derived parameters for the model of the tissue are shown in figure 4.6. For the same reason as previously, series resistance values, particularly for dry configurations,

show a wide variation, even within repeats of the same measurement. The wet measurements, by virtue of their higher capacitance and lower parallel resistance, did exhibit a frequency range at which the series resistance was the dominant contribution to the overall impedance, allowing it to be measured more reliably in these cases. The model in figure 4.3 ascribes the series resistance to the deeper tissues below the skin. Were this the case, the measured series resistance values would be expected to have a direct, linear correlation with distance. While the resistance value does increase in an approximately linear fashion, the constant offset along with the decrease induced by higher masses, implies there is a significant contribution from the upper layers of the skin and the interface from the electrodes as well.

The parallel resistance and capacitance values behave as the model predicts. Showing no correlation with distance is consistent with their being sourced from the upper layers of the skin. The increase in capacitance and decrease in resistance when the electrodes are wet is to be expected as well: the majority of the epidermis' impedance comes from the *stratum corneum*, the layer of dry, dead cells that make up the outer most layer of the skin. Applied water will get absorbed by this layer, increasing both its conductivity and permittivity.

Taken together, these results imply that the impedance of the skin – electrode system is equivalent to that presented in figure 4.3. However the physical source of each component of that impedance appears to differ from those given in the literature.

4.3 The Finite Element Skin Model

4.3.1 Finite Element Model Construction

Finite element analysis is a simulation methodology that works by breaking a system down into small sections, then solving a set of equations for each section using numerical methods. To verify the accuracy of the equivalent circuit model described above, a finite element simulation model was created using the modelling software COMSOL (COMSOL Inc. Stockholm, Sweden).

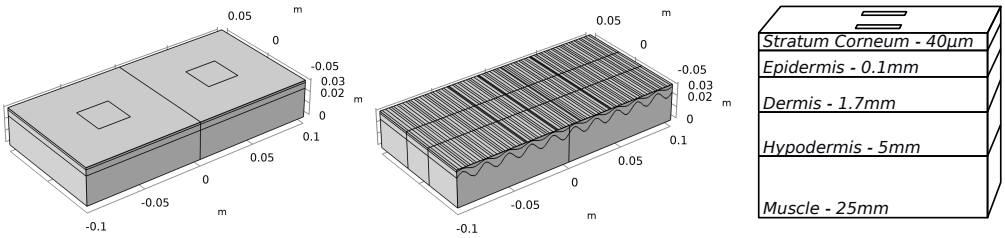

FIGURE 4.7: Basic version of the COMSOL simulation model (left) and version with uneven layer boundaries (centre). The image on the right shows how each layer of the skin was represented by a layer in the model.

Tissue	ε_∞	$\Delta\varepsilon_n$	τ_n / s	α_n	σ_i / S/m	Depth / mm
Stratum Corneum	100	1400 1×10^4	5.3×10^{-7} 1.59×10^{-2}	0.05 0.4	1.3×10^{-5}	0.04
Epidermis	$\epsilon_r = 1.14 \times 10^3$, $\sigma = 0.55\,S/m$					0.1
Dermis	$\epsilon_r = 1.14 \times 10^3$, $\sigma = 2.9\,S/m$					1.7
Hypodermis	5.5	15 2×10^5 1×10^7	15.92×10^{-9} 159.15×10^{-6} 7.95×10^{-3}	0.2 0.05 0.01	0.01	5
Muscle	54	7000 1.2×10^6 2.5×10^7	353.86×10^{-9} 318.83×10^{-6} 2.274×10^{-3}	0.1 0.1 0	0.2	25

TABLE 4.1: Electrical parameters and depths of the stratum corneum [59], epidermis and dermis [33], hypodermis and muscle [177].

This model, shown in figure 4.7 (left), consisted of five layers, representing the *stratum corneum*, the epidermis, the dermis, the hypodermis and the muscle. The electrical properties of each layer were taken from values published in the literature and are shown in table 4.1. The data for the *stratum corneum* is specific to the ventral forearm [59], the other layers' data is for generic skin.

Where available, the properties of the Cole–Cole dispersion equation are used. As opposed to the impedance version used in the physical modelling above, this version of the equation, (4.3), calculates the complex permittivity of a material as a function of frequency. This value can then be split into permittivity and conductivity according to equation 4.4 [177].

$$\epsilon^*(\omega) = \epsilon_\infty + \sum_n \frac{\Delta\epsilon_n}{1 + (\mathrm{j}\omega\tau_n)^{(1-\alpha_n)}} + \frac{\sigma_i}{\mathrm{j}\omega\epsilon_0} \tag{4.3}$$

$$\epsilon^*(\omega) = \epsilon_r - \frac{\mathrm{j}\sigma}{\omega\epsilon_0} \tag{4.4}$$

The data for the stratum corneum was collected using electrodes with a gel interface [59], meaning this model corresponds best to the moistened version of the equivalent circuit model given above.

Interface impedances, for example, the double layer impedance effect, were ignored in the finite simulation model. While COMSOL does support parametrised boundary impedances, no suitable data was available which this facet of the model could be based upon.

The model was 20 cm long and 10 cm wide, approximating an adult's forearm. The electrodes were modelled as two, 2–d squares, 28 × 28 mm in size, of variable distance apart, centred at the top of the *stratum corneum*. One of these squares was tied to

ground, the other given a 1 V sinusoidal input signal, at frequencies from 1 Hz to 1 MHz. Simulations were repeated with the electrodes 3, 5, 7 and 9 cm apart, as with the physical tests.

The model was divided into its elements using COMSOL's 'extra fine' meshing setting, producing elements no larger than 4 mm in size.

As well as measuring the impedance with this default model, versions were tested with the thickness of each layer increased and then decreased by 10% in turn. This was done to assess the sensitivity of the results to the inevitable variations in skin layers that exist between different areas of the body and between different people.

Similarly, a version was constructed which, instead of having the interfaces between layers flat, replaced them with sinusoidally oscillating surface, as shown in figure 4.7 (centre). The wavelength of these oscillations was 2 cm, creating 10 oscillations across the length of the model. Even with these modifications, the model is not a perfect representation of the geometry of the skin, but adding these oscillations is a practical way of gauging the inaccuracies caused by the model's simplifications.

4.3.2 Finite Element Model Results

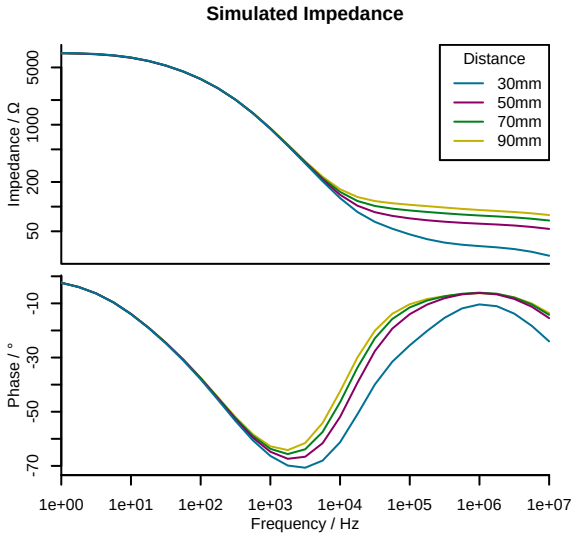

FIGURE 4.8: Simulated impedance spectrum between two electrodes on skin at 4 different distances. Low frequencies face a large impedance of around 7.5 kΩ, unaffected by changing distance. Higher frequencies show less than 100 Ω when the electrodes are 9 cm apart, falling as low as 25 Ω at 3 cm.

The impedance between electrodes in the standard version of the model is shown in figure 4.8. The overall shape of the impedance curve is as expected: low frequencies face a large resistive impedance that is not affected by the distance between electrodes.

As the frequency of the input is increased, the impedance decreases as current is able to pass through the *stratum corneum*. What remains is a smaller impedance that is affected by distance: the result of the lower tissues.

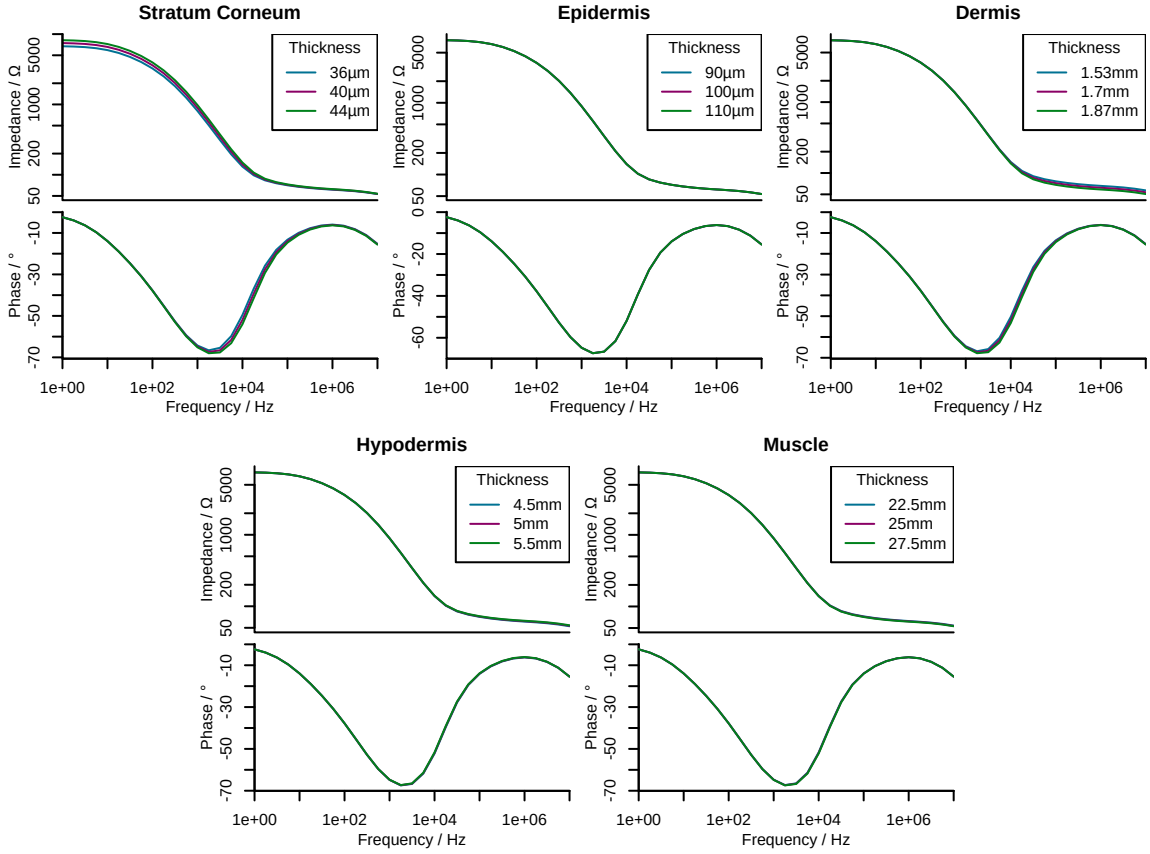

FIGURE 4.9: Simulated tissue impedance with varied layer thicknesses. Changing the thickness of most layers has only a very minor effect. The exceptions are the *stratum corneum* which affects the low frequency impedance, and the dermis which affect the value at high frequencies.

Varying the thickness of each layer, the results of which are shown in figure 4.9, confirms this interpretation. Changing the thickness of the *stratum corneum*, induced a proportional change in the impedance at low frequencies, while having very little effect on the high frequency impedance. Changing the thickness of the dermis, the most conductive of the layers, had an equivalent effect on the higher frequencies.

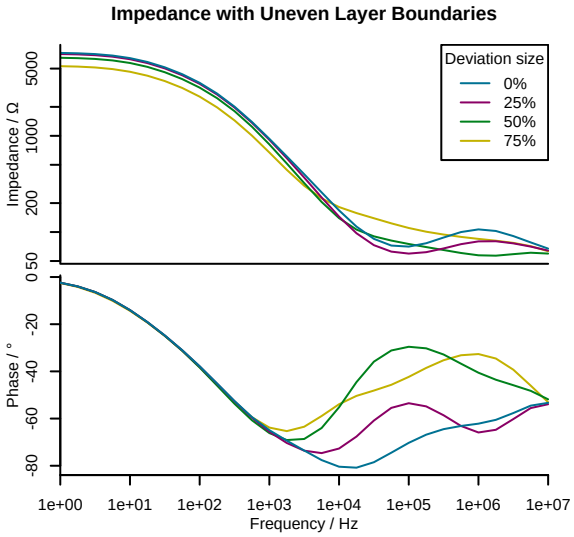

FIGURE 4.10: Simulated impedance between two electrodes, 5 cm apart, when the boundary between layers varies by 0, 25, 50 or 75% the height of the layer above it.

Creating oscillations in the boundary between layers causes changes across the whole frequency spectrum (figure 4.10). Creating a shortcut across the *stratum corneum*, reduces the low frequency impedance, in much the same way that changing the thickness did. Changes in the high frequency impedance are also caused as the effective resistance and capacitance of each layer changes.

These two tests can be used to draw conclusions about the reliability of the model. The fact that changing the heights of the tissue layers causes only a small change in the model's output indicates that errors in the data on layer thicknesses would not greatly impact the model's predictions. Conversely, the larger effect changing the layer boundary shape has on the results at high frequencies means that, if accurate predictions about the tissue's high frequency impedance are needed, accurate information about the layer boundary topography would be required.

4.4 Comparison of Finite Element and Equivalent Circuit Models

A comparison of the two models is shown in figure 4.11. While they are in approximate agreement about the impedance at high frequencies and about how the impedance transitions from high to low, there is a large discrepancy in their predictions about low frequencies.

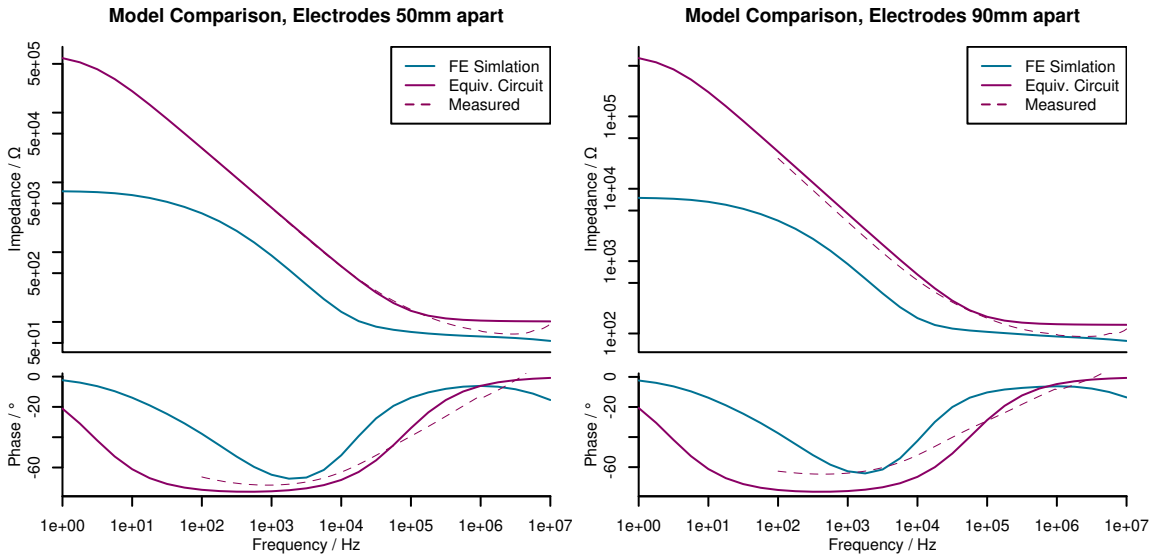

FIGURE 4.11: Simulated impedance results from the two models with the electrodes 50 mm (left) and 90 mm apart (right). The equivalent circuit plot is calculated from the 50 g, wet case, as this was closest, reliably derived case to the finite element simulation results and because the finite element model was derived from data collected on wet skin. The average of the measured plots, from which the equivalent circuit model was derived, is also given.

Some amount of this difference will result from the equivalent circuit's inclusion of the electrodes and the double–layer interface impedances, which the COMSOL model lacks. However, the tests of the electrode's impedance on to a copper sheet showed that this should account for less than 1 kΩ, far less than the 50 kΩ required to explain the discrepancy. The double–layer impedance effect, meanwhile, primarily adds capacitance to material interfaces so its inclusion in the COMSOL model would only serve to separate the models further in their transition from high to low impedance.

The fact that the error is largest at low frequencies implies that it is associated with the modelling of the *stratum corneum*. The COMSOL model can be made to resemble the equivalent circuit by increasing the thickness of the *stratum corneum* from 40 µm to 400 µm. However, it is known with confidence that the *stratum corneum* on the ventral forearm is not this thick. A more likely explanation is that an inaccuracy exists in the electrical properties of the layer. These values can be difficult to measure given the layer's small size and the difficultly in isolating a sample as well as its propensity to change properties depending on how much moisture has been applied and whether any layers have been physically removed [57, 59]. And because the electrical properties of the *stratum corneum* are dependent on the eight individual values shown in table 4.1, it is difficult to derive corrected values from these results alone.

4.5 Conclusions

Both the finite element simulation and the equivalent circuit model developed here, show the impedance between two electrodes to consist of a large resistive impedance at low frequencies, shifting to a decreasing capacitive impedance at 10 to 100 Hz. This is caused by the thin, low conductivity layers at the top of the skin.

The relationship between the impedance of the electrodes when placed on a copper sheet to the applied mass and the permittivity of the electrolyte, shown in figure 4.5, indicates that the capacitive component of the impedance is likely to arise, at least in part, from the electrolyte beneath the electrode rather from the electrode–electrolyte boundary or the electrode itself, as originally proposed. Aside from this, the physically measured impedance data, correlated well with that predicted by the model in figure 4.3 from [50].

The two models disagree about the exact frequencies these changes occur at and, most significantly, about the total impedance at low frequencies. These differences indicate an error in the literature data used to model the *stratum corneum*.

Nevertheless, these models can be used to make predictions about how current passes through the tissue. For example they show that low frequency stimulation, below 100 Hz, will mainly deliver energy to the high resistance, outer layers of the skin, whereas higher frequencies, above 10 kHz will use the capacitive properties of the upper layers to penetrate deeper.

When stimulating open wounds, the lack of skin under the wound electrode will mean that relatively more current and energy will be delivered with a DC or low frequency stimulation waveform.

However, as the return electrode must still be on intact skin, away from the wound, a high frequency stimulation signal is still needed if a significant electric field strength is desired in the living tissue. This, along with the fact that DC stimulation causes the build up of charged ions under each electrode, helps to explain the why modern stimulation waveforms primarily use high frequency waveforms or short pulses: these waveforms are able to deliver more energy to the dermis and deeper tissue layers where the mechanisms of wound healing are taking place.

Chapter 5

Evaluation of Stimulation Waveforms for Inducing Cell Migration

5.1 Introduction

Electrotaxis, the propensity of cells to migrate directionally in an electric field, is thought to be a key component of how the current of injury and external electrical stimulation assist in wound healing [12]. During the healing process, the directional migration of immune system cells, fibroblasts and keratinocytes is required for eradicating infections, rebuilding tissue and reepithelialisation respectively [25, 31].

As discussed in section 2.5, many studies have found that applying a directional electric field to cells *in vitro* can induce this directional migration [38, 39, 40, 41, 43, 44, 74, 77, 78]. These experiments provide a means of comparing different stimulation waveforms, a task that has proven difficult in clinical trials where confounding factors and small sample sizes have prevented statistically significant results. A thorough investigation of different stimulation waveforms *in vitro* would provide clearer data on which is the most effective, which could be used to inform the design of stimulation devices.

While the majority of past electrotaxis studies have just tested various intensities of DC electric field, one, Tsai et al. [41], did evaluate several waveforms previously used in clinical trials. Their work found that constant, low strength electric fields (600 mV/mm) were more effective than pulsed, high voltage ones (2000 mV/mm, 0.025% duty cycle). This study did not, however, account for the impedance of skin and the effect that would have on the electric field cells would experience; they simply applied the same voltage that would be connected to a pair of electrodes across the chamber containing their cells. As shown in chapter 4, the impedance of the skin primarily attenuates DC

and low frequency signals so discounting its effects gives a relative advantage to low frequency stimulation that would not exist *in vivo*.

The aim of the following experiment was to repeat this work, accounting for the impedances that would be faced when stimulating an actual wound, to try to gain a more accurate understanding of the effects of waveform choice on cell migration.

5.2 Migration Assay

5.2.1 Method

The tests were conducted separately on available HaCaTs (human keratinocytes) and 3T3-L1s (mouse fibroblasts). Both of these cells need to migrate towards or across the wound during the healing process as previously defined in section 2.2 [29, 25]. The cells were cultured in a media of Dulbecco's modified Eagle's medium (DMEM) supplemented with 10%v/v foetal bovine serum and 1%v/v penicillin/streptomycin as an antibiotic and antifungal. The DMEM included a HEPES buffer which helps to keep the pH of the media constant and phenol red, a pH indicator and was sourced from Sigma Aldrich.

The cells' media was changed three times a week and once the cells reached 70% confluence they were divided by washing with phosphate buffered saline (PBS) and detaching them from their flask using trypsin. The cells were then centrifuged at 200 rcf (centrifugal force relative to 1g) for 5 minutes using an Eppendorf 5810 centrifuge. The trypsin supernatant was removed, the cells were resuspended in media and seeded in new flasks at a density of approximately 1500 cells/cm^2, following standard practice [41, 80].

When performing experiments, cells were removed from their flask as described above, but instead of placing them into a new flask, they were seeded into the wells of either a 12- or 24-well well plate (Corning Costar). The seeding density was between 1000 and 2000 cells/cm^2 and the well plate was incubated for between 48 and 72 hours with the aim of producing cell colonies of various sizes with enough empty space that the cells could move freely. A typical result is shown in figure 5.1.

The image on the left of figure 5.1 shows the 3T3s which typically exist as single cells or small groups and have long lamellipodia protruding from the edge of the cell which they use to move around. The HaCaTs in the right hand image are more inclined towards forming colonies. They have broader lamellipodia which form a sheet around the cell. When a cell detaches from the base of the well, it shows up with a bright white outline in the microscope image. This can occur when a cell dies or when it is dividing.

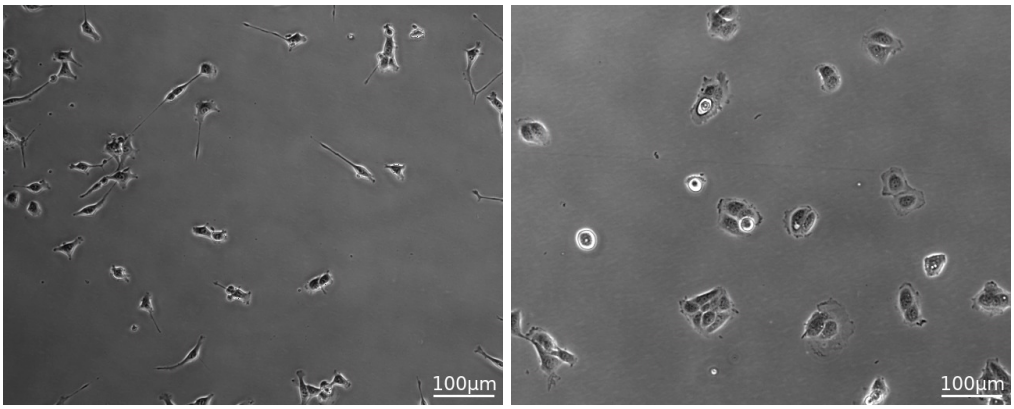

FIGURE 5.1: Cell densities prior to experimenting. Left: 3T3s, right: HaCaTs.

Tests were done, both with silver coated wires inserted directly into the media (figure 5.3 left), and with wires inserted into adjacent wells filled with PBS connected via tubes of PBS with 3%v/v agarose. These tubes had a diameter of 2.5 mm and were at least 10 cm long. This is shown on the right of figure 5.3.

A custom made voltage generator, shown in figure 5.2, was configured to provide an electric field between 0 and 200 mV/mm. This voltage generator received power through a USB port and used an LT1072 boost converter IC to increase this to 30 V. This 30 V supply was used to power an LM358 operational amplifier, which amplified the digital-to-analogue converter output of an ATSam D21 microcontroller. The output was connected to a set of screw terminals to which the electrode in the well plate could be attached. One terminal was connected to the output of the op-amp, the other to either the 30 V supply rail or to ground as controlled by the microcontroller and a transistor switch. This gave an effective output range of -30 to +30 V with a resolution of 11 bits.

The system was given a simple interface consisting of two buttons and two LEDs. The buttons could be used to cycle between the various programmed waveforms while the LEDs would flash to show a representation of the current output (reduced to a human parsable frequency were needed).

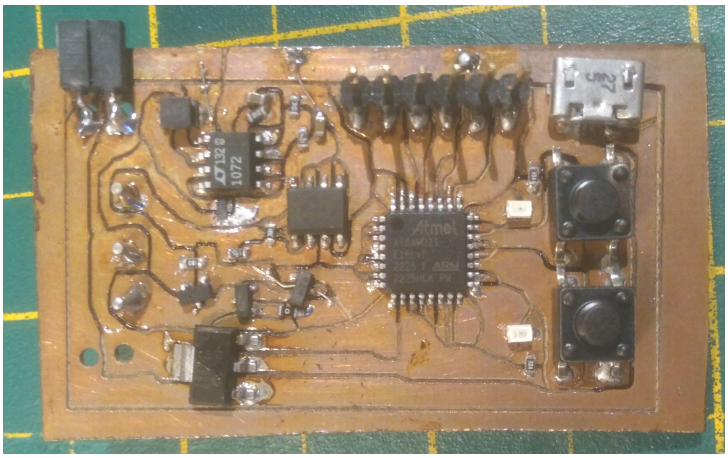

FIGURE 5.2: The voltage generator used to apply the electric field to the well plate. The circuit board was produced using a CNC milling machine which expanded each net into a Voronoi region to minimise the required cutting distance, creating the unorthodox trace outlines on the PCB.

Each experiment was performed with three well in parallel, and with three identical wells left with no electric field as controls.

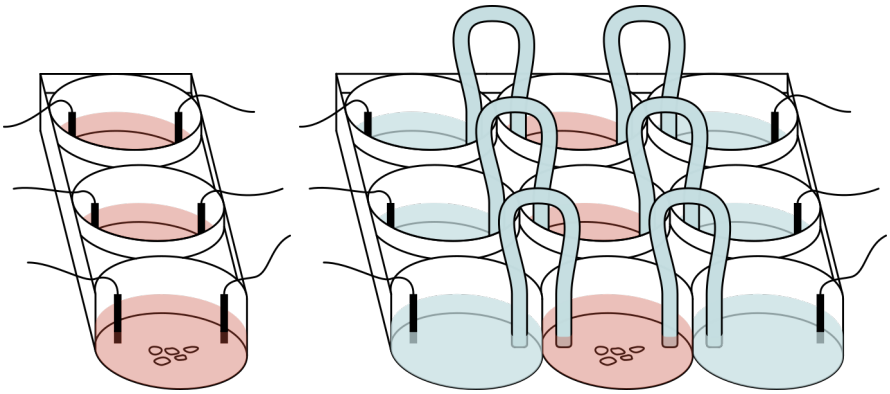

FIGURE 5.3: In some tests, the electric field was applied to the cells by placing metal electrodes directly into the cells' media with three wells connected in parallel. In others, the electrodes were placed into adjacent wells filled with PBS and which were bridged to the cells' wells with tubes of PBS and 3%v/v agarose.

Timelapse videos were recorded on a Nikon Eclipse Ti microscope set to 10× magnification. The microscope had an enclosure around it which held the cells at 37°C and at 5% CO_2 to emulate physiological conditions.

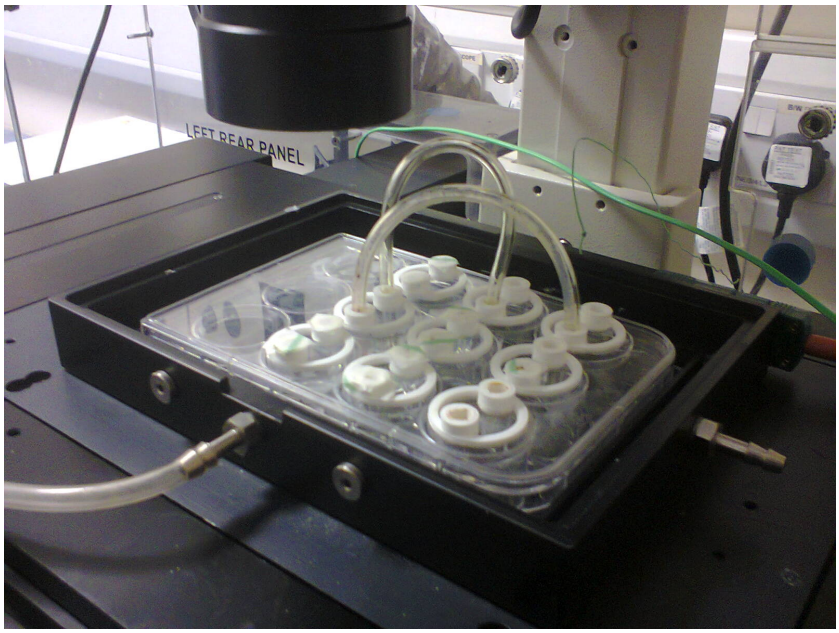

FIGURE 5.4: A 12 well plate with two tubes for agar bridges placed inside a Nikon Eclipse Ti microscope.

5.2.2 Results

With silver coated wires inserted directly into the cell's media, high voltages caused the cells to die. For HaCaTs, the threshold at which this happened was between 250 and 300 mV/mm and for 3T3 was around 200 mV/mm. Any voltage below this threshold had no visible effect on the cells.

At particularly high voltages, greater than 300mV/mm, chemical reactions at the electrodes caused a pH change to occur and a turquoise residue to form in the media, shown in figure 5.5, but there were also cases when cells died with no change to the pH of the media.

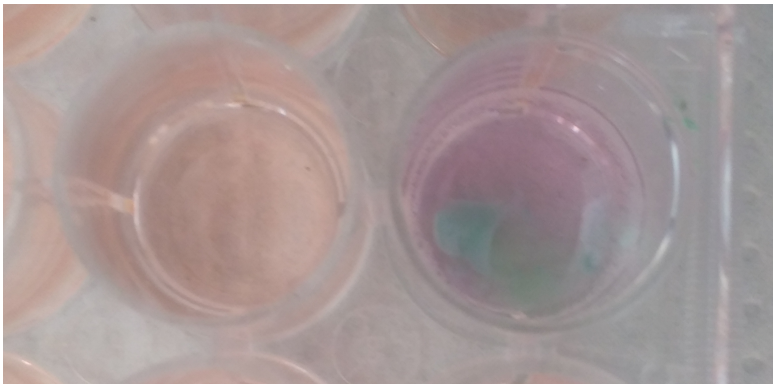

FIGURE 5.5: The pink colour of the right hand well, indicating that the media has become significantly alkaline, compared to the approximately neutral media in the control well on the left.

In tests conducted with the connecting agar tubes, a voltage approximately 10 time higher was required from the generator, in order to get equivalent field strengths across the well. Field strengths up to 260 mV/mm were tested, but no change could be induced in the cells at all.

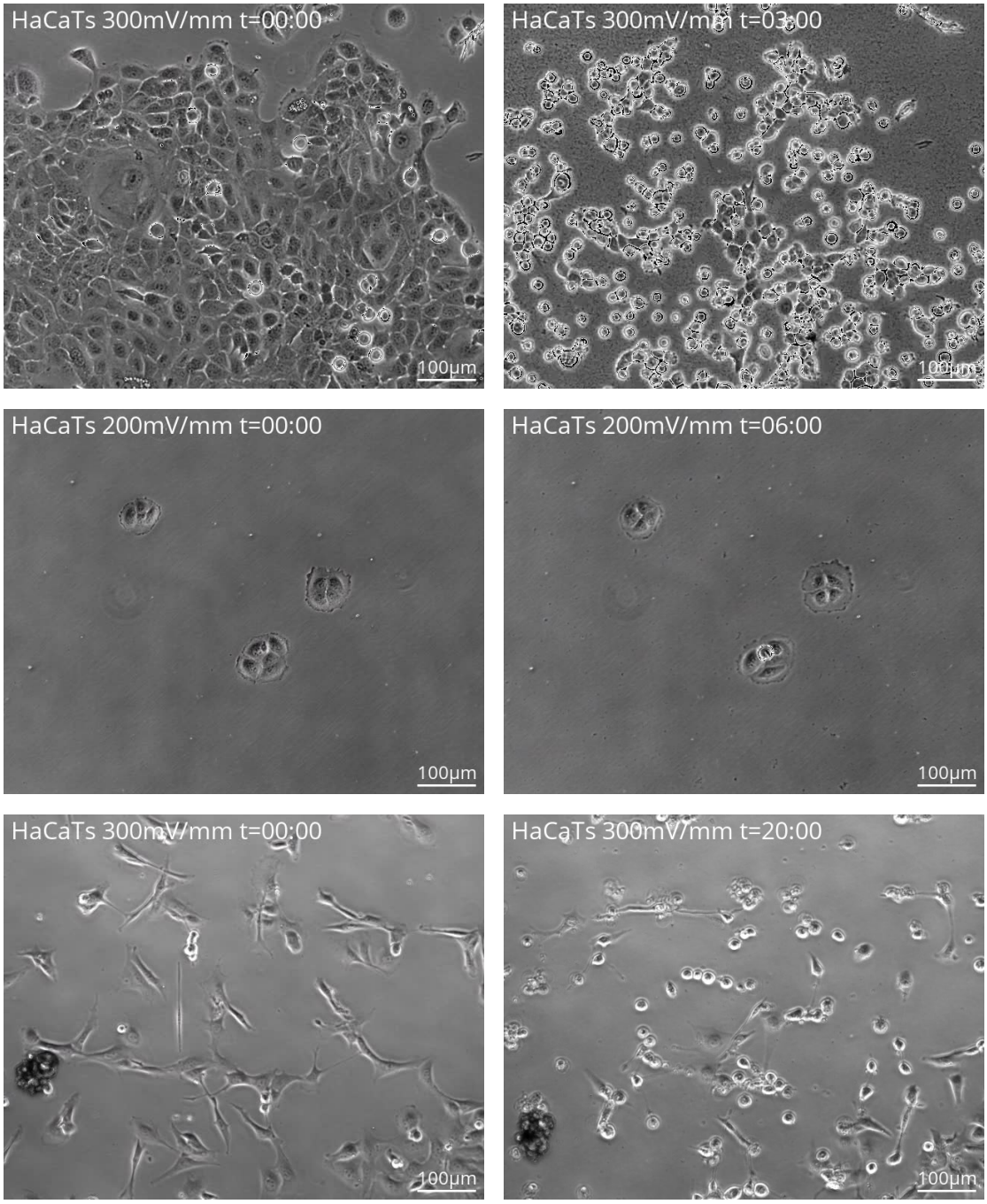

FIGURE 5.6: Microscope images of the cells at the beginning (left) and end (right) of the experiments. Top: HaCaTs, exposed to 3 V (300 mV/mm), directly into their wells, 2nd row: HaCaTs exposed to 2 V (200 mV/mm), directly into their wells, 3rd row: 3T3s, 2 V (200 mV/mm), directly into the well. Timestamps are given in hours and minutes. Full videos are available at https://doi.org/10.5258/SOTON/D2796.

5.3 Scratch Test

A variation on the migration assay which has also been used to evaluate electrical stimulation is a scratch test [178, 179]. This involves allowing the cell culture to become 100% confluent, completely covering the base of the well. A small, plastic pipette tip is then dragged across the centre of the well to create a gap approximately 500 µm wide. The well plate was then placed in the timelapse microscope and monitored as the gap was closed.

In this test, only HaCaTs were used as their physiological role is to form complete layers while fibroblasts typically do not.

As previously, three wells were left as controls in each test while another three wells were given electrical stimulation using wires placed directly into their media. Tests were conducted with constant fields of 100 and 200 mV/mm and with 300mV/mm pulsed with a 50% duty cycle.

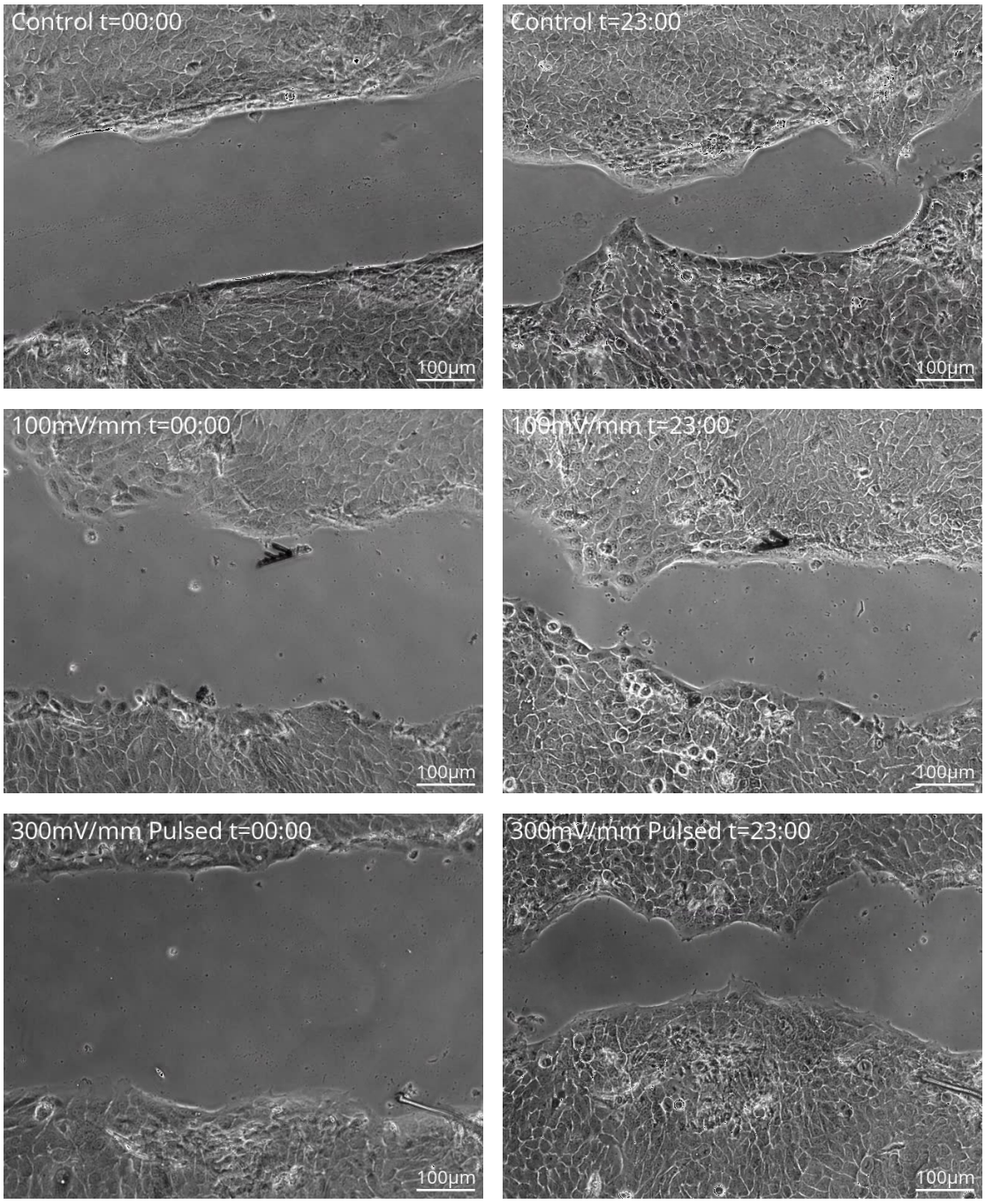

FIGURE 5.7: Microscope images of cells at the beginning (left) and end (right) of the scratch test. Top: Controls, 2nd row: 1V (100mV/mm), 3rd row: 3V (300mV/mm) pulsed. Timestamps are given in hours and minutes. Full videos are available at https://doi.org/10.5258/SOTON/D2796.

As shown in figure 5.7, the scratch in the cell layer shrinks significantly in all tests over the course of 23 hours. However, there is no visible difference between any of the cells which were exposed to stimulation and the controls.

In one case, when testing with 1 V, the cells on both sides of the gap visibly receded, with many of the cells dying by the end of the experiment. This only happened in one

instance out of 6 tests with that stimulation, so is likely to be the result of contamination in that particular well.

The remaining results show that the HaCaTs are continuing their usual behaviour of proliferation and migration across a scratch in the environment of the experiment, and are doing so both with and without an electrical field. However, the fact that electrical stimulation neither speeds up the closing of the scratch nor makes one side advance faster than the other is unexpected given the cells' reported sensitivity to electric fields.

5.4 Alamar Blue Metabolism Test

To identify possible problems in the experimental procedure, an alamar blue metabolism assay was conducted. It has been shown that electrical stimulation, applied through metallic electrodes directly into the cell's media can increase metabolism as a result of the chemical reactions occurring around the electrodes [180]. This can be assessed using alamar blue, a non-fluorescent blue dye which cells are able to metabolise into resorufin which is pink and highly fluorescent. By adding alamar blue to a culture's media and later measuring the media's florescence, a measure of the total metabolic activity of the culture can be acquired [181].

Wells of both HaCaTs and 3T3s were plated and incubated for 72 hours, before having electrical stimulation applied for 1 hour a day for three days using steel electrodes. Initially, this was done with an electric field of 100 mV/mm, as recommended by [180], but this caused complete cell death and discolouration of the media, so was reduced to 60 mV/mm. The cell media was changed after 48 hours of incubation before the second day's stimulation was applied. As well as the one well of each cell type that received the stimulation, two wells were kept as controls and were grown as normal.

Immediately following the final day's stimulation, the media was changed to introduce 10%v/v alamar blue. An additional well which contained no cells was also filled with this media as a reference. The well plate was incubated for 4 hours and the media was transferred to an opaque walled well plate. From each well of the cells' plate, two media samples of 200 µl were taken.

The fluorescence of the media was measured using a Promega GloMax plate reader and the results are shown in figure 5.8.

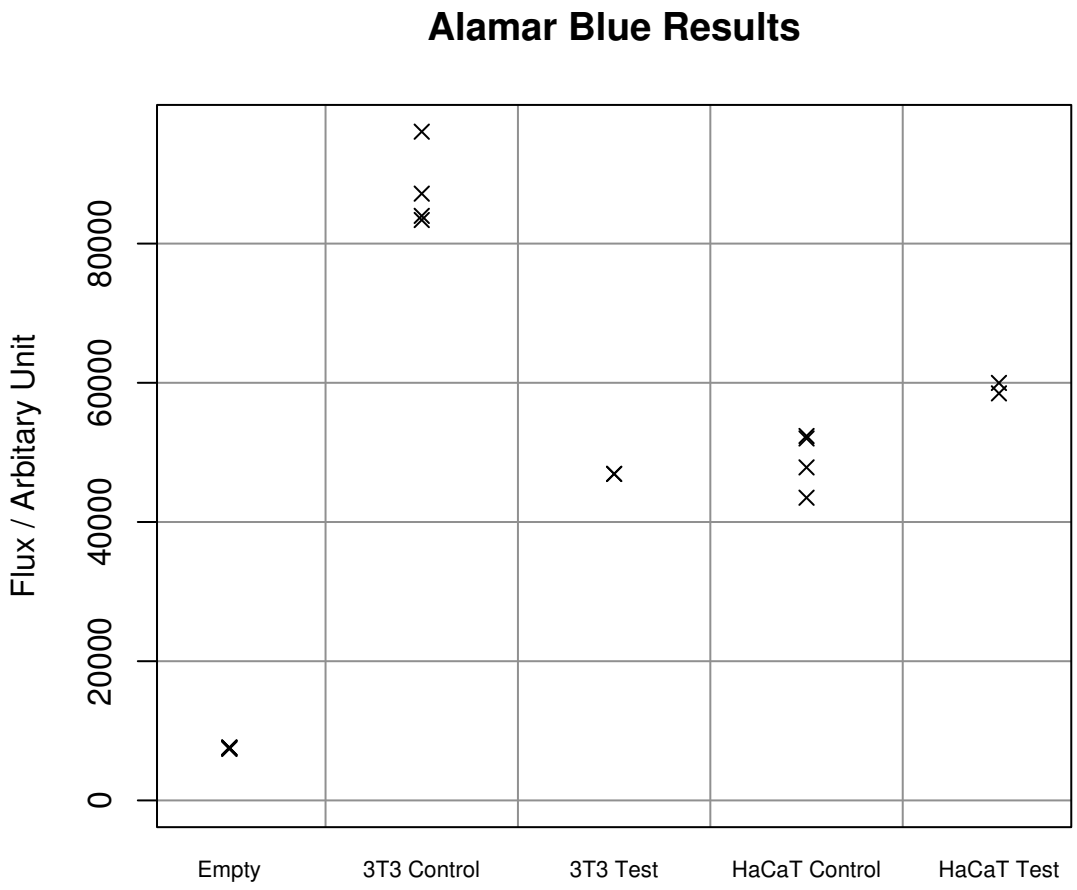

FIGURE 5.8: Results of the alamar blue metabolism assay. The higher the calculated flux, the more metabolism occurred. The 'empty' column is from the well which contained no cells at all.

While the stimulated HaCaTs do show a slight increase in metabolism compared to their controls, the difference is small and given the low number of repeats cannot be considered conclusive. The 3T3s meanwhile should a remarkable decrease in metabolism when given electrical stimulation. Again the number of repeats is small, but the large distance between the control and test results implies that the stimulation was actively harmful to the cells.

5.5 Conclusions

The experiments in this chapter were intended to identify the optimal stimulation waveform for inducing directional migration in cells responsible for wound healing. This information could then be used to inform the design of new stimulation circuits.

However, both experiments described above gave predominantly negative results, failing to show any induced migration. The fact that the methods used were copied from

successful reports in the literature implies that something unaccounted for was causing the failures, rather than it being a case of incorrect experimental parameters.

One possible explanation is that the precise cell lines used were not suitable. This is unlikely however, as both keratinocytes and fibroblasts have been successfully used in electrotaxis studies [39, 40, 41, 43, 44, 74, 77, 78] which, combined with the fact that several other cell types have also yielded positive results, indicates that using a slightly different cell line should not have caused the entire experiment to fail.

Another potential source of problems is the chemical reactions occurring at the electrodes. Cell growth media contains a large variety of complex chemicals [182] and a wide variety of chemical reactions can occur at the surface of the electrodes when a current is passed through them. As such, the choice of electrode material is very important. Most studies choose to use platinum [180] or silver-chloride [41] which are particularly inert, however, both silver and steel have yielded positive results in the past [74, 81].

Further work would be needed, focusing on these areas, to identify the precise issue limiting the experiment. For example, a thorough chemical analysis of the changes induced in the media or a repetition of the experiment with cell lineages identical to those used in the literature may offer more information on the problems with this experiment.

Chapter 6

Stimulation System Design and Integration

6.1 Introduction

To show that e-textile manufacturing techniques can produce a wound stimulation device that would be comfortable and unobtrusive to a patient, the required components of such a device were investigated. Such a device should be small enough to be worn under a patient's clothing. As much of the electronics as possible should be removable from the dressing so that it can be reused when a dressing is replaced.

The aim of the work in this chapter was to produce a prototype device that fulfilled these requirements as well as to explore the possibility of adding additional sensing and interface capabilities.

6.2 Flexible High-Voltage Stimulation Circuit

The core of the stimulator is the circuit that generates the stimulation voltage. With the experiments in the previous chapter offering no further information on the best stimulation waveform, it was chosen to target a high voltage pulsed waveform, favoured by more recent investigations [67]. However, generating the up to 200 V used in these protocols on a small, battery powered circuit, presents a challenge. The lithium polymer based batteries that are the current state of the art for small electronic devices provide around 3.7 V so a boost converter is required to generate the higher voltage which can then be switched using a transistor to produce the stimulation waveform.

To keep the completed stimulation device small and flexible, it was necessary to choose components that were themselves as small as possible. This limited to voltage that could

be generated in two ways. First, small, surface mount boost conversion ICs typically have output voltages limited to little more than 100 V. Secondly, smaller lithium polymer batteries are only able to produce a certain amount of current without overheating and becoming dangerous.

The LT1072 boost converter chip was chosen for this design. It is available in a 5 × 6 mm SOIC-8 package and has a maximum output voltage of 65 V. Similarly sized chips exist with higher output voltages, for example the LT8300 and MP6000 series, but the LT1072 was chosen because it was available for purchase and because other parts of the circuit limited the output voltage even further. Specifically, the LP-402025-1S-3 battery is only able to provide 60 mA of continuous current which limits the voltage particularly during start up when the large output capacitor is first being charged.

The problem of start up current draw is partially mitigated with the addition of a second capacitor in parallel with the upper resistor of the feedback potential divider. The boost converter controls its output by ensuring that the voltage of a potential divider connected to the output is the same as a constant reference (1.24 V for the LT1072). Placing an extra capacitor in parallel with the upper resistor effectively short circuits that resistor when the converter is first turned on, giving it a very low target voltage. As this capacitor charges up, the target voltage rises, causing the output capacitor to be charged gradually and keeping the total current draw of the system as low as possible.

The complete boost converter circuit is shown in figure 6.1.

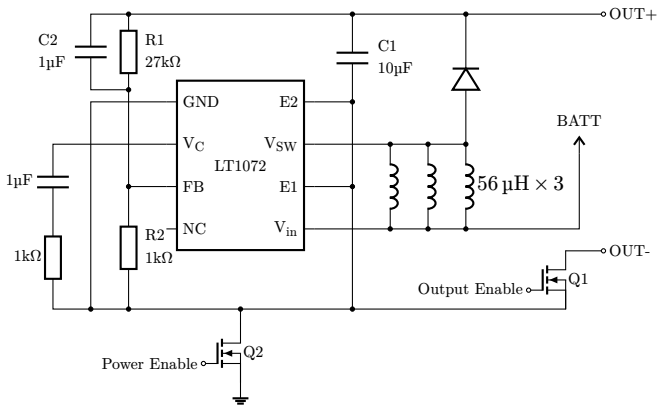

FIGURE 6.1: Boost converter circuit used to generate the high-voltage stimulation signal. The circuit is based around the LT1072 boost converter IC in a SOIC-8 package. The output can be switched using transistor Q1 to provide the pulsed waveform wound healing stimulation requires. Transistor Q2 can be used to disable the entire boost converter to save power.

Larger batteries are capable of providing greater currents, but to use one of these would be to enlarge what is already the largest and least flexible component of the device. The LP-402025-1S-3 battery is 20 × 25 × 3 mm in size, taking up as much space as the rest of the boost circuit and its controller (figure 6.2).

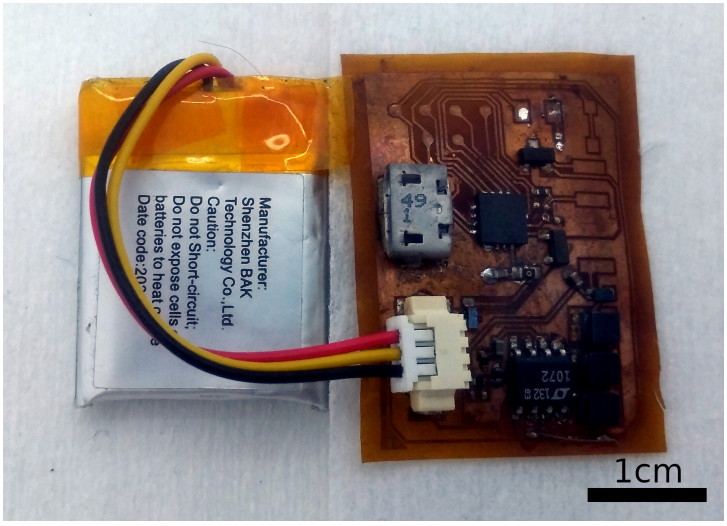

FIGURE 6.2: Miniature flexible high-voltage stimulation circuit connected to the battery that powers it.

The flexible circuit board was created using copper coated polyimide (GTS Flexible Materials Ltd, Rassau, Wales): a 25µm thick sheet of polyimide coated with an 18µm layer of copper. Unwanted copper was removed using a variation of the photolithographic etching process described in [18]. The copper was spin coated with Microposit S1813 G2 positive photoresist (Micro Resist Technology GmbH, Berlin, Germany) as 2000 rpm. The areas where the copper needed to be removed were exposed using the screen of an Elegoo Saturn 8K resin 3D printer (Elegoo Inc, Shenzhen, China) with the exposure time set to 3 minutes and the photoresist was washed off using AZ 400K developer (Merck KGaA, Darmstadt, Germany). The exposed copper was then etched using a solution of sodium persulphate etching crystals (Fortex Ltd, Lincoln, UK) in a PA104 bubble etch tank (Mega Electronics, New Brunswick, USA).

Based on the skin impedances measured in chapter 4, the converter was connected to a 560 kΩ resistor in parallel with a 10 nF capacitor with an additional 100 Ω resistor in series for testing. Measuring the output across this load with a Tektronix MSO 3014 oscilloscope yielded the plot shown in figure 6.3. The figure shows a 100 ms pulse, but the circuit was able to maintain its voltage across that load continuously, meaning that the frequency and duty cycle are limited only by the speed of the microcontroller.

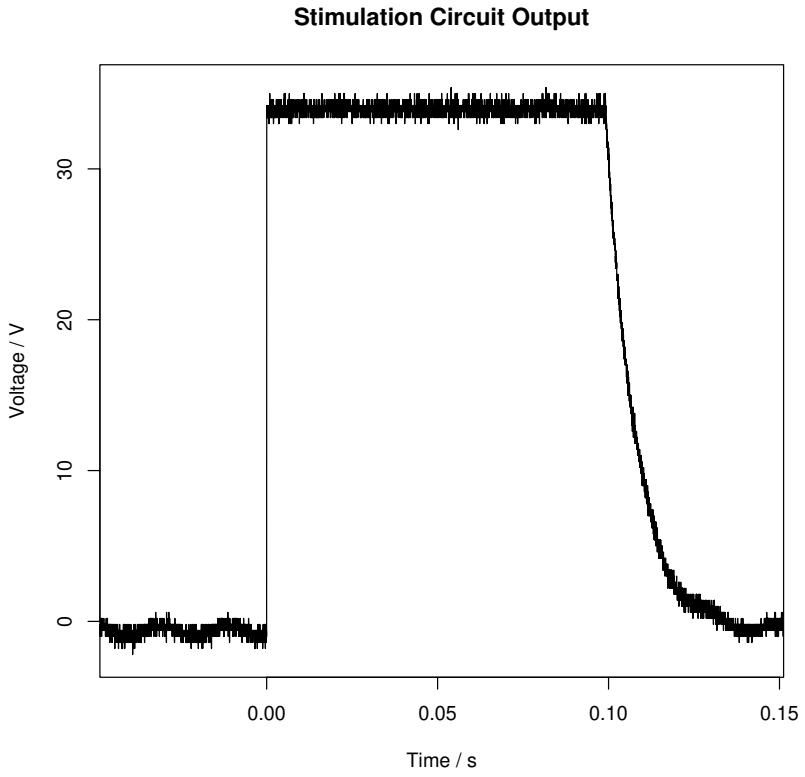

FIGURE 6.3: Output voltage of the boost converter, showing that it is able to produce 100 ms pulses of up to 35 V.

Most high voltage stimulation waveforms used in the literature use pulses that are only microseconds in duration [67]. 100 ms pulses at 10 Hz were chosen to test the stimulation circuit, both because the lower output voltage would need to be compensated with a higher duty cycle, and because, if the voltage generator can sustain its output for 100 ms, it is very likely to manage the shorter pulses of a more typical HVPC waveform.

6.3 A Magnetic E-Textiles Connector Concept

Wound dressings have an inherently limited lifespan and several different types of dressings are often applied as a wound moves thought the stages of healing. Were the battery and stimulation circuity permanently integrated into the dressing, they too would need to be disposed of and replaced several times during a wound's healing. This is an issue that affects many other e-textile devices: in attempting to keep the delicate electronic components protected and unobtrusive, they are completed ensconced within the textile host, making separation for recycling very challenging and meaning that parts cannot be replaces as they wear out. This, being both environmentally and financially undesirable, creates a need for an impermanent connector between the parts of the device that have different lifespans.

A number of different approaches to the problem of flexible, e-textile connectors have been considered in the past [169]. Some use a permanent fixture such as an eyelet [183] or crimp [184] to attach to the textile, then use a standard rigid connector to attach to that. This system allows the connection to the textile to be much more robust than if it had to be removable, though it does require adding rigid components to the device, the boundaries of which are known to be a common point of mechanical failure for flexible conductors [18].

Other designs have adapted components native to textiles which share their flexible properties, for example, creating conductive Velcro. However, the conductive coating used on Velcro has been shown to wear off after repeated use [185]. The opening and closing of a zip has been employed as an electrical switching mechanism [186], but zips are not useful for increasing modularity as the parts of an e-textile device are rarely just two sheets needing to be joined edge to edge.

An alternative basis for e-textile connectors is the combination of magnets and spring loaded contacts. Magnetic fastenings are attractive because they are self-aligning and, with judicious use of polarity, can enforce correct orientation. Magnets have been used directly as connectors [187], but their inability to be soldered without demagnetising makes this challenging. Using magnets to hold sprung connectors in place solves this problem and has the advantage that the receiving side of the connector is simply an exposed conductive pad. This makes manufacturing easier and increases the flexibility afforded to the design. It also means that when disconnected, the connection mechanism is completely unobtrusive.

Thus far, such systems have only been realised using spring loaded "pogo" pins [169, 188]. Shown in figure 6.4, these consist of a spring loaded pin inside a hollow metallic cylinder. As a result, pogo pins cannot compress to less than half their original height. This creates a compromise between the total thickness of the device and the working contact range of the connector. Because the spacing between the tips of the pins needs to remain the same as that of the bases, the material the pins are attached to must also be rigid.

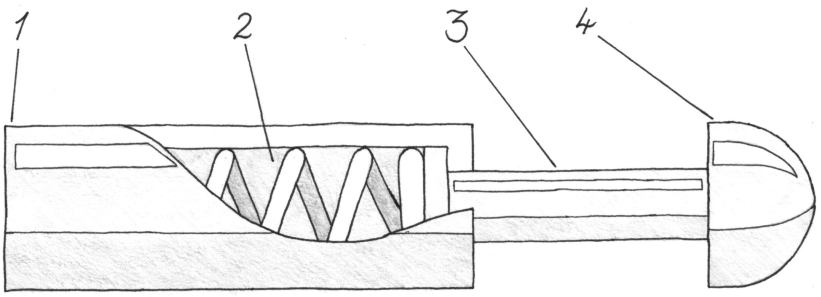

FIGURE 6.4: Pogo pin mechanism. (1) Fixed barrel which is permanently attached to one side of the connector, (2) Spring, (3) Movable pin, (4) Contact head.

An alternative that is more suited to connections between two flexible devices is spring finger connectors. These are 'C' shaped metal contacts, the bottom of which is soldered to a PCB. When compressed onto an opposing contact pad, they form a reliable, electrical connection. While this system occupies more lateral space than one based on pogo pins, it can compress almost flat so is better suited for devices where a low profile is a requirement.

Such a connector would itself have properties beneficial for sustainability: the easily accessible spring fingers contacts can be replaced in situ if broken and the encapsulated magnets are unlikely to demagnetise during standard use and can be easily recovered at the end of the product's lifetime. The metallic construction, using materials already present in most electronic devices, means that the recycling process is not complicated by the connector's inclusion.

Detailed below, is the evaluation of such a system, identifying the key requirements of its design to allow development of future reliable connectors for e-textiles.

6.3.1 Method

6.3.1.1 E-Textile Connector Test Device Design

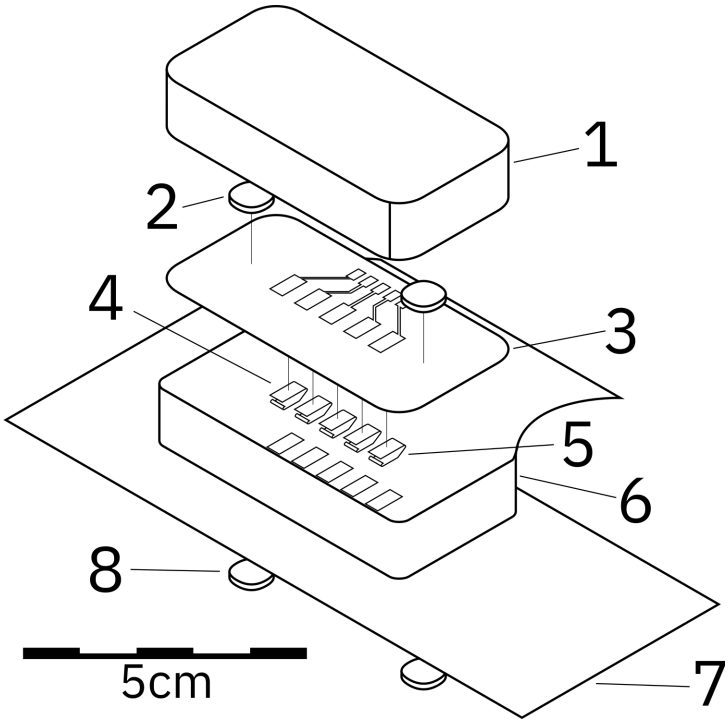

FIGURE 6.5: Design of the test device. (1) Foam backing, (2) Magnets × 2, (3) Flexible PCB connecting contacts to test pads, (4) Spring finger connectors, pin 1, (5) pin 5, (6) Fabric cover, (7) Copper sheet, (8) Magnets used to hold device down × 2.

The proposed connector system was tested using the design shown in figure 6.5. A flexible, copper coated polyamide (GTS Flexible Materials Ltd, Rassau, Wales) circuit board was produced, using the photolithographic etching technique described in [18], with five pads 5 mm apart to which the spring finger contacts were soldered. Two different spring contacts were tested, both from TE Connectivity: the smaller 1447360-8 (1.3 mm high) and the larger 1438259-6 (4 mm high). The flexible circuit board connected each spring contact to a copper pad, to which a length of light weight litz wire was soldered to connect to an oscilloscope.

Either side of the contacts, N850 cylindrical magnets (Eclipse Magnetics, Sheffield, UK) were attached using double sided tape. The magnets were 6 mm in diameter, 1 mm high and had a pull force of 0.3 kgf. Their small size allowed them to be incorporated into the device without noticeably impacting its flexibility.

Above the PCB, was a 10 mm thick layer of foam (Anyfoam Ltd, Welwyn Garden City, UK). This was used to add some rigidity to the device so that the middle pins did not completely fold up and lose contact. Five different types of foam, described in table 6.1, were tested.

	Density kg/m^3	Hardness N	Flexural Rigidity Nm^2
1 (Softest)	21 - 24	86 - 110	1.62×10^{-5}
2	31 - 34	100 - 130	1.07×10^{-4}
3	38 - 40	180 - 220	1.16×10^{-4}
4	48 - 52	225 - 265	1.51×10^{-4}
5 (Hardest)	20 - 22	225 - 275	1.83×10^{-4}

TABLE 6.1: Backing foam properties [189].

The whole device was enclosed in a polyester-cotton cover with holes cut in the bottom to allow the contacts through (figure 6.6). This design was chosen for the purpose of easier testing, in a final application it could be significantly more compact.

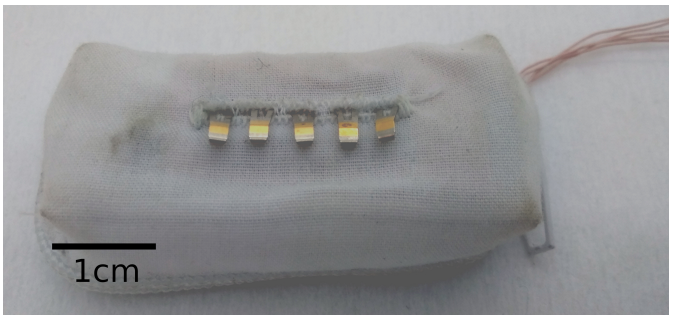

FIGURE 6.6: Test device with spring finger contacts protruding from the underside. A zip was included in the cover to allow the backings to be easily swapped but would not be required in a real application.

A sheet of copper coated polyamide was used as the other side of the connector for all five pins. Two more N850, 6 × 1 mm magnets were placed underneath it. It was given a fabric backing and litz wire was used to connect the sheet to the oscilloscope.

6.3.1.2 Testing Procedure for the Magnetic E-Textile Connector

Methods for testing e-textile devices are slowly becoming standardised [190, 163], however, no completed standard exists describing the type of test needed here. As such, a testing methodology was devised to simulate the conditions the connector would endure as part of a wearable, e-textile device, optimised to reveal the differences between the various configurations. Since this work began, a draft standard for measuring the resistance of e-textiles during bending has been published [162] which has some similarity with the method presented here, but it focuses on conductive materials rather than the connection between modules.

The method used here involved mounting the copper sheet into a bespoke bending rig [18], shown in figure 6.7. The bending rig holds a length of fabric under tension while pulling it back and forth over a cylindrical axle. In this case, a 90 mm diameter axle was used. During each test, the connector was passed across the axle at approximately 1.25 Hz for 5 s.

FIGURE 6.7: Test device mounted on the bespoke bending rig [18]. The real time connection between the copper sheet and each pin of the device was tested as it was pulled back and forth over the grey cylindrical axle.

Data was collected on whether a connection occurred between the copper sheet and the each pin of the connector via a potential divider connected to an oscilloscope. If the

pin made contact, the voltage between it and the copper sheet would be zero, if not, a voltage would appear. The reliability of each pin was quantified as the fraction of the time it maintained a connection as it moved over the axle of the bending rig.

6.3.2 Results & Discussion

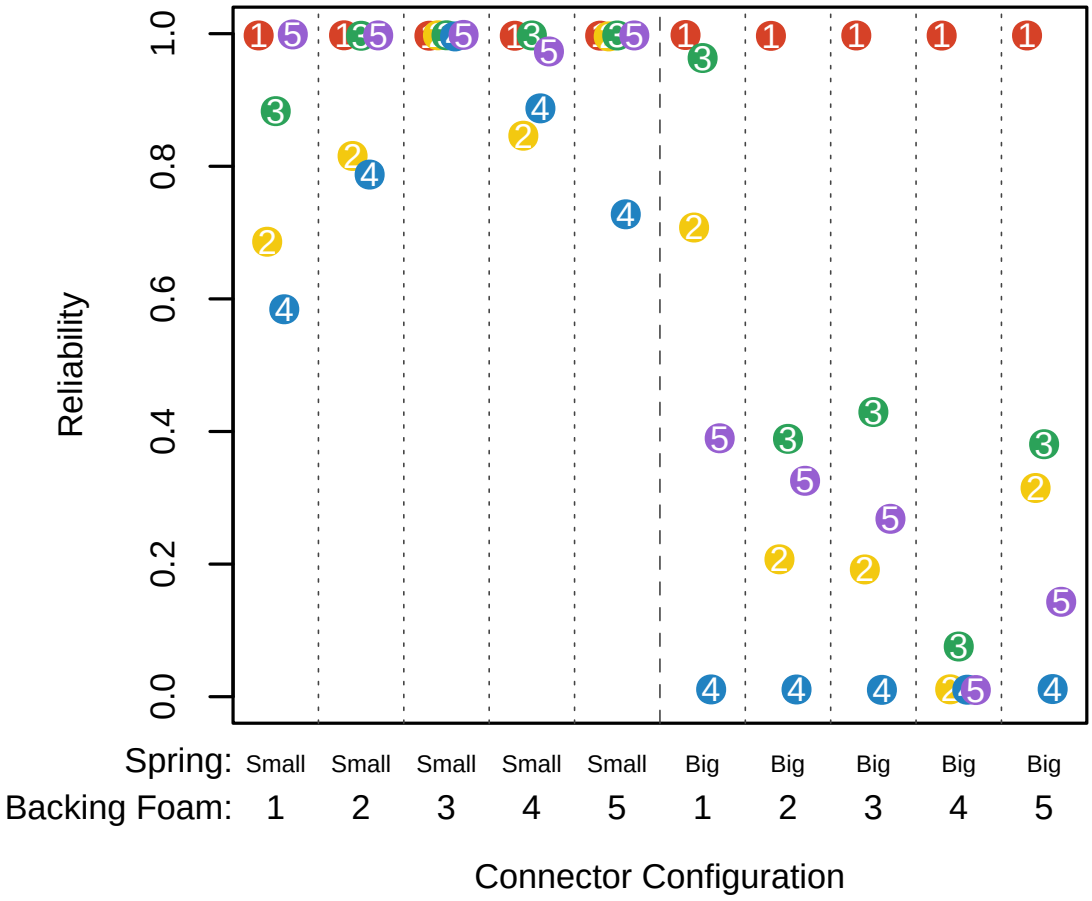

FIGURE 6.8: Pin reliability for each connector configuration. Reliability is the fraction of the time a connection was made. The result for each pin is shown by the position of the corresponding number.

The reliability values for each pin in each configuration are shown in figure 6.8. The most common failure mechanism observed during the experiment, illustrated in figure 6.9, was when the magnets, pulling the connector down on either end, combined with the outer two pins to lever the central pins up, preventing them from making contact. This is shown in results as pins 1 and 5 being always more reliable than pins 2 and 4 respectively. With the softest backing (foam 1) and the smaller pins, the dent in the foam caused by this effect reached far enough to affect pin 3 as well.

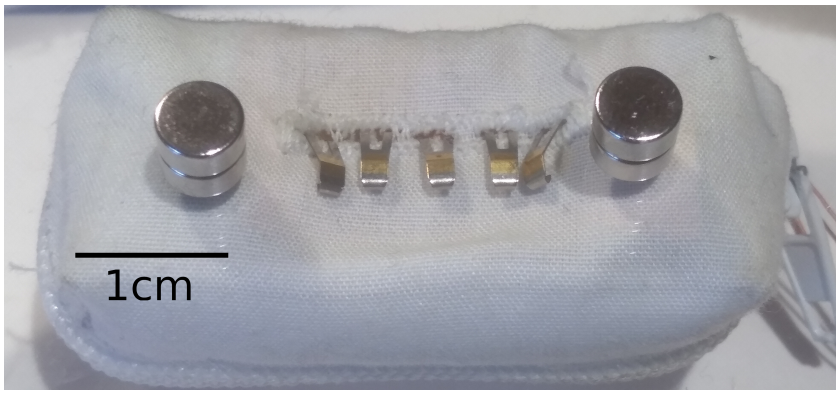

FIGURE 6.9: Underside of the test device with backing foam 1, shown through glass so that the compression could be viewed. The magnets pull the ends of the connector down to the surface, creating an angle that lifts the central pins away.

In the case of the larger springs, pin 1 was sufficiently large for the levering effect to affect every other pin. With the more flexible backings, the magnet at the far end was able to bend the connector and make pin 5 connect some of the time, but with more rigid backings, this happens less frequently. At the points where pin 5 does make contact, that end of the connector is at a sufficiently steep angle that pin 4 is still much farther up, keeping its reliability at 0. Despite the symmetry of the connector, pin 1 is always favoured because it was initially the farthest from the axle of the bending rig: as the copper sheet was bent, it peeled away from pin 5 first, allowing pin 1 to establish a reliable connection at the expense of the pins at the other end.

Using the optimal backing, with a rigidity of $1.16 \times 10^{-4} Nm^2$, the smaller pins were able to reach 100% reliability in this test, however, the smooth surface of the copper sheet they were connecting to is not necessarily representative of a real e-textile application. Were the contact surface less uniform, the small working range of these pins may have caused them to become less effective. A solution to this would be to use spring finger contacts with a larger size but a lower spring constant. This would allow the pins near the magnets to simply compress, rather than levering the inner contacts upwards. However, because spring finger contacts are primarily used in rigid electronics [191], the spring constant is not often specified, making suitable versions difficult to identify so a bespoke design for e-textiles would be required.

The need to control the rigidity of the connector's backing can reduce the overall flexibility of the device slightly. Using contacts with a lower spring constant would help here too as softer springs will need a less rigid backing to hold them down.

6.3.3 Conclusions

Magnetically secured, spring finger connectors have several properties that make them appealing as e-textile connectors: their small size, mechanical compliance and simplicity

make them good candidates for integration into e-textile devices.

However, the results presented here show that size of the springs and the rigidity of their backing must be carefully chosen to ensure reliability in the dynamic environment in which e-textile devices can be used. If the device's backing is too soft, pins near the fixing magnets can push their neighbouring contacts upwards, causing their connection to break. A backing that is too rigid however, is unable to respond when the surface to which it is connected bends.

Using larger contacts increases the risk of them lifting each other up, but smaller ones have a smaller working range, which would cause them to be less reliable when placed on uneven surfaces. Pins which require less force to compress would circumvent this trade-off, but due to the usual applications of spring finger connectors, these are not currently widely available.

While greater care is needed to ensure that this form of connector is electrically reliable, the complete lack of rigid components in the conducting path significantly reduces mechanical stress compared to standard electronics connector designs.

6.4 Integration of Temperature Sensing

While the various types of wound dressing are an essential tool in the treatment of wounds, covering up the wound makes it difficult to track its state and to monitor the progress of healing. This is particularly important when considering infections because how quickly an intervention can be applied can have a significant effect on the outcome [25].

This has created an interest in adding sensing capabilities to wound dressings, so that a wound may be monitored without having to remove the dressing [192]. A property of wounds that is easy to monitor electronically, and is a strong indicator of infection is temperature [25]. Because of this, a temperature sensor was chosen to add as a simple example of sensing.

6.4.1 Method

Panasonic ERTJ0ET102J, negative temperature coefficient thermistors were used in this work. These have a 1×0.5 mm footprint and a resistance of approximately 1 kΩ at 20°C. The thermistor was mounted on a small polyimide PCB (GTS Flexible Materials Ltd, Rassau, Wales) (shown in figure 6.10) which facilitated the connection to a Keithley 2000 multimeter for taking resistance measurements.

FIGURE 6.10: Thermistor mounted on a flexible polyamide PCB. It is shown here, encapsulated with interface.

The heat of the skin was simulated using a CIMAREC HP121220-33 hotplate set to 40°C, the precise temperature of which was measured using an Etekcity Lasergrip 1080 infrared thermometer before each test.

The thermistor's measurement accuracy and response time were measured by placing it on the hot plate for at least 60 seconds, then removing it and holding it loose in the air (approximately 10 cm to the side of the hotplate, to avoid its influence). When placed on the hotplate, the sensor was held in place with a length of Kapton adhesive tape, stuck across the middle of the circuit in figure 6.10, not over the thermistor itself. This provided constant force at the interface with the hotplate, without adding additional insulation around the thermistor. During the experiments, the resistance of the thermistor was logged to a PC at a rate of 10 Hz.

A number of different relevant materials were placed above and below the thermistor to identify how its placement around a dressing would affect the readings. The different configurations are shown in table 6.2.

	Above	Below
1	—	Polyamide PCB
2	Polyamide PCB	—
3	Fabinks IF-UV-1004 interface	Polyamide PCB
4	Polyamide PCB	Fabinks IF-UV-1004 interface
5	PCB and Molynlyke Mepore dressing	—

TABLE 6.2: Material placed above and below the thermistor in the different testing configurations. 'Below' means between the thermistor and the hotplate, 'above' means insulating the thermistor from the surrounding air.

To know the relative extents to which the air and hotplate temperatures were influencing the thermistor's reading, it was necessary to obtain a precise mapping between the thermistor's temperature and its resistance. This was done by placing the thermistor in a Weiss WKL100 environmental chamber, setting it to a variety of temperatures between 20 and 45°C and, once the temperature had settled, measuring the thermistor's resistance. These values were then used to find the parameters R_{25} and B in equation 6.1 which governs the resistance R of a thermistor at temperature T, in °C.

$$R = R_{25} e^{B \frac{25-T}{(25+273.15)(T+273.15)}} \tag{6.1}$$

6.4.2 Results

The calibration measurements closely followed the predicted curve, shown in figure 6.11, giving $R_{25} = 854.6\Omega$ and $B = 3870.8K$.

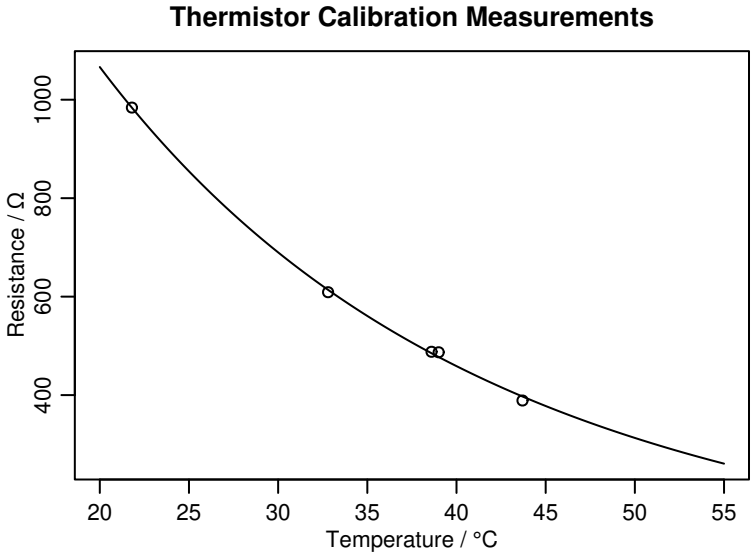

FIGURE 6.11: Thermistor calibration data. The circles show the recorded data points; the line is the best fit of equation 6.1.

For all configurations, the relationship between the thermistor's reading and the time since its movement was an exponential curve, as would be expected for Newtonian heating. An example is shown in figure 6.12. Similar graphs were plotted for each configuration and from the heating cases, the time constant and resistance asymptote (and thus relative surface and ambient temperature influence) were extracted. These values are shown in figure 6.13.

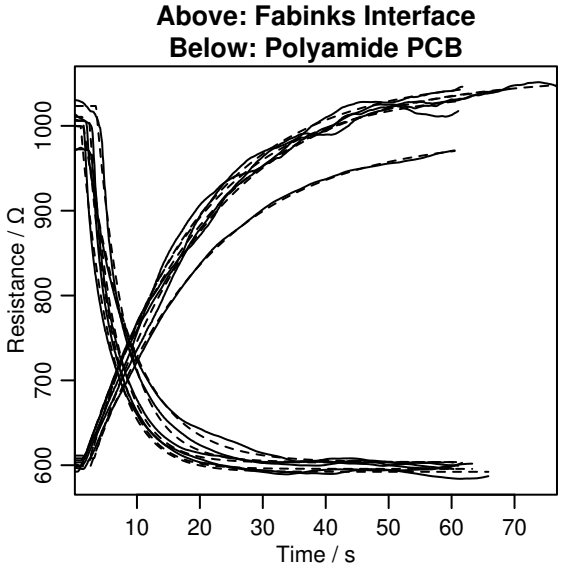

FIGURE 6.12: An example transient resistance response as the thermistor is placed on and removed from the hotplate. In this case, the thermistor's PCB was underneath it and a layer of Fabinks IF-UV-1004 interface was on top.

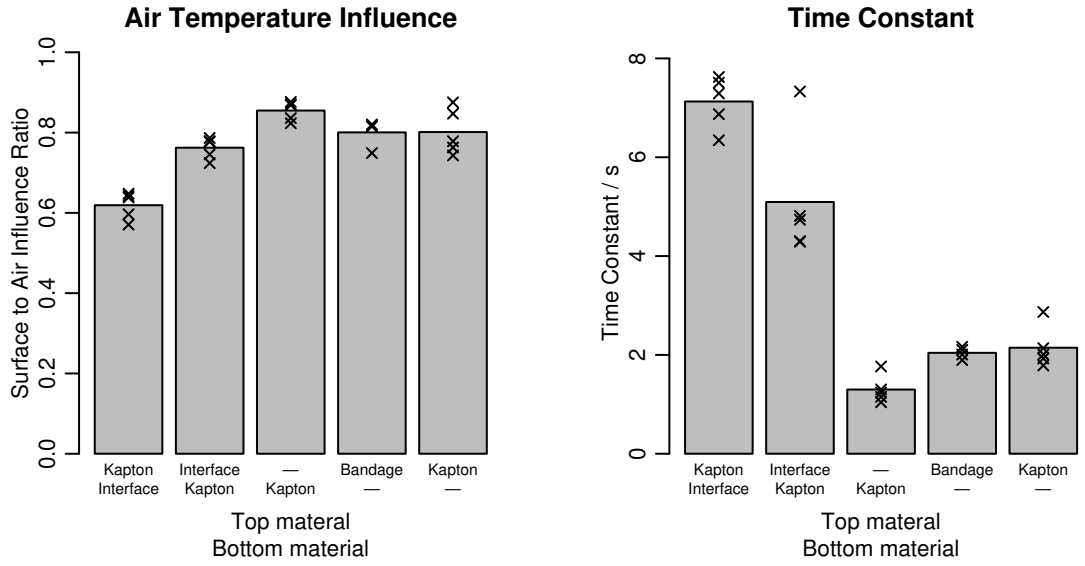

FIGURE 6.13: Effects of different materials placed around the thermistor. The left graph shows the weighting of the hotplate surface temperature and the air temperature in the thermistor's readings. The right hand graph shows the time constant of the thermistor's response to a sudden change in temperature.

The graph of air temperature influence in figure 6.13 shows that, in most cases, about 80% of the thermistor's reading comes from the surface it is placed on and 20% is dependent on the surrounding temperature. This means that large changes in ambient temperature, for example, a patient moving from inside to outside, would produce a change in reading as large, if not larger than the changes in skin temperature that are being looked for.

The best configuration for avoiding air temperature interference was having the polyamide PCB against the hotplate with nothing on top. This performed even better than having the thermistor directly touching the hotplate surface. The implication of this is than having good thermal contact with the surface being measured is more important that having close proximity or having insulation on the top side.

Having the PCB below and nothing above also gave the fastest response, with a time constant under 2 seconds. Adding interface either on the top or on the underside, significantly increased the response time, however it remained under 10 seconds, meaning the system would still accurately track temperature changes due to an inflammation reaction which typically happen over the span of a few minutes [25].

6.4.3 Conclusions

To prevent a thermistor from being short circuited when mounted on a wound dressing, it would be necessary to encapsulate it under a non-porous coating. The results presented above show having interface paste between the thermistor and the surface it is measuring significantly worsened both the influence of ambient temperature and the response time. Given this, it would be advisable to use the thinnest coating layer possible and the have a second thermistor mounted further away from the skin to compensate for ambient temperature changes.

6.5 System Integration and Conclusions

An e-textile device was designed and fabricated to provide a wound healing stimulation signal. This included a 30 V voltage generator to provide the stimulation voltage, a magnetic connector to hold the device to a dressing and basic sensing capabilities to track wound temperature. The complete circuit is show in figure 6.14.

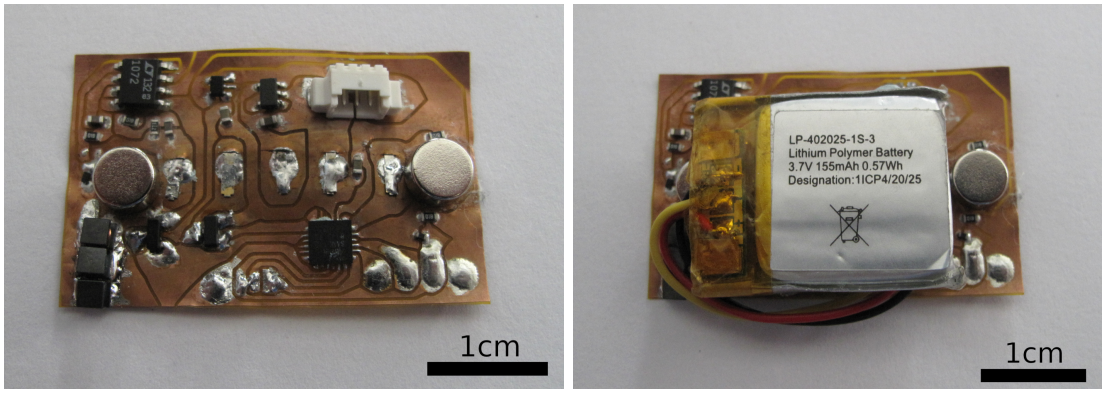

FIGURE 6.14: The complete stimulation circuit, including the high voltage boost converter, control thermistor and a microcontroller (left) and shown with its battery (right).

The connector used the smaller size of spring finger contacts, found to be the most reliable in section 6.3. The fabric cover was padded with loose stuffing, which could wrap around the battery and was compressed to approximately the same stiffness as the most effective backing foam. The five pins of the connector are used for ground, a connection to the embedded thermistor, the positive and negative stimulation voltages and a supply connection for recharging the battery. This last pin is not connected on the dressing, but allows the device to be recharged by simply placing it on a charging pad.

The device is shown, attached to an example printed electrode dressing, in figure 6.15. The outward facing contacts were provided using a second, etched, flexible PCB, attached to the printed traces and exposed through a notch cut in the edge of the dressing.

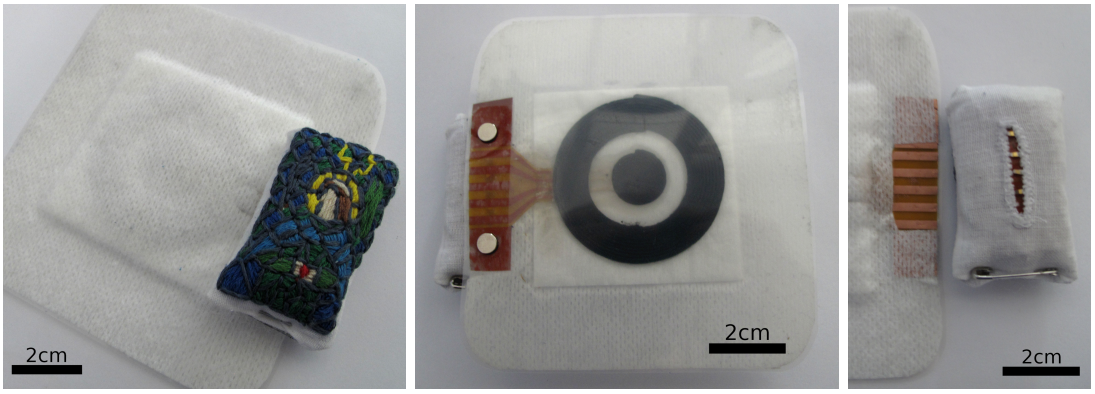

FIGURE 6.15: The encased stimulation device mounted to a dressing with a printed electrode and thermistor, shown from the front and back (left and centre) and with the connector separated (right).

Because the non-permeable interface layer is only printed beneath the electrodes and the interconnects, the dressing would still be able to transfer moisture, air and heat. The addition of the electrode does increase the height of the dressing, but the pressure applied to the wound can be kept constant relative to an unaltered dressing, by adjusting how tightly the dressing is stretched as it is applied.

In total the device is approximately 10 mm in height. As with many e-textile devices, the majority of the thickness is taken up by the battery which also constitutes the main limitation on the device's flexibility. The battery is however, small enough that this limitation does not prevent it from sitting reasonably flush against most parts of the body or being worn under clothing.

The small size, along with the newly developed connector, demonstrate the potential for e-textile techniques to produce a ergonomic and user friendly wound stimulation device. At this stage, the device has only a very basic user interface: a single button for toggling the output and an LED to show that it is activated. This was sufficient for testing. The device was designed to allow the creation of a more advanced interface,

the same contacts which connect to a dressing can be used as digital IO to connect to a PC, and this would need to be implemented before the device could fully utilised. The device also lacks explicit safety features which would be necessary for it to achieve approval as a medical device.

Chapter 7

Conclusions

It is clear from the evidence presented in the literature review that electrical stimulation has a positive effect on wound healing. The fact that some studies found the healing rate of patients who were treated with electrostimulation to be twice that of control group patients suggests that, if optimised, the treatment could significantly reduce the burden on health systems presented by wounds and ulcers. The issue preventing the adoption of electrostimulation is that, while a large number of studies have investigated the treatment, they have all used different experimental equipment, protocols and inclusion criteria, meaning that they can not be combined into a single piece of evidence with enough significance to support its adoption.

E-textile printing techniques have been used for fabricating electrodes in the past, but the work in chapter 3 shows that dispenser printing can be used fabricate them directly onto uneven, compressible surface of wound dressings, using a newly developed system of height compensation. This system used a laser displacement metre and a modified the interface material, coloured in a way which complimented the wavelength of the laser's light. The results in chapter 3 showed that adding red or yellow pigment to an interface paste fulfilled this requirement with no negative effects on the printing or curing of the paste itself. The software that was written to automate the process of measuring and compensating for height changes allows new electrode designs to be printed on a wide variety of materials quickly and with minimal manual intervention.

To gain a better understanding of how electric current passes through the tissue, a pair of skin models were created, one an equivalent circuit of passive components, derived from physical measurements, and the other a COMSOL simulation derived from parameters found in the literature. While these two models agreed on the overall shape of the skin's impedance, they were not in agreement about the magnitude of the impedance at low frequencies, indicating that the data for the *stratum corneum* is inaccurate or incomplete.

An attempt was made to use this modelling data to simulate the effects of different simulation waveforms on cells *in vitro* to identify which produced the strongest migration. This is something clinical trials have so far been unable to identify, and is part of the reason why the methodologies of clinical trials have differed from each other. However, due to delays in access to the necessary cell culture laboratories at the Southampton General Hospital imposed by the coronavirus pandemic restrictions, there was insufficient time to fully explore this part of the work.

Finally, the necessary components for implementing a miniature, flexible stimulation circuit that could be connected to a wound dressing were investigated and combined into a prototype device for electrical stimulation of wounds. To improve the robustness of the system and allow for easy removal and replacement of the electronics, a magnetic connector was designed and optimised which allows the stimulator to be reused with multiple dressings. A battery powered, flexible circuit was designed and built which could provide a 30 V, high voltage stimulation waveform and interface with simple temperature sensors. The placement of these sensors was also investigated and it was found that the necessary encapsulation would affect the readings and would need to be compensated for.

This thesis has provided a prototype platform for the deployment of bespoke electrode wound healing devices which can provide electrostimulation in a more user friendly manner and would provide an opportunity for more consistent results from future clinical trials.

7.1 Future Work

The modelling work in chapter 4 revealed a discrepancy between the impedance predicted by the available data and that which was measured using real electrodes and an impedance meter. This occurred particularly with the data surrounding the *stratum corneum*. Obtaining better data for the electrical properties of that layer or otherwise resolving that discrepancy would allow the electric field inside the body to be calculated with much more confidence. It has also been shown that the electrical properties of the *stratum corneum* change when exposed to higher voltages such as those used in HVPC treatments [193]. To accurately model such waveforms, the model presented in chapter 4 would need to take these effects into account.

Future work would also continue investigations of the electrotaxis experiments, to identify why exactly the experiment in chapter 5 failed when equivalent experiments in the literature have reported positive results. If this can be done, the experiment could then be run to verify whether the results from Tsai et al. [41], hold when electrical losses in the skin considered. This would help to generate a consensus about what the optimal wound healing waveform is, and encourage future clinical trails, like the ones reviews

in section 2.6, to produce results that could be better aggregated then the data that is currently available.

The stimulation device itself, presented in chapter 6, is primarily limited by its source of power. The lithium polymer battery being used is only able to supply about 60 mA of current which limits the achievable output voltage. Additionally, despite being one of the smallest commercially available batteries, it is the largest component in the device, significantly increasing the overall thickness and decreasing the flexibility. As such, work increasing the current output and decreasing the size of batteries would be beneficial, as would efforts to make more flexible batteries.

Outside of wound healing, the connector described in section 6.3 could be used in other e-textile devices which would benefit from a modular design. The investigations of how moisture and pressure affect the electrode – skin impedance could be used in other treatments such electrography, impedance tomography, FES and TENS.

Appendix A

Miniature Flexible Reprogrammable Microcontroller Circuits for E-Textiles

This work was originally presented as a conference poster at E-Textiles 2022. The design did not end up being used in the device described in chapter 6, but has been used in other projects in the group, so is included here as an appendix.

A.1 Introduction

Microcontrollers are vital components in many e-textile devices [194, 164]. Their reprogrammability and wide range of peripheral functions means that they can fulfil the digital processing requirements of almost any small electronic product while their small size makes them possible to include in e-textile devices.

The ability of be reprogrammed is key to a microcontroller's utility, and most provide some means of uploading new programs while *in situ*, for example, AVRs' SPI based 'ICSP' protocol [195]. However, such systems typically only work with one brand of microcontroller and require specialised programming circuits to use. The connectors required to use these systems also occupy a large area: the header needed to connect the ATMEL ICE programmer to a QFN ATTiny occupies 4 times the area and 12 times the height of the chip itself, see figure A.1.

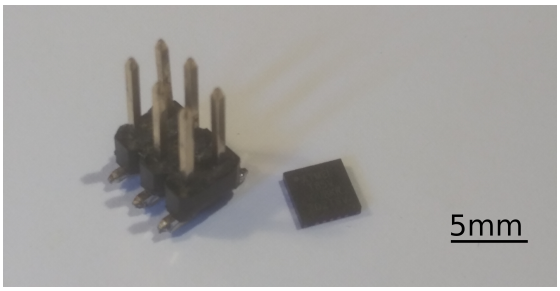

FIGURE A.1: A standard 2.54 mm, 6 pin programming header (left) compared to the ATTiny85 microcontroller it programs (right).

The first problem can be solved using a USB bootloader. This is a small program which is used to load new software via a USB connection. However, event micro-USB connectors are relatively large components in the context of e-textiles and would restrict the textile integration of a microcontroller circuit. A potential solution to this is to use an edge connector. These consist of a series of exposed pads near the edge of the circuit board. The board itself is then inserted into a receptacle with contacts arranged to connect with the pads. However, existing solutions are typically thicker (0.3 mm) flat flexible cables (FFCs), therefore connections can be difficult and unreliable.

A.2 Design

The system developed here uses five, 1 mm pitch, pads which need only protrude a few millimetres from the body of a flexible circuit board to connect to an external clip. The five connections are used for power, ground, positive and inverted USB data and a button operated reset line which prompts the microcontroller to run its bootloader. The clip contains all the additional components needed for USB programming: the micro USB connector, a 3.3 V voltage regulator, a reset button and several passive components. A diagram of this system is shown in figure A.2.

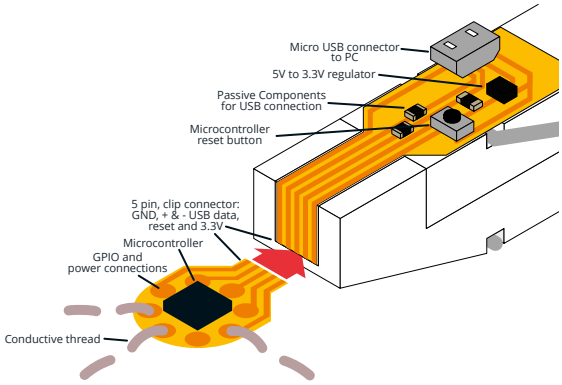

FIGURE A.2: Design of the microcontroller and programmer. Placing the components needed for USB programming on the clip means that only the microcontroller's IC needs to be integrated into the textile.

The system was tested using an ATTiny85 microcontroller [195] with the micronucleus bootloader [196].. Both the flexible microcontroller circuit board and the programming clip's PCB were made using a standard photolithographic etching process described in [18].

The contacts on both sides are tinned with solder to prevent corrosion and to raise the contact point slightly, making the connection more reliable.

A.3 Applications

The test implementation was incorporated into both woven (figure A.3, top left), and stretchable, knitted fabrics (figure A.3, right) by couching the conductive thread soldered to the general purpose input/output (GPIO) pins of the controller. Another version was made by inserting the device and its connecting wires into woven pockets in a custom made fabric (figure A.3, bottom left).

FIGURE A.3: Microcontroller circuit integrated into the collar of a garment (top left), a stretchable knitted fabric (right) and a custom woven textile (bottom left).

Because of its small size, the impact on the flexibility and stretchability of the fabric is minor. This is a major improvement over existing prototyping boards designed for e-textiles which are much larger and use rigid PCBs (figure A.4).

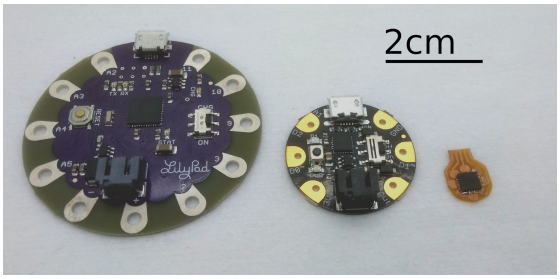

FIGURE A.4: Existing prototyping boards designed for e-textiles, left to right: an Arduino Lilypad (diameter 50 mm [197]), an Adafruit Gemma (diameter 28 mm [198]) and this work (10 × 12.5 mm)

This programming system can easily be adapted to other microcontrollers which are reprogrammable via USB.

A.4 Conclusions

This work presents an easy to use programmer, compatible with many different types of microcontroller. It occupies significantly less circuit board space than existing commercial equivalents; the prototype displayed here is 80% smaller than an Adafruit Gemma, and requires no additional components on the microcontroller board itself.

This is important in e-textile applications where a large size or additional rigid components can compromise the textile's properties of comfort and flexibility.

The small connector size and minor impact on integration mean that, when moving beyond the prototyping stage, the connector footprint may not even need to be removed, and if it is, only a small change to the circuit layout is needed.

The initial demonstrators also show that this methodology of flexible microcontroller integration and flexible connection points works with both couching into existing garment structures and integration during weaving.

References

[1] T. Greig, R. Torah, and K. Yang, "Electrical stimulation for wound healing: Opportunities for e-textiles," *IEEE Reviews in Biomedical Engineering*, pp. 1–14, 2022, doi: *10.1109/RBME.2022.3210598*.

[2] T. Greig, R. Torah, and K. Yang, "Investigation of Nozzle Height Control to Improve Dispenser Printing of E-Textiles," *Proceedings*, vol. 68, p. 6, Jan. 2021, doi: *10.3390/proceedings2021068006*.

[3] T. Greig, R. Torah, and K. Yang, "Investigation of the effects of ink pigmentation on substrate profiling for e-textile dispenser printing," in *2021 IEEE International Conference on Flexible and Printable Sensors and Systems (FLEPS)*, pp. 1–4, 2021, doi: *10.1109/FLEPS51544.2021.9469756*.

[4] T. Greig, K. Yang, and R. Torah, "Evaluation of a spring-finger based, magnetic connector concept for reliable e-textile interconnects," *IEEE Transactions on Components, Packaging and Manufacturing Technology*, vol. 12, no. 10, pp. 1723–1725, 2022, doi: *10.1109/TCPMT.2022.3209591*.

[5] T. Greig, K. Yang, and R. Torah, "Miniature flexible reprogrammable microcontroller circuits for e-textiles," *Engineering Proceedings*, vol. 30, no. 1, 2023, doi: *10.3390/engproc2023030015*.

[6] T. Greig, K. Yang, and R. Torah, "A comparative evaluation of equivalent circuit and finite element electrical skin modelling techniques," *Biomedical Engineering Express*, 2023, doi: *10.1088/2057-1976/acfb04*.

[7] J. M. Monfre, "Pressure Ulcers," *Wound Healing - New insights into Ancient Challenges*, Oct. 2016, doi: *10.5772/63572*.

[8] G. V. Torres, A. M. Pergola-Marconato, T. C. Mansano- Schlosser, R. O. Araújo, D. C. Silva, A. Gómez-Morales, S. M. S. G. S. O. Torres, F. R. P. Mendes, and E. M.C. Maia, "Aspects Related to Venous Ulcer Healing and its Influence on Quality of Life," *Worldwide Wound Healing - Innovation in Natural and Conventional Methods*, Dec. 2016, doi: *10.5772/64913*.

[9] NHS, "National Diabetes Foot Care Audit, 2014-2018." https://digital.nhs.uk/data-and-information/publications/statistical/national-diabetes-footcare-audit/2014-2018, May 2019.

[10] NHS, "National Diabetes Foot Care Audit, 2014-2021." https://digital.nhs.uk/data-and-information/publications/statistical/national-diabetes-footcare-audit/2014-2021, May 2022.

[11] A. Polak, L. C. Kloth, E. Blaszczak, J. Taradaj, A. Nawrat-Szoltysik, T. Ickowicz, E. Hordynska, A. Franek, and C. Kucio, "The Efficacy of Pressure Ulcer Treatment With Cathodal and Cathodal-Anodal High-Voltage Monophasic Pulsed Current: A Prospective, Randomized, Controlled Clinical Trial," *Physical Therapy*, vol. 97, pp. 777–789, Aug. 2017, doi: *10.1093/ptj/pzx052*.

[12] J. Hunckler and A. de Mel, "A current affair: Electrotherapy in wound healing," *Journal of Multidisciplinary Healthcare*, vol. 10, pp. 179–194, Apr. 2017, doi: *10.2147/JMDH.S127207*.

[13] G. D. Gentzkow, S. V. Pollack, L. C. Kloth, and H. A. Stubbs, "Improved Healing of Pressure Ulcers Using Dermapulse, A New Electrical Stimulation Device," *Wounds*, vol. 3, pp. 158–170, Jan. 1991.

[14] P. E. Houghton, C. B. Kincaid, M. Lovell, K. E. Campbell, D. H. Keast, M. G. Woodbury, and K. A. Harris, "Effect of Electrical Stimulation on Chronic Leg Ulcer Size and Appearance," *Physical Therapy*, vol. 83, pp. 17–28, Jan. 2003, doi: *10.1093/ptj/83.1.17*.

[15] L. Wolcott, P. Wheeler, H. Hardwicke, and B. Rowley, "Accelerated Healing of Skin Ulcers by Electrotherapy: Preliminary Clinical Results," *Southern Medical Journal*, vol. 62, pp. 795–801, July 1969.

[16] W. R. Gault and P. F. Gatens, "Use of Low Intensity Direct Current in Management of Ischemic Skin Ulcers," *Physical Therapy*, vol. 56, pp. 265–269, Mar. 1976, doi: *10.1093/ptj/56.3.265*.

[17] O. Fakhri and M. A. Amin, "The Effect of Low-Voltage Electric Therapy on the Healing of Resistant Skin Burns," *The Journal of Burn Care & Rehabilitation*, vol. 8, pp. 15–18, Jan. 1987, doi: *10.1097/00004630-198701000-00003*.

[18] A. Komolafe, R. Torah, Y. Wei, H. Nunes-Matos, M. Li, D. Hardy, T. Dias, M. Tudor, and S. Beeby, "Integrating Flexible Filament Circuits for E-Textile Applications," *Advanced Materials Technologies*, vol. 4, no. 7, p. 1900176, 2019, doi: *10.1002/admt.201900176*.

[19] S. Beeby, R. Torah, J. Tudor, N. Grabham, S. Yong, S. Arumugam, Y. Li, and J. Shi, "Energy Harvesting Power Supplies for Electronic Textiles," in *2019 IEEE*

International Conference on Flexible and Printable Sensors and Systems (FLEPS), pp. 1–3, July 2019, doi: *10.1109/FLEPS.2019.8792260*.

[20] G. Paul, R. Torah, S. Beeby, and J. Tudor, "Novel active electrodes for ECG monitoring on woven textiles fabricated by screen and stencil printing," *Sensors and Actuators A: Physical*, vol. 221, pp. 60–66, Jan. 2015, doi: *10.1016/j.sna.2014.10.030*.

[21] C. G. Bartone, L. Moore, and M. Kohli, "An e-textile antenna for body area network," in *2016 IEEE International Symposium on Antennas and Propagation (APSURSI)*, pp. 999–1000, June 2016, doi: *10.1109/APS.2016.7696208*.

[22] M. de Vos, R. Torah, and J. Tudor, "Dispenser printed electroluminescent lamps on textiles for smart fabric applications," *Smart Materials and Structures*, vol. 25, p. 045016, Mar. 2016, doi: *10.1088/0964-1726/25/4/045016*.

[23] K. Yang, R. Torah, Y. Wei, S. Beeby, and J. Tudor, "Waterproof and durable screen printed silver conductive tracks on textiles," *Textile Research Journal*, vol. 83, pp. 2023–2031, Nov. 2013, doi: *10.1177/0040517513490063*.

[24] G. M. Paul, F. Cao, R. Torah, K. Yang, S. Beeby, and J. Tudor, "A Smart Textile Based Facial EMG and EOG Computer Interface," *IEEE Sensors Journal*, vol. 14, pp. 393–400, Feb. 2014, doi: *10.1109/JSEN.2013.2283424*.

[25] M. J. Morison, L. G. Ovington, and K. Wilkie, eds., *Chronic Wound Care*. Mosby, 2004.

[26] A. Hoffbrand, J. Pettit, and P. Moss, "Platelets, blood coagulation and haemostasis," in *Haematology*, pp. 236–249, Blackwell Science, fourth ed., 2001.

[27] K. Murphey, *Janeway's Immunobiology*. Garland Science, eighth ed., 2012.

[28] P. Lydyard, A. Whelan, and M. Fanger, *BIOS Instant Notes in Immunology*. London, UNITED KINGDOM: Taylor & Francis Group, 2011.

[29] M. Flanagan, ed., *Wound Healing and Skin Integrity: Principals and Practice*. Wiley-Blackwell, 2013.

[30] R. Graham-Brown and J. F. Bourke, *Mosby's Colour Atlas and Text of Dermatology*. London: Mosby, 1st ed., 1998.

[31] C. Martin-Granados and C. D. McCaig, "Harnessing the Electric Spark of Life to Cure Skin Wounds," *Advances in Wound Care*, vol. 3, pp. 127–138, Feb. 2014, doi: *10.1089/wound.2013.0451*.

[32] I. S. Foulds and A. T. Barker, "Human skin battery potentials and their possible role in wound healing," *British Journal of Dermatology*, vol. 109, no. 5, pp. 515–522, 1983, doi: *10.1111/j.1365-2133.1983.tb07673.x*.

[33] Z. Li, *Textile Electrode Design and Simulation for Bio-Signal Recording.* PhD thesis, University of Southampton, Oct. 2018.

[34] F. Lin, F. Baldessari, C. C. Gyenge, T. Sato, R. D. Chambers, J. G. Santiago, and E. C. Butcher, "Lymphocyte Electrotaxis In Vitro and In Vivo," *The Journal of Immunology*, vol. 181, pp. 2465–2471, Aug. 2008, doi: *10.4049/jimmunol.181.4.2465*.

[35] M. Zhao, B. Song, J. Pu, T. Wada, B. Reid, G. Tai, F. Wang, A. Guo, P. Walczysko, Y. Gu, T. Sasaki, A. Suzuki, J. V. Forrester, H. R. Bourne, P. N. Devreotes, C. D. McCaig, and J. M. Penninger, "Electrical signals control wound healing through phosphatidylinositol-3-OH kinase-γ and PTEN," *Nature*, vol. 442, pp. 457–460, July 2006, doi: *10.1038/nature04925*.

[36] M. R. Cho, H. S. Thatte, R. C. Lee, and D. E. Golan, "Integrin-Dependent Human Macrophage Migration Induced by Oscillatory Electrical Stimulation," *Annals of Biomedical Engineering*, vol. 28, pp. 234–243, Mar. 2000, doi: *10.1114/1.263*.

[37] K. Franke and H. Gruler, "Galvanotaxis of human granulocytes: Electric field jump studies," *European Biophysics Journal*, vol. 18, pp. 334–346, July 1990, doi: *10.1007/BF00196924*.

[38] C. A. Erickson and R. Nuccitelli, "Embryonic fibroblast motility and orientation can be influenced by physiological electric fields.," *The Journal of Cell Biology*, vol. 98, pp. 296–307, Jan. 1984, doi: *10.1083/jcb.98.1.296*.

[39] M. J. Brown and L. M. Loew, "Electric field-directed fibroblast locomotion involves cell surface molecular reorganization and is calcium independent.," *The Journal of Cell Biology*, vol. 127, pp. 117–128, Oct. 1994, doi: *10.1083/jcb.127.1.117*.

[40] E. Finkelstein, W. Chang, P.-H. G. Chao, D. Gruber, A. Minden, C. T. Hung, and J. C. Bulinski, "Roles of microtubules, cell polarity and adhesion in electric-field-mediated motility of 3T3 fibroblasts," *Journal of Cell Science*, vol. 117, pp. 1533–1545, Mar. 2004, doi: *10.1242/jcs.00986*.

[41] C.-H. Tsai, B.-J. Lin, and P.-H. G. Chao, "*A2*β1 integrin and RhoA mediates electric field-induced ligament fibroblast migration directionality," *Journal of Orthopaedic Research*, vol. 31, no. 2, pp. 322–327, 2012, doi: *10.1002/jor.22215*.

[42] A. Guo, B. Song, B. Reid, Y. Gu, J. V. Forrester, C. A. B. Jahoda, and M. Zhao, "Effects of Physiological Electric Fields on Migration of Human Dermal Fibroblasts," *Journal of Investigative Dermatology*, vol. 130, pp. 2320–2327, Sept. 2010, doi: *10.1038/jid.2010.96*.

[43] H. K. Soong, W. C. Parkinson, S. Bafna, G. L. Sulik, and S. C. Huang, "Movements of cultured corneal epithelial cells and stromal fibroblasts in electric fields.," *Investigative Ophthalmology & Visual Science*, vol. 31, pp. 2278–2282, Nov. 1990.

[44] D. M. Sheridan, R. Rivkah Isseroff, and R. Nuccitelli, "Imposition of a Physiologic DC Electric Field Alters the Migratory Response of Human Keratinocytes on Extracellular Matrix Molecules," *Journal of Investigative Dermatology*, vol. 106, pp. 642–646, Apr. 1996, doi: *10.1111/1523-1747.ep12345456*.

[45] G. Zhange, Y. Gu, R. Begum, H. Chen, X. Gao, J. A. McGrath, M. Parsons, and B. Song, "Kindlin-1 regulates keratinocyte electrotaxis," *Journal of Investigative Dermatology*, vol. 136, Oct. 2016, doi: *10.1016/j.jid.2016.05.129*.

[46] Z. M. I. I. S. W. O. Ibrahim, "Negative pressure wound therapy versus microcurrent electrical stimulation in wound healing in burns," *Journal of Wound Care*, Apr. 2019, doi: *10.12968/jowc.2019.28.4.214*.

[47] B. A. Rowley, "Electrical Current Effects on E. coil Growth Rates," *Proceedings of the Society for Experimental Biology and Medicine*, vol. 139, pp. 929–934, Mar. 1972, doi: *10.3181/00379727-139-36269*.

[48] J. A. Spadaro, T. J. Berger, S. D. Barranco, S. E. Chapin, and R. O. Becker, "Antibacterial Effects of Silver Electrodes with Weak Direct Current," *Antimicrobial Agents and Chemotherapy*, vol. 6, pp. 637–642, Nov. 1974, doi: *10.1128/AAC.6.5.637*.

[49] C. Assambo, A. Baba, R. Dozio, and M. J. Burke, "Determination of the parameters of the skin-electrode impedance model for ecg measurement," in *Proceedings of the 6th WSEAS Int. Conf. on Electronics, Hardware, Wireless and Optical Communications*, pp. 90–95, February 2007.

[50] M. Neuman, "Biopotential electrodes," in *Medical instrumentation: application and design* (J. Webster, ed.), ch. 5, pp. 189–240, Wiley, 4th ed., 2010.

[51] B. Taji, S. Shirmohammadi, and V. Groza, "Measuring skin-electrode impedance variation of conductive textile electrode under pressure," in *2014 IEEE International Instrumentation and Measurement Technology Conference (I2MTC) Proceedings*, May 2014, doi: *10.1109/I2MTC.2014.6860909*.

[52] F. Xiong, D. Chen, Z. Chen, C. Jin, and S. Dai, "Impedance characteristics of the skin-electrode interface of dry textile electrodes for wearable electrocardiogram," in *Advances in Body Area Networks I* (G. Fortino and Z. Wang, eds.), pp. 343–356, Springer International Publishing, 2019.

[53] K. Kaczmarek and J. Webster, "Voltage-current characteristics of the electrotactile skin-electrode interface," in *Images of the Twenty-First Century. Proceedings of the Annual International Engineering in Medicine and Biology Society*, pp. 1526–1527, November 1989, doi: *10.1109/IEMBS.1989.96322*.

[54] W. Schmickler, *Interfacial Electrochemistry*. Oxford University Press, 1996.

[55] Y. Lee and K. Hwang, "Skin thickness of korean adults," *Surgical and Radiological Anatomy*, vol. 24, pp. 183–189, 2002, doi: *10.1007/s00276-002-0034-5*.

[56] K. A. Holbrook and G. F. Odland, "Regional differences in the thickness (cell layers) of the human stratum corneum," *The Journal of Investigative Dermatology*, vol. 62, no. 4, pp. 415–422, 1974, doi: *10.1111/1523-1747.ep12701670*.

[57] Ø. G. Martinsen, S. Grimnes, and O. Sveen, "Dielectric properties of some keratinised tissues. Part 1:Stratum corneum and nailin situ," *Medical and Biological Engineering and Computing*, vol. 35, pp. 172–176, May 1997, doi: *10.1007/BF02530033*.

[58] C. Gabriel, A. Peyman, and E. H. Grant, "Electrical conductivity of tissue at frequencies below 1 mhz," *Physics in Medicine and Biology*, vol. 54, pp. 4863–4878, 2009, doi: *10.1088/0031-9155/54/16/002*.

[59] T. Yamamoto and Y. Yamamoto, "Electrical properties of the epidermal stratum corneum," *Medical and biological engineering*, vol. 14, pp. 151–158, Mar. 1976, doi: *10.1007/BF02478741*.

[60] C. Gabriel, S. Gabriel, and E. Corthout, "The dielectric properties of biological tissues: I. literature survey," *Physics in Medicine and Biology*, vol. 41, pp. 2231–2249, 1996, doi: *10.1088/0031-9155/41/11/003*.

[61] U. Birgersson, E. Birgersson, I. Nicander, and S. Ollmar, "A methodology for extracting the electrical properties of human skin," *Phisiological Measurement*, vol. 34, pp. 723–736, 2013, doi: *10.1088/0967-3334/34/6/723*.

[62] M. A. Stuchly and S. S. Stuchly, "Coaxial line reflection methods for measuring dielectric properties of biological substances at radio and microwave frequencies - a review," *IEEE Transactions on Instrumentation and Measurement*, vol. IM-29, no. 3, pp. 176–183, 1980, doi: *10.1109/TIM.1980.4314902*.

[63] T. Lahtinen, J. Nuutinen, and E. Alanen, "Dielectric properties of the skin," *Physics in Medicine and Biology*, vol. 42, pp. 1471–1472, 1997, doi: *10.1088/0031-9155/42/7/020*.

[64] S. I. Alekseev and M. C. Ziskin, "Human skin permittivity determined by millimeter wave reflection measurements," *Bioelectromagnetics*, vol. 28, pp. 331–339, 2007, doi: *10.1002/bem.20308*.

[65] B. Tsai, H. Xue, E. Birgersson, S. Ollmar, and U. Birgersson, "Dielectrical properties of living epidermis and dermis in the frequency range from 1 khz to 1 mhz," *Journal of Electrical Bioimpedance*, vol. 10, pp. 14–23, 2019, doi: *10.2478/joeb-2019-0003*.

[66] S. A. R. Naqvi, M. Manoufali, B. Mohammed, A. T. Mobashsher, D. Foong, and A. M. Abbosh, "In vivo human skin dielectric properties characterization and statistical analysis at frequencies from 1 to 30 ghz," *IEEE Transactions on Instrumentation and Measurement*, vol. 70, 2021, doi: *10.1109/TIM.2020.3036767*.

[67] L. C. Kloth, "Electrical Stimulation Technologies for Wound Healing," *Advances in Wound Care*, vol. 3, pp. 81–90, Feb. 2014, doi: *10.1089/wound.2013.0459*.

[68] H. P. Schwan, "Electrical Properties of Tissue and Cell Suspensions* *This work was supported in part by grants from the United States Public Health Service, H-1253(c2-4) and in part by the Office of Naval Research, 119–289.," in *Advances in Biological and Medical Physics* (J. H. Lawrence and C. A. Tobias, eds.), vol. 5, pp. 147–209, Elsevier, Jan. 1957. doi: *10.1016/B978-1-4832-3111-2.50008-0*.

[69] Ørjan J. Martinsen, S. Grimnes, and P. Mirtaheri, "Non-invasive measurements of post-mortem changes in dielectric properties of haddock muscle - a pilot study," *Journal of Food Engineering*, vol. 43, pp. 189–192, 2000, doi: *10.1016/S0260-8774(99)00151-X*.

[70] S. Grimnes and Ørjan G. Martinsen, "Alpha-dispersion in human tissue," in *International Conference on Electrical Bioimpedance*, vol. 224, 2010, doi: *10.1088/1742-6596/224/1/012073*.

[71] K. S. Cole and R. H. Cole, "Dispersion and absorption in dielectrics ii. direct current characteristics," *The Journal of Chemical Physics*, vol. 10, no. 2, pp. 98–105, 1942, doi: *10.1063/1.1723677*.

[72] B. H. Brown, R. H. Smallwood, D. C. Barber, P. V. Lawford, and D. R. Hose, *Medical Physics and Biomedical Engineering*. Taylor & Francis, 1999.

[73] M. Zhao, A. Agius-Fernandez, J. V. Forrester, and C. D. McCaig, "Orientation and directed migration of cultured corneal epithelial cells in small electric fields are serum dependent," *Journal of Cell Science*, vol. 109, pp. 1405–1414, June 1996.

[74] X. Ren, H. Sun, J. Liu, X. Guo, J. Huang, X. Jiang, Y. Zhang, Y. Huang, D. Fan, and J. Zhang, "Keratinocyte electrotaxis induced by physiological pulsed direct current electric fields," *Bioelectrochemistry*, vol. 127, pp. 113–124, June 2019, doi: *10.1016/j.bioelechem.2019.02.001*.

[75] P.-H. G. Chao, R. Roy, R. L. Mauck, W. Liu, W. B. Valhmu, and C. T. Hung, "Chondrocyte Translocation Response to Direct Current Electric Fields," *Journal of Biomechanical Engineering*, vol. 122, pp. 261–267, June 2000, doi: *10.1115/1.429661*.

[76] R. Nuccitelli and T. Smart, "Extracellular Calcium Levels Strongly Influence Neural Crest Cell Galvanotaxis," *The Biological Bulletin*, vol. 176, pp. 130–135, Apr. 1989, doi: *10.2307/1541662*.

[77] K. Y. Nishimura, R. R. Isseroff, and R. Nuccitelli, "Human keratinocytes migrate to the negative pole in direct current electric fields comparable to those measured in mammalian wounds," *Journal of Cell Science*, vol. 109, pp. 199–207, Jan. 1996.

[78] P.-H. G. Chao, H. H. Lu, C. T. Hung, S. B. Nicoll, and J. C. Bulinski, "Effects of Applied DC Electric Field on Ligament Fibroblast Migration and Wound Healing," *Connective Tissue Research*, vol. 48, pp. 188–197, Jan. 2007, doi: *10.1080/03008200701424451*.

[79] Z. Zhao, C. Watt, A. Karystinou, A. Roelofs, C. McCaig, I. Gibson, and C. De Bari, "Directed migration of human bone marrow mesenchymal stem cells in a physiological direct current electric field," *European Cells and Materials*, vol. 22, pp. 344–358, Nov. 2011, doi: *10.22203/eCM.v022a26*.

[80] N. J. Gunja, D. Dujari, A. Chen, A. Luengo, J. V. Fong, and C. T. Hung, "Migration responses of outer and inner meniscus cells to applied direct current electric fields," *Journal of Orthopaedic Research*, vol. 30, no. 1, pp. 103–111, 2012, doi: *10.1002/jor.21489*.

[81] M. Moarefian, R. V. Davalos, M. D. Burton, and C. N. Jones, "Electrotaxis-on-chip to quantify neutrophil migration towards electrochemical gradients," *Frontiers in Immunology*, vol. 12, Aug. 2021, doi: *10.3389/fimmu.2021.674727*.

[82] A. J. Bullock, A. T. Barker, L. Coulton, and S. MacNeil, "The effect of induced biphasic pulsed currents on re-epithelialization of a novel wound healing model," *Bioelectromagnetics*, vol. 28, no. 1, pp. 31–41, 2007, doi: *10.1002/bem.20267*.

[83] N. M. Kanof, "Gold Leaf in the Treatment of Cutaneous Ulcers," *Journal of Investigative Dermatology*, vol. 43, pp. 441–442, Nov. 1964, doi: *10.1038/jid.1964.181*.

[84] J. P. Gallagher and C. F. Geschickter, "The Use of Charged Gold Leaf in Surgery," *JAMA*, vol. 189, pp. 928–933, Sept. 1964, doi: *10.1001/jama.1964.03070120050012*.

[85] K. Digby, *Choice and Experimented Receipts in Physick and Chirurgery, as Also Cordial and Distilled Waters and Spirits, Perfumes, and Other Curiosities. Collected by the Honourable and Truly Learned Sir Kenelm Digby Kt. Chancellour to Her Majesty the Queen Mother. Translated out of Several Languages by G.H.* London: printed for the author, 1668.

[86] B. A. Rowley, J. M. McKenna, and L. E. Wolcott, "Proceedings: The use of low level electrical current for enhancement of tissue healing," *Biomedical Sciences Instrumentation*, vol. 10, pp. 111–114, Apr. 1974.

[87] P. J. Carley and S. F. Wainapel, "Electrotherapy for acceleration of wound healing: Low intensity direct current," *Archives of Physical Medicine and Rehabilitation*, vol. 66, pp. 443–446, July 1985.

[88] P. M. Katelaris, J. P. Fletcher, J. M. Ltttle, R. J. Mcentyre, and K. W. Jeffcoate, "Electrical Stimulation in the Treatment of Chronic Venous Ulceration," *Australian and New Zealand Journal of Surgery*, vol. 57, no. 9, pp. 605–607, 1987, doi: *10.1111/j.1445-2197.1987.tb01434.x*.

[89] P. L. Bigliardi, S. A. L. Alsagoff, H. Y. El-Kafrawi, J.-K. Pyon, C. T. C. Wa, and M. A. Villa, "Povidone iodine in wound healing: A review of current concepts and practices," *International Journal of Surgery*, vol. 44, pp. 260–268, Aug. 2017, doi: *10.1016/j.ijsu.2017.06.073*.

[90] D. L. Nelson and M. M. Cox, *Lehringer Principles of Biochemistry*. Macmillan Higher Education, 7th international ed., 2017.

[91] J. A. Feedar, L. C. Kloth, and G. D. Gentzkow, "Chronic Dermal Ulcer Healing Enhanced with Monophasic Pulsed Electrical Stimulation," *Physical Therapy*, vol. 71, pp. 639–649, Sept. 1991, doi: *10.1093/ptj/71.9.639*.

[92] M. Jünger, A. Arnold, D. Zuder, H.-W. Stahl, and S. Heising, "Local therapy and treatment costs of chronic, venous leg ulcers with electrical stimulation (Dermapulse®): A prospective, placebo controlled, double blind trial," *Wound Repair and Regeneration*, vol. 16, no. 4, pp. 480–487, 2008, doi: *10.1111/j.1524-475X.2008.00393.x*.

[93] J. M. Wood, P. E. Evans, K. U. Schallreuter, W. E. Jacobson, R. Sufit, J. Newman, C. White, and M. Jacobson, "A Multicenter Study on the Use of Pulsed Low-Intensity Direct Current for Healing Chronic Stage II and Stage III Decubitus Ulcers," *Archives of Dermatology*, vol. 129, pp. 999–1009, Aug. 1993, doi: *10.1001/archderm.1993.01680290071011*.

[94] B. O. Adegoke and K. A. Badmos, "Acceleration of pressure ulcer healing in spinal cord injured patients using interrupted direct current," *African Journal of Medicine and Medical Sciences*, vol. 30, pp. 195–197, Sept. 2001.

[95] L. L. Baker, S. Rubayi, F. Villar, and S. K. Demuth, "Effect of electrical stimulation waveform on healing of ulcers in human beings with spinal cord injury," *Wound Repair and Regeneration*, vol. 4, no. 1, pp. 21–28, 1996, doi: *10.1046/j.1524-475X.1996.40106.x*.

[96] L. C. Kloth and J. A. Feedar, "Acceleration of Wound Healing with High Voltage, Monophasic, Pulsed Current," *Physical Therapy*, vol. 68, pp. 503–508, Apr. 1988, doi: *10.1093/ptj/68.4.503*.

[97] J. W. Griffin, R. E. Tooms, R. A. Mendius, J. K. Clifft, R. Vander Zwaag, and F. El-Zeky, "Efficacy of High Voltage Pulsed Current for Healing of Pressure Ulcers in Patients with Spinal Cord Injury," *Physical Therapy*, vol. 71, pp. 433–442, June 1991, doi: *10.1093/ptj/71.6.433*.

[98] A. Franek, A. Polak, and M. Kucharzewski, "Modern application of high voltage stimulation for enhanced healing of venous crural ulceration," *Medical Engineering & Physics*, vol. 22, pp. 647–655, Nov. 2000, doi: *10.1016/S1350-4533(00)00077-1*.

[99] P. E. Houghton, K. E. Campbell, C. H. Fraser, C. Harris, D. H. Keast, P. J. Potter, K. C. Hayes, and M. G. Woodbury, "Electrical Stimulation Therapy Increases Rate of Healing of Pressure Ulcers in Community-Dwelling People With Spinal Cord Injury," *Archives of Physical Medicine and Rehabilitation*, vol. 91, pp. 669–678, May 2010, doi: *10.1016/j.apmr.2009.12.026*.

[100] A. Franek, R. Kostur, A. Polak, J. Taradaj, Z. Szlachta, E. Blaszczak, P. Dolibog, P. Dolibog, B. Koczy, and C. Kucio, "Using High-Voltage Electrical Stimulation in the Treatment of Recalcitrant Pressure Ulcers: Results of a Randomized, Controlled Clinical Study," *Ostomy Wound Management*, vol. 58, pp. 30–44, Mar. 2012.

[101] E. J. Peters, L. A. Lavery, D. G. Armstrong, and J. G. Fleischli, "Electric stimulation as an adjunct to heal diabetic foot ulcers: A randomized clinical trial," *Archives of Physical Medicine and Rehabilitation*, vol. 82, pp. 721–725, June 2001, doi: *10.1053/apmr.2001.23780*.

[102] K. Zhou, K. Krug, J. Stachura, P. Niewczyk, M. Ross, J. Tutuska, and G. Ford, "Silver-Collagen Dressing and High-voltage, Pulsed-current Therapy for the Treatment of Chronic Full-thickness Wounds: A Case Series," *Ostomy/Wound Management*, vol. 62, pp. 36–44, Mar. 2016.

[103] B. Kaada and M. Emru, "PROMOTED HEALING OF LEPROUS ULCERS BY TRANSCUTANEOUS NERVE STIMULATION," *Acupuncture & Electro-Therapeutics Research*, vol. 13, no. 4, pp. 165–176, 1988, doi: *info:doi/10.3727/036012988816358589*.

[104] W. Gibson, B. M. Wand, C. Meads, M. J. Catley, and N. E. O'Connell, "Transcutaneous electrical nerve stimulation (TENS) for chronic pain - an overview of Cochrane Reviews," *The Cochrane Database of Systematic Reviews*, vol. 2019, Apr. 2019, doi: *10.1002/14651858.CD011890.pub3*.

[105] T. Lundeberg, S. Eriksson, and M. Malm, "Electrical Nerve-Stimulation Improves Healing of Diabetic Ulcers," *Annals of Plastic Surgery*, vol. 29, pp. 328–331, Oct. 1992, doi: *10.1097/00000637-199210000-00009*.

[106] S. García-Pérez, M. C. García-Ríos, J. M. Pérez-Mármol, R. M. Tapia-Haro, M. Albornoz-Cabello, M. C. Valenza, and M. E. Aguilar-Ferrándiz, "Effectiveness of Transcutaneous Electrical Nerve Stimulation Energy in Older Adults: A Pilot Clinical Trial," *Advances in Skin & Wound Care*, vol. 31, pp. 462–469, Oct. 2018, doi: *10.1097/01.ASW.0000544614.18501.b4*.

[107] T. Lundeberg, J. Kjartansson, and U. Samuelsson, "EFFECT OF ELECTRICAL NERVE STIMULATION ON HEALING OF ISCHAEMIC SKIN FLAPS," *The Lancet*, vol. 332, pp. 712–714, Sept. 1988, doi: *10.1016/S0140-6736(88)90187-0*.

[108] A. Jerčinović, R. Karba, L. Vodovnik, A. Stefanovska, P. Krošelj, R. Turk, I. Džidić, H. Benko, and R. Šavrin, "Low frequency pulsed current and pressure ulcer healing," *IEEE Transactions on Rehabilitation Engineering*, vol. 2, pp. 225–233, Dec. 1994, doi: *10.1109/86.340876*.

[109] D. Lawson and J. S. Petrofsky, "A randomized control study on the effect of biphasic electrical stimulation in a warm room on skin blood flow and healing rates in chronic wounds of patients with and without diabetes," *Medical Science Monitor: International Medical Journal of Experimental and Clinical Research*, vol. 13, pp. CR258–263, June 2007.

[110] S. Farnia, M. Casarotto, M. Benelle, M. Tinazzi, A. Fiaschi, M. Goldoni, and N. Smania, "A randomized controlled study on the effect of two different treatments (FREMS and TENS) in myofascial pain syndrome - ProQuest," *Europa Medicophysica*, vol. 40, pp. 293–301, Dec. 2004.

[111] E. Bosi, M. Conti, C. Vermigli, G. Cazzetta, E. Peretti, M. C. Cordoni, G. Galimberti, and L. Scionti, "Effectiveness of frequency-modulated electromagnetic neural stimulation in the treatment of painful diabetic neuropathy," *Diabetologia*, vol. 48, pp. 817–823, May 2005, doi: *10.1007/s00125-005-1734-2*.

[112] E. Bosi, G. Bax, L. Scionti, V. Spallone, S. Tesfaye, P. Valensi, D. Ziegler, and FREMS European Trial Study Group, "Frequency-modulated electromagnetic neural stimulation (FREMS) as a treatment for symptomatic diabetic neuropathy: Results from a double-blind, randomised, multicentre, long-term, placebo-controlled clinical trial," *Diabetologia*, vol. 56, pp. 467–475, Mar. 2013, doi: *10.1007/s00125-012-2795-7*.

[113] M. Bevilacqua, L. J. Dominguez, M. Barrella, and M. Barbagallo, "Induction of vascular endothelial growth factor release by transcutaneous frequency modulated neural stimulation in diabetic polyneuropathy," *Journal of Endocrinological Investigation*, vol. 30, pp. 944–947, Dec. 2007, doi: *10.1007/BF03349242*.

[114] A. Janković and I. Binić, "Frequency rhythmic electrical modulation system in the treatment of chronic painful leg ulcers," *Archives of Dermatological Research*, vol. 300, p. 377, July 2008, doi: *10.1007/s00403-008-0875-9*.

[115] A. Margara, F. Boriani, F. D. Obbialero, and M. A. Bocchiotti, "Frequency rhythmic electrical modulation system in the treatment of diabetic ulcers.," *Estratto da Chirugia*, vol. 21, no. 6, pp. 311–314, 2008.

[116] A. Santamato, F. Panza, F. Fortunato, A. Portincasa, V. Frisardi, G. Cassatella, M. Valente, D. Seripa, M. Ranieri, and P. Fiore, "Effectiveness of the Frequency Rhythmic Electrical Modulation System for the Treatment of Chronic and Painful Venous Leg Ulcers in Older Adults," *Rejuvenation Research*, vol. 15, pp. 281–287, June 2012, doi: *10.1089/rej.2011.1236*.

[117] C. Magnoni, E. Rossi, C. Fiorentini, A. Baggio, B. Ferrari, and G. Alberto, "Electrical stimulation as adjuvant treatment for chronic leg ulcers of different aetiology: An RCT," *Journal of Wound Care*, vol. 22, pp. 525–533, Oct. 2013, doi: *10.12968/jowc.2013.22.10.525*.

[118] M. M. V. Miguel, I. F. Mathias-Santamaria, A. Rossato, L. F. F. Ferraz, A. M. Figueiredo-Neto, A. C. de Marco, R. C. V. Casarin, S. M. Wallet, D. N. Tatakis, M. A. Mathias, and M. P. Santamara, "Microcurrent electrotherapy improves palatal wound healing: Randomized clinical trial," *Journal of Periodontology*, vol. 92, pp. 244–253, May 2021, doi: *10.1002/JPER.20-0122*.

[119] NICE, "Evidence | Diabetic foot problems: Prevention and management | Guidance | NICE." https://www.nice.org.uk/guidance/ng19/evidence, 2015.

[120] NICE, "Pressure ulcers: Prevention and management," Tech. Rep. CG179, National Institute for Health and Care Excellence, Apr. 2014.

[121] BNF, "Wound management products and elasticated garments." https://bnf.nice.org.uk/wound-management/.

[122] K. Yang, M. Liu, T. Ward, D. Young, H. Matos, Y. Wei, and J. Adams, "Electronic textiles based wearable electrotherapy for pain relief," *Sensors and Actuators A: Physical*, vol. 303, p. 111701, Mar. 2020, doi: *10.1016/j.sna.2019.111701*.

[123] B. G. Tuna, G. Goncu Berk, N. Topcuoglu, and U. Ozorhan, "A Pilot Study on Electrode–Skin Impedance Analysis of Embroidered EMG Electrodes," in *13th EAI International Conference on Body Area Networks* (C. Sugimoto, H. Farhadi, and M. Hämäläinen, eds.), EAI/Springer Innovations in Communication and Computing, (Cham), pp. 365–371, Springer International Publishing, 2020, doi: *10.1007/978-3-030-29897-5_31*.

[124] C. W. Bae, P. T. Toi, B. Y. Kim, W. I. Lee, H. B. Lee, A. Hanif, E. H. Lee, and N.-E. Lee, "Fully Stretchable Capillary Microfluidics-Integrated Nanoporous Gold Electrochemical Sensor for Wearable Continuous Glucose Monitoring," *ACS Applied Materials & Interfaces*, vol. 11, pp. 14567–14575, Apr. 2019, doi: *10.1021/acsami.9b00848*.

[125] J. W. Matiko, Y. Wei, R. Torah, N. Grabham, G. Paul, S. Beeby, and J. Tudor, "Wearable EEG headband using printed electrodes and powered by energy harvesting for emotion monitoring in ambient assisted living," *Smart Materials and Structures*, vol. 24, p. 125028, Nov. 2015, doi: *10.1088/0964-1726/24/12/125028*.

[126] L. S. Vidyaratne and K. M. Iftekharuddin, "Real-Time Epileptic Seizure Detection Using EEG," *IEEE Transactions on Neural Systems and Rehabilitation Engineering*, vol. 25, pp. 2146–2156, Nov. 2017, doi: *10.1109/TNSRE.2017.2697920*.

[127] E. M. Ahmed, "Hydrogel: Preparation, characterization, and applications: A review," *Journal of Advanced Research*, vol. 6, pp. 105–121, Mar. 2015, doi: *10.1016/j.jare.2013.07.006*.

[128] A. M. Stewart, C. G. Pretty, and X. Chen, "An Evaluation of the Effect of Stimulation Parameters and Electrode Type on Bicep Muscle Response for a Voltage-controlled Functional Electrical Stimulator," *IFAC-PapersOnLine*, vol. 50, pp. 15109–15114, July 2017, doi: *10.1016/j.ifacol.2017.08.2242*.

[129] K. Yang, C. Freeman, R. Torah, S. Beeby, and J. Tudor, "Screen printed fabric electrode array for wearable functional electrical stimulation," *Sensors and Actuators A: Physical*, vol. 213, pp. 108–115, July 2014, doi: *10.1016/j.sna.2014.03.025*.

[130] B. Moineau, C. Marquez-Chin, M. Alizadeh-Meghrazi, and M. R. Popovic, "Garments for functional electrical stimulation: Design and proofs of concept," *Journal of Rehabilitation and Assistive Technologies Engineering*, vol. 6, p. 2055668319854340, Jan. 2019, doi: *10.1177/2055668319854340*.

[131] T.-G. La, S. Qiu, D. K. Scott, R. Bakhtiari, J. W. P. Kuziek, K. E. Mathewson, J. Rieger, and H.-J. Chung, "Two-layered and stretchable e-textile patches for wearable healthcare electronics," *Advanced Healthcare Materials*, vol. 7, no. 22, p. 1801033, 2018, doi: *https://doi.org/10.1002/adhm.201801033*.

[132] G. Acar, O. Ozturk, A. J. Golparvar, T. A. Elboshra, K. Böhringer, and M. K. Yapici, "Wearable and Flexible Textile Electrodes for Biopotential Signal Monitoring: A review," *Electronics*, vol. 8, p. 479, May 2019, doi: *10.3390/electronics8050479*.

[133] T. Perera, M. Mohotti, and M. Perera, "Stretchable Conductive Yarn for Electronic Textiles Made Using Hollow Spindle Spinning," in *2018 Moratuwa Engineering Research Conference (MERCon)*, pp. 544–548, May 2018, doi: *10.1109/MERCon.2018.8421958*.

[134] J. Jianming, P. Wei, Y. Shenglin, and L. Guang, "Electrically conductive PANI-DBSA/Co-PAN composite fibers prepared by wet spinning," *Synthetic Metals*, vol. 149, pp. 181–186, Mar. 2005, doi: *10.1016/j.synthmet.2004.12.008*.

[135] D. Bowman and B. R. Mattes, "Conductive Fibre Prepared From Ultra-High Molecular Weight Polyaniline for Smart Fabric and Interactive Textile Applications," *Synthetic Metals*, vol. 154, pp. 29–32, Sept. 2005, doi: *10.1016/j.synthmet.2005.07.017*.

[136] J. Foroughi, G. M. Spinks, G. G. Wallace, and P. G. Whitten, "Production of polypyrrole fibres by wet spinning," *Synthetic Metals*, vol. 158, pp. 104–107, Feb. 2008, doi: *10.1016/j.synthmet.2007.12.008*.

[137] Y. Wang, M. Rouabhia, and Z. Zhang, "PPy-coated PET fabrics and electric pulse-stimulated fibroblasts," *Journal of Materials Chemistry B*, vol. 1, no. 31, pp. 3789–3796, 2013, doi: *10.1039/C3TB20257G*.

[138] H. Okuzaki, Y. Harashina, and H. Yan, "Highly conductive PEDOT/PSS microfibers fabricated by wet-spinning and dip-treatment in ethylene glycol," *European Polymer Journal*, vol. 45, pp. 256–261, Jan. 2009, doi: *10.1016/j.eurpolymj.2008.10.027*.

[139] T. Bashir, M. Skrifvars, and N.-K. Persson, "Surface modification of conductive PEDOT coated textile yarns with silicone resin," *Materials Technology*, vol. 26, pp. 135–139, July 2011, doi: *10.1179/175355511X13007211258926*.

[140] B. Ding, X. Wang, and J. Yu, eds., *Electrospinning: Nanofabrication and Applications*. Elsevier, 2019, doi: *10.1016/C2016-0-01374-8*.

[141] Y. Merhi and S. Agarwala, "Direct write of dry electrodes on healthcare textiles," in *2021 IEEE International Conference on Flexible and Printable Sensors and Systems (FLEPS)*, pp. 1–2, 2021, doi: *10.1109/FLEPS51544.2021.9469835*.

[142] M. Liu, S. Beeby, and K. Yang, "Electrode for Wearable Electrotherapy," *Proceedings*, vol. 32, no. 1, p. 5, 2019, doi: *10.3390/proceedings2019032005*.

[143] A. Komolafe, H. Nunes-Matos, M. Glanc-Gostkiewicz, and R. Torah, "Influence of textile structure on the wearability of printed e-textiles," in *2020 IEEE International Conference on Flexible and Printable Sensors and Systems (FLEPS)*, pp. 1–4, Aug. 2020, doi: *10.1109/FLEPS49123.2020.9239562*.

[144] G. Paul, R. Torah, S. Beeby, and J. Tudor, "The development of screen printed conductive networks on textiles for biopotential monitoring applications," *Sensors and Actuators A: Physical*, vol. 206, pp. 35–41, Feb. 2014, doi: *10.1016/j.sna.2013.11.026*.

[145] T. Kuroda, H. Takahashi, and A. Masuda, "Chapter 3.2 - Woven Electronic Textiles," in *Wearable Sensors* (E. Sazonov and M. R. Neuman, eds.), pp. 175–198, Oxford: Academic Press, Jan. 2014. doi: *10.1016/B978-0-12-418662-0.00021-0*.

[146] Y. Tajitsu, "Development of e-textile sewn together with embroidered fabric having motion-sensing function using piezoelectric braided cord for embroidery," *IEEE Transactions on Dielectrics and Electrical Insulation*, vol. 27, pp. 1644–1649, Oct. 2020, doi: *10.1109/TDEI.2020.008448*.

[147] K. Fobelets, G. Hammour, and K. Thielemans, "Knitted ecg electrodes in relaxed fitting garments," *IEEE Sensors Journal*, vol. 23, no. 5, pp. 5263–5269, 2023, doi: *10.1109/JSEN.2023.3236723*.

[148] Z. Ahmed, R. Torah, K. Yang, S. Beeby, and J. Tudor, "Investigation and improvement of the dispenser printing of electrical interconnections for smart fabric applications," *Smart Materials and Structures*, vol. 25, p. 105021, Sept. 2016, doi: *10.1088/0964-1726/25/10/105021*.

[149] N. Karim, S. Afroj, A. Malandraki, S. Butterworth, C. Beach, M. Rigout, K. S. Novoselov, A. J. Casson, and S. G. Yeates, "All inkjet-printed graphene-based conductive patterns for wearable e-textile applications," *Journal of Materials Chemistry C*, vol. 5, no. 44, pp. 11640–11648, 2017, doi: *10.1039/C7TC03669H*.

[150] C. Cie, "6 - ink jet print heads," in *Ink Jet Textile Printing* (C. Cie, ed.), Woodhead Publishing Series in Textiles, pp. 73–84, Woodhead Publishing, 2015. doi: *https://doi.org/10.1016/B978-0-85709-230-4.00006-6*.

[151] C. Goth, S. Putzo, and J. Franke, "Aerosol Jet printing on rapid prototyping materials for fine pitch electronic applications," in *2011 IEEE 61st Electronic Components and Technology Conference (ECTC)*, pp. 1211–1216, May 2011, doi: *10.1109/ECTC.2011.5898664*.

[152] M. G. Honarvar and M. Latifi, "Overview of wearable electronics and smart textiles," *The Journal of The Textile Institute*, vol. 108, pp. 631–652, Apr. 2017, doi: *10.1080/00405000.2016.1177870*.

[153] Y. Merhi, P. H. Mikkelsen, C. Suetta, J. V. Nygaard, and S. Agarwala, "Mechanical performance of electronically functional smart textiles," *Transactions on Additive Manufacturing Meets Medicine*, vol. 2, no. 1, 2020.

[154] K. Garbacz, L. Stagun, S. Rotzler, M. Semenec, and M. von Krshiwoblozki, "Modular e-textile toolkit for prototyping and manufacturing," *Proceedings*, vol. 68, no. 1, 2021, doi: *10.3390/proceedings2021068005*.

[155] A. O. Komolafe, R. N. Torah, K. Yang, J. Tudor, and S. P. Beeby, "Durability of screen printed electrical interconnections on woven textiles," in *2015 IEEE 65th Electronic Components and Technology Conference (ECTC)*, pp. 1142–1147, 2015, doi: *10.1109/ECTC.2015.7159738*.

[156] C. Zhu, Y. Li, and X. Liu, "Polymer interface molecular engineering for e-textiles," *Polymers*, vol. 10, no. 6, 2018, doi: *10.3390/polym10060573*.

[157] X.-F. Wang, M.-L. Li, Q.-Q. Fang, W.-Y. Zhao, D. Lou, Y.-Y. Hu, J. Chen, X.-Z. Wang, and W.-Q. Tan, "Flexible electrical stimulation device with Chitosan-Vaseline® dressing accelerates wound healing in diabetes," *Bioactive Materials*, vol. 6, pp. 230–243, Jan. 2021, doi: *10.1016/j.bioactmat.2020.08.003*.

[158] J. Petrofsky, E. Schwab, M. Cúneo, J. George, J. Kim, A. Almalty, D. Lawson, E. Johnson, and W. Remigo, "Current distribution under electrodes in relation to stimulation current and skin blood flow: Are modern electrodes really providing the current distribution during stimulation we believe they are?," *Journal of Medical Engineering & Technology*, vol. 30, pp. 368–381, Jan. 2006, doi: *10.1080/03091900500183855*.

[159] J. Petrofsky and E. Schwab, "A re-evaluation of modelling of the current flow between electrodes: Consideration of blood flow and wounds," *Journal of Medical Engineering & Technology*, vol. 31, pp. 62–74, Jan. 2007, doi: *10.1080/03091900600687698*.

[160] H. Suh, J. Petrofsky, A. Fish, V. Hernandez, E. Mendoza, K. Collins, T. Yang, A. Abdul, J. Batt, and D. Lawson, "A New Electrode Design to Improve Outcomes in the Treatment of Chronic Non-Healing Wounds in Diabetes," *Diabetes Technology & Therapeutics*, vol. 11, pp. 315–322, May 2009, doi: *10.1089/dia.2008.0092*.

[161] Y.-S. Sun, "Electrical Stimulation for Wound-Healing: Simulation on the Effect of Electrode Configurations," *BioMed Research International*, vol. 2017, 2017, doi: *10.1155/2017/5289041*.

[162] "BS IEC 63203-204-2. wearable electronic devices and technologies. part 204-2. electronic textile. test method to characterize resistance change in bending test of e-textile systems," 2022.

[163] S. Rotzler, M. von Krshiwoblozki, and M. Schneider-Ramelow, "Washability of e-textiles: current testing practices and the need for standardization," *Textile Research Journal*, vol. 91, no. 19-20, pp. 2401–2417, 2021, doi: *https://-doi.org/10.1177/0040517521996727*.

[164] A. Komolafe, B. Zaghari, A. S. Weddell, H. Khanbareh, Z. M. Tsikriteas, M. Vousden, M. Wagih, U. T. Jurado, J. Shi, S. Yong, S. Arumugam, Y. Li, K. Yang, G. Savelli, N. M. White, and S. Beeby, "E-textile technology review - from materials to applications," *IEEE Access*, vol. 9, pp. 97152 – 97179, 2021, doi: *https://-doi.org/10.1109/ACCESS.2021.3094303*.

[165] M. H. Kim, C. H. Cho, J. S. Kim, T. U. Nam, W.-S. Kim, T. Il Lee, and J. Y. Oh, "Thermoelectric energy harvesting electronic skin (e-skin) patch with reconfigurable carbon nanotube clays," *Nano Energy*, vol. 87, p. 106156, 2021, doi: *https://doi.org/10.1016/j.nanoen.2021.106156*.

[166] Z. Cao, E. Koukharenko, M. Tudor, R. Torah, and S. Beeby, "Flexible screen printed thermoelectric generator with enhanced processes and materials," *Sensors and Actuators A: Physical*, vol. 238, pp. 196–206, 2016, doi: *https://doi.org/10.1016/j.sna.2015.12.016*.

[167] M. Bouklachi, M. Biancheri-Astier, A. Diet, and Y. L. Bihan, "Energy harvesting of a nfc flexible patch for medical applications," in *2019 IEEE Wireless Power Transfer Conference (WPTC)*, pp. 249–252, 2019, doi: *10.1109/WPTC45513.2019.9055686*.

[168] D. Hardy, R. Wickenden, and A. McLaren, "Electronic textile reparability," *Journal of Cleaner Production*, vol. 276, p. 124328, 2020, doi: *https://doi.org/10.1016/j.jclepro.2020.124328*.

[169] J. Stanley, J. A. Hunt, P. Kunovski, and Y. Wei, "A review of connectors and joining technologies for electronic textiles," *Engineering Reports*, p. e12491, 2021, doi: *https://doi.org/10.1002/eng2.12491*.

[170] Renishaw plc, "Renishaw: Products." http://www.renishaw.com/en/products–32083.

[171] C. Votzke, N. Alteir, V. Vasquez, Y. Mengüç, and M. L. Johnston, "Auger-based 3d printing of stretchable liquid metal paste interconnects: A brief tutorial," in *2021 IEEE International Conference on Flexible and Printable Sensors and Systems (FLEPS)*, pp. 1–4, 2021, doi: *10.1109/FLEPS51544.2021.9469786*.

[172] S. Li, X. Jia, M. Chen, and Y. Yang, "Error analysis and correction for color in laser triangulation measurement," *Optik*, vol. 168, pp. 165–173, Sept. 2018, doi: *10.1016/j.ijleo.2018.04.057*.

[173] Z. Ahmed, R. Torah, and J. Tudor, "Optimisation of a novel direct-write dispenser printer technique for improving printed smart fabric device performance," in *2015 Symposium on Design, Test, Integration and Packaging of MEMS/MOEMS (DTIP)*, pp. 1–5, Apr. 2015, doi: *10.1109/DTIP.2015.7160978*.

[174] M. Liu, Z. Ahmed, N. Grabham, S. Beeby, J. Tudor, and K. Yang, "An all dispenser printed electrode structure on textile for wearable healthcare," in *3rd International Conference on the Challenges, Opportunities, Innovations and Applications in Electronic Textiles*, April 2022, doi: *10.3390/engproc2022015016*.

[175] R Core Team, *R: A Language and Environment for Statistical Computing*. R Foundation for Statistical Computing, Vienna, Austria, 2022, URL: *https://www.R-project.org*.

[176] D. G. Archer and P. Wang, "The dielectric constant of water and debye-hückel limiting law slopes," *Journal of Physical and Chemical Reference Data*, vol. 19, no. 2, pp. 371–411, 1990, doi: *10.1063/1.555853*.

[177] S. Gabriel, R. W. Lau, and C. Gabriel, "The dielectric properties of biological tissues: III. parametric models for the dielectric spectrum of tissues," *Physics in Medicine and Biology*, vol. 41, pp. 2271–2293, 1996, doi: *10.1088/0031-9155/41/11/003*.

[178] Y.-S. Sun, S.-W. Peng, and J.-Y. Cheng, "In vitro electrical-stimulated wound-healing chip for studying electric field-assisted wound-healing process," *Biomicrofluidics*, vol. 6, 09 2012, doi: *10.1063/1.4750486*. 034117.

[179] J. C. Yarrow, Z. E. Perlman, N. J. Westwood, and T. J. Mitchison, "A high-throughput cell migration assay using scratch wound healing, a comparison of image-based readout methods," *BMC Biotechnology*, vol. 4, Sept. 2004, doi: *https://doi.org/10.1186/1472-6750-4-21*.

[180] K. Srirussamee, R. Xue, S. Mobini, N. J. Cassidy, and S. H. Cartmell, "Changes in the extracellular microenvironment and osteogenic responses of mesenchymal stem/stromal cells induced by in vitro direct electrical stimulation," *Journal of Tissue Engineering*, vol. 12, p. 2041731420974147, 2021, doi: *10.1177/2041731420974147*. PMID: 33643602.

[181] J. O'Brien, I. Wilson, T. Orton, and F. Pognan, "Investigation of the alamar blue (resazurin) fluorescent dye for the assessment of mammalian cell cytotoxicity," *European Journal of Biochemistry*, vol. 267, no. 17, pp. 5421–5426, 2000, doi: *https://doi.org/10.1046/j.1432-1327.2000.01606.x*.

[182] Merck. https://www.sigmaaldrich.com/GB/en/technical-documents/technical-article/cell-culture-and-cell-culture-analysis/mammalian-cell-culture/dulbecco-modified-eagle-medium-formulation. Accessed: 2023-04-23.

[183] J. Leśnikowski, "Research on poppers used as electrical connectors in high speed textile transmission lines," *Autex Research Journal*, vol. 16, no. 4, pp. 228–235, 2016, doi: *doi:10.1515/aut-2016-0025*.

[184] M. Liu, T. Ward, D. Young, H. Matos, Y. Wei, J. Adams, and K. Yang, "Electronic textiles based wearable electrotherapy for pain relief," *Sensors*

and Actuators A: Physical, vol. 303, p. 111701, 2020, doi: *https://doi.org/10.1016/j.sna.2019.111701*.

[185] H. G. Joo, Y. H. Jang, and H. S. Choi, "Electrical contact resistance for a conductive velcro system," *Tribology International*, vol. 80, pp. 115–121, 2014, doi: *https://doi.org/10.1016/j.triboint.2014.06.016*.

[186] L. Stark, "Soft switches." http://thesoftcircuiteer.net/soft-switches/, 2018. Accessed: 2022-06-01.

[187] X. Righetti and D. Thalmann, "Proposition of a modular i2c-based wearable architecture," in *Melecon 2010 - 2010 15th IEEE Mediterranean Electrotechnical Conference*, pp. 802–805, 2010, doi: *10.1109/MELCON.2010.5475965*.

[188] R. Freire, B. R. Glowacki, R. R. Williams, M. Wonnacott, A. Jamieson-Binnie, and D. R. Glowacki, "Omg-vr: Open-source mudra gloves for manipulating molecular simulations in vr," 2019, doi: *10.48550/ARXIV.1901.03532*.

[189] Anyfoam ltd. https://anyfoam.co.uk/. Accessed: 2022-06-01.

[190] "BS IEC 63203-204-1. wearable electronic devices and technologies. part 204-1. electronic textile. washable durability test method for leisure and sportswear e-textile system," 2018.

[191] TE Connectivity. https://www.te.com/global-en/products/connectors/pcb-connectors/board-to-board-connectors/spring-finger-contacts.html. Accessed: 2022-06-08.

[192] R. Dong and B. Guo, "Smart wound dressings for wound healing," *Nano Today*, vol. 41, p. 101290, 2021, doi: *https://doi.org/10.1016/j.nantod.2021.101290*.

[193] U. Pliquett, R. Langer, and J. C. Weaver, "Changes in the passive electrical properties of human stratum corneum due to electroporation," *Biochimica et Biophysica Acta (BBA) - Biomembranes*, vol. 1239, no. 2, pp. 111–121, 1995, doi: *https://doi.org/10.1016/0005-2736(95)00139-T*.

[194] L. M. Castano and A. B. Flatau, "Smart fabric sensors and e-textile technologies: a review," *Smart Materials and Structures*, vol. 32, 2014.

[195] Microchip. https://www.microchip.com/en-us/product/ATtiny85. Accessed: 2022-12-02.

[196] micronucleus. https://www.github.com/micronucleus/micronucleus. Accessed: 2022-12-02.

[197] https://docs.arduino.cc/retired/boards/lilypad-arduino-usb. Accessed: 2022-12-05.

[198] Adafruit Industries. https://www.adafruit.com/product/1222. Accessed: 2022-12-05.